

IDŐJÁRÁS

QUARTERLY JOURNAL OF THE HUNGAROMET
HUNGARIAN METEOROLOGICAL SERVICE

CONTENTS

<i>András Peterka, Gabriella Schmeller, Noémi Sarkadi, and István Geresdi: Comparison of horizontal visibility observed by present weather sensor and human eye-based method and evaluated from ceilometer's vertical backscattering profile over two Hungarian meteorological stations</i>	1
<i>İhsan Çiçek, Necla Türkoğlu, Zerrin Demirörs, Edanur Gözet, Batuhan Ateş Yılmaz, and İlker Alan: Temporal and spatial analysis of lightning density in Türkiye</i>	15
<i>Pak-wai Chan and Junyi He: An observational study of a long-lived monsoon depression over the South China Sea</i>	39
<i>Nour Elhouda Maria Chellil, and Sabah Chermat: Assessment of climate change impact on temperature and rainfall trend in the Setifian High Plains of Algeria.....</i>	53
<i>Ana Milanović Pešić, Dejana Jakovljević, Vesna Rajčević, and Slobodan Gnjato: Assessment of hydroclimatic trends in southeast Europe – Examples from two adjacent countries (Bosnia & Herzegovina and Serbia)</i>	69
<i>Aslı Ulke Keskin, Gurkan Kır, and Utku Zeybekoğlu: Clustering of the Black Sea Region meteorological stations of Türkiye with fuzzy c-means, k-means, and silhouette index analysis methods by precipitation, temperature and wind speed</i>	89

IDŐJÁRÁS

Quarterly Journal of the HungaroMet Hungarian Meteorological Service

Editor-in-Chief
LÁSZLÓ BOZÓ

Executive Editor
KRISZTINA LABANCZ

EDITORIAL BOARD

ANTAL, E. (Budapest, Hungary)	MIKA, J. (Budapest, Hungary)
BARTHOLY, J. (Budapest, Hungary)	MERSICH, I. (Budapest, Hungary)
BATCHVAROVA, E. (Sofia, Bulgaria)	MÖLLER, D. (Berlin, Germany)
CZELNAI, R. (Dörgicse, Hungary)	PINTO, J. (Res. Triangle Park, NC, U.S.A.)
FERENCZI, Z. (Budapest, Hungary)	PRÁGER, T. (Budapest, Hungary)
GERESDI, I. (Pécs, Hungary)	PROBÁLD, F. (Budapest, Hungary)
HASZPRA, L. (Budapest, Hungary)	RADNÓTI, G. (Surány, Hungary)
HORVÁTH, Á. (Siófok, Hungary)	S. BURÁNSZKI, M. (Budapest, Hungary)
HORVÁTH, L. (Budapest, Hungary)	SZEIDL, L. (Budapest, Hungary)
HUNKÁR, M. (Keszthely, Hungary)	SZUNYOGH, I. (College Station, TX, U.S.A.)
LASZLO, I. (Camp Springs, MD, U.S.A.)	TAR, K. (Debrecen, Hungary)
MAJOR, G. (Budapest, Hungary)	TOTH, Z. (Camp Springs, MD, U.S.A.)
MÉSZÁROS, E. (Veszprém, Hungary)	VALI, G. (Laramie, WY, U.S.A.)
MÉSZÁROS, R. (Budapest, Hungary)	WEIDINGER, T. (Budapest, Hungary)

Editorial Office: Kitaibel P.u. 1, H-1024 Budapest, Hungary
P.O. Box 38, H-1525 Budapest, Hungary
E-mail: journal.idojaras@met.hu

**Indexed and abstracted in Science Citation Index Expanded™ and
Journal Citation Reports/Science Edition**
Covered in the abstract and citation database SCOPUS®
Included in EBSCO's database

Subscription by mail:
IDŐJÁRÁS, P.O. Box 38, H-1525 Budapest, Hungary
E-mail: journal.idojaras@met.hu

IDŐJÁRÁS

*Quarterly Journal of the HungaroMet Hungarian Meteorological Service
Vol. 129, No. 1, January – March, 2025, pp.1–14*

Comparison of horizontal visibility observed by present weather sensor and human eye-based method and evaluated from ceilometer's vertical backscattering profile over two Hungarian meteorological stations

András Peterka*, Gabriella Schmeller, Noémi Sarkadi, and István Geresdi

*Institute of Geography and Earth Sciences
Faculty of Sciences
University of Pécs
Ifjúság útja 6., H-7624 Pécs, Hungary*

** Correspondening Author E-mail: peterka.andras@gmail.com*

(Manuscript received in final form February 1, 2024)

Abstract— This research aims to evaluate a quantitative comparison of the visibilities detected by three different methods: (i) human eye-based observations; (ii) calculated from the measured values of forward scatter visibility sensor; and (iii) evaluated from ceilometer's vertical backscattering profiles. Visibility data observed at two meteorological stations, Pestszentlőrinc and Szeged (Hungary) were analyzed. The paper focuses on the fog events observed during the periods of October-December in 2019 and November 21-24 in 2020. The results reveal that the visibility observed by the three methods can be significantly different. Comparison of the values of visibility detected by the three different techniques shows, that visibility evaluated from the ceilometer data is the largest, and the human eye-based observation detects the smallest values. Analysis of the data about fog detection (yes or no) reveals that the ceilometer detects significantly shorter duration of the fog than the other two methods.

Key-words: visibility, ceilometer, fog, present weather sensor, human-eye based observation

1. Introduction

Visibility has a direct and indirect effect on our everyday life. It significantly influences the safety of transport (road traffic, aviation, shipping, etc.) (Wang *et al.*, 2017; Shepard, 1996) and human health (Hameed *et al.*, 2000) as well. Visibility is impacted by meteorological parameters, e.g., relative humidity, temperature, and wind speed (Zhao *et al.*, 2013). Thus, through measurement of visibility, conclusions may be derived for the atmospheric circumstances.

Visibility is usually observed by human-eye observation or sensors that are based on different optical principles, e.g., light transmission, and forward scattering (transmissometers and forward scatter sensors) (Chan, 2016). Because visibility depends on the backscattering of light, it can be determined by a ceilometer (Taillade *et al.*, 2008; Czarnecki *et al.*, 2014).

Kim (2018) compared the visibility values detected by human eye-based, image-based, and optical-based methods. While the human eye-based and optical-based measurements were performed at the Seoul Meteorological Observatory, the image-based measurements occurred about 3 km northwest of the observatory. The author asserted that the calculated image-based visual range agreed better with the human eye-based visual range than that detected by the optical-based meteorological optical range (hereafter MOR) sensor. Cheng *et al.* (2018) emphasized that the worldwide used optical measurement techniques had several limitations, thus alternative methods for determining atmospheric visibility are needed. The authors implemented a novel algorithm to test the accuracy of visibility data measured by a vision-based method (video surveillance cameras). They concluded that the “variation approach provides an effective and efficient framework for real-time atmospheric visibility estimation” (Cheng *et al.*, 2018). Wang *et al.* (2014) suggested a new Digital Photography Visiometer System (DPVS) for automatic visibility determination which operates in the same way as the human eye-based method (hereafter HEM) and could replace them in any kind of weather conditions. They compared the data detected by DPVS with a forward scattering visibility instrument (FD12), and manual observations in heavy rainfall, even- and uneven rainfall, non-rainy and foggy conditions. They concluded that during heavy rainfall events, visibility is negatively correlated to the intensity of the precipitation. During even- and uneven rainfall events, the visibility values detected by manual observation and DPVS agreed well. However, the visibility detected by the forward scatter meter was smaller, and the variability of its values was significantly larger. In the case of non-rainy (or clear) conditions, the visibility values detected by each of the three methods agreed well. In foggy conditions, the bias between the values was small. They found that comparing values detected by the forward scatter meter and DPVS to that observed by the HEM during e.g., rainy conditions, the DPVS gives more accurate visibility values, while the forward scatter meter seems to be less accurate.

As ceilometers can be operated during any kind of weather conditions and both daytime and nighttime, these devices give continuous information about the vertical profile of the atmosphere. Based on these properties, ceilometers can be efficiently used as tools for automated mixing height measurements, for the estimation of in situ PM₁₀ concentrations (Münkel *et al.*, 2006), surface PM_{2.5} concentrations even during cloudy and nighttime conditions (Li *et al.*, 2017), and also for the monitoring of diurnal, seasonal, and vertical changes of aerosol layers (Muñoz *et al.*, 2012). Furthermore, ceilometers have been implemented in the fog alert systems (Haeffelin *et al.*, 2016) and in skyglow simulations (Kolláth *et al.*, 2020).

Continuously working ceilometer CHM15k systems are already deployed over 11 places in Hungary. Integrating them to the current visibility measuring systems does not require further investment, and it would spatially improve the availability of visibility data. Utilizing them to evaluate visibility would fit in the global trend to rely more on automated systems over human observers.

Molnar *et al.* (2008) elaborated the spatial distribution of visibility observed in 1996 and 2002 in Hungary. They found that the annual average visibility was 4 km larger in 2002 than in 1996. The regional variability is ambiguous: while in the northern and western parts of the country the increase of visibility was larger than the average, in the central region (mainly the Great Hungarian Plain) the increase of the visibility was smaller. This difference stems from that fact that while in the northern and western parts of the country the visibility reduction is the consequence of the industrial emission, in the Great Hungarian Plain the dust particles emitted from the sandy soil reduces the visibility. The reduction of the industrial emission at the end of the last century must have resulted in significant increase of the visibility.

In this study, horizontal visibility was calculated from ceilometer data based on the Koschmieder formula and the Klett-Fernald algorithm. This visibility data was compared with that observed by the human eye and present weather-visibility sensors. Data observed during 39 foggy events (when the visibility detected by any of the methods is less than 1000 m) occurred at two locations were analyzed to characterize the differences between the three methodologies. Furthermore, 2 cases were chosen to make a more detailed analysis. Section 2 describes the visibility measurement methods, the calculation from ceilometer data, and the selected cases. Section 3 presents the results, and summary of the paper is given in Section 4.

2. Data and methods

The Hungarian Meteorological Service (hereafter HungaroMet) operates the national meteorological measurement network. In this network, regular human eye-based visibility observations are carried out at 14 meteorological stations and

3 air force bases. Trained observers estimate the horizontal visibility values based on the regulations of the WMO (WMO, 2021). The observation methods in these stations are either human eye-based or remote sensing including the data of forward scatter meters, disdrometers, and/or sky cameras installed at the stations.

Few stations (including the Marczell György Main Observatory in Budapest and the Upper Air Observatory in Szeged) are equipped with the PWD22 (Vaisala, Finland) Present Weather Detector and Visibility Sensor (henceforth: PWVS) which is designed to observe the horizontal visibility within a range from 10 to 20,000 meters. The device operates by the right of the forward scatter principle. Both the emitter and receiver units are tilted down at a 45° angle. The scattering of emitted light depends on its wavelength and the size of the drops. The intensity of the forward scattered light is proportional to the number concentration of the particles. Because the droplet size in the fog is significantly smaller than the size of the precipitating hydrometeors, this instrument can distinguish the fog from the falling precipitation (and even more types of precipitation can be determined, such as snow or freezing rain). Besides visibility and precipitation type, the intensity of precipitation is also measured.

CHM15k Nimbus ceilometers (Lufft, Germany) are installed at four meteorological stations in the Hungaromet network: Marczell György Main Observatory in Pestszentlőrinc, Upper Air Observatory in Szeged, Storm Warning Observatory in Siófok, and the meteorological station at the University of Pécs. The wavelength of the radiation emitted by the CHM15k Nimbus ceilometers is 1.064 μm (User Manual CHM 15k.).

In this study visibility values retrieved by three different methods are compared: 1) human eye-based observations, 2) visibility values from forward scatter visibility sensor (PWVS), and 3) visibility values calculated from the backscatter profile of ceilometer measurements. To the authors' knowledge, the observers can utilize data from sky cameras or PWVS in the HEM. Therefore, HEM and PWVS may not be independent.

Due to the low number of ceilometers in the network, visibility data observed at two Hungarian meteorological stations (Pestszentlőrinc and Szeged) were selected for comparison. At these two stations, the selected optical-based sensors and regular human eye-based visibility observations are available.

The vertical profile of the backscattered energy assessed by a ceilometer was used to evaluate the visibility. The evaluation of visibility based on the Koschmieder formula (*Larson and Cass, 1989*):

$$VIS = \frac{-\ln 0.02}{\sigma_{ext}}, \quad (1)$$

where σ_{ext} is the extinction coefficient. The vertical profile of the extinction coefficient and the mean extinction coefficient of the column at a given time were evaluated by the Klett-Fernald algorithm (*Werner et al., 2006; 28902-1:2012 ISO*

standard) implemented in MATLAB R2020b. For this evaluation, the following conditions were set:

1. Due to the attenuation of the beam, ceilometers cannot detect the upper part of the fog (Nowak *et al.*, 2008). Therefore, negative backscatter values can appear. These values cannot be incorporated into the calculations, thus they are treated as NaN.
2. If the sky condition index of the ceilometer indicates fog, but the column contains less than 10 non-NaN values due to the attenuation of the beam, that indicates a rather dense fog. In those cases the mean of the extinction coefficient for the column is set to 0.03

We hypothesize that the fog is isotropic in the surroundings of the ceilometer, thus the backscattered energy detected vertically (calculated from the backscatter profile) equals to the horizontal one (note that data near to the surface in the so-called blind range are not available, this may also cause error in visibility detection). Please note that while the condition of the isotropic surroundings is often met, currently we cannot distinguish those cases where it fails. If the surrounding area was not isotropic, the evaluated visibility would not be correct.

Fog events detected in October-December 2019 and November 2020 were selected for comparison. Data observed on total of 20 days at Budapest (Marcell György Main Observatory in Pestszentlőrinc), and at Szeged (Upper Air Observatory) were analyzed. Furthermore, a well-observed radiation fog event on November 24, 2020 (Gandhi *et al.*, 2023) was chosen for a case study (Table 1).

Table 1. Days selected for data evaluation. The data observed on the day highlighted with bold letters are chosen for case study.

	Pestszentlőrinc	Szeged
October 2019	-	10 / 26
November 2019	04 / 05 / 07 / 08 / 09 / 27 / 28 / 29	04 / 05 / 08 / 09 / 15 / 25 / 29
December 2019	04 / 05 / 07 / 08 / 09 / 12 / 13 / 16 / 19 / 21	03 / 05 / 06 / 07 / 08 / 09 / 10
November 2020	23 / 24	21 / 22 / 23 / 24
Total	20	20

The visibility values evaluated from the ceilometer backscattering profile and the PWVS visibility data have a 1-minute temporal resolution. However, the frequency of human eye-based observations is only 1 hour. For the comparison of the data, 15-minute averages were created from the 1-minute data set, and the 1-hour dataset was divided into sections with a duration of 15 minutes. That means there are 1920 elements of the dataset observed at Budapest station, and there are 1920 elements of the dataset observed at Szeged station.

The difference between the visibility values derived from different methods is quantified by plotting histograms and by evaluation of contingency tables. The

histograms reveal the frequency of the relative difference x between the visibilities evaluated by the two different methods:

$$x = \frac{h1-h2}{(h1+h2)/2}, \quad (2)$$

where $h1$ and $h2$ are the visibilities evaluated by method 1 and method 2, respectively. The histogram was normalized, the height of a bar was calculated by the following formula:

$$y = \frac{n}{w*N}, \quad (3)$$

where n is the count of the bin, w is the width of the bin, and N is the total count. The bin's width of the histogram is 0.25. The data for the evaluation of the histogram were involved if any of the two methods detected fog. The differences are plotted for the following pairs of methods: (a) PWVS – Ceilometer, (b) PWVS - HEM, and (c) HEM - Ceilometer.

The reliability of simple fog detection (yes or no) is also an important characteristic of the fog detection methods. For the comparison of the fog detection, contingency tables were prepared using visibility data evaluated for intervals of 15 minutes. Based on the contingency table, the frequencies of fog detection by the different methods are compared. The critical success index (hereafter *CSI*) and *bias* were evaluated:

$$CSI = a/(a + b + c), \quad (4)$$

$$bias = (a + b)/(a + c), \quad (5)$$

where a is the number of hits (top left corner of the contingency table), b is the number of misses (top right corner of the contingency table), and c is the number of false alarms (bottom left corner of the contingency table).

3. Results and discussion

3.1. Comparison of PWVS and ceilometer

Histograms in *Fig.1* reveal the differences between the visibilities detected by different methods. The frequency of the relative differences (see Eq.(2)) for the comparison of the PWVS and ceilometer at the Budapest and Szeged stations are plotted in the first row in panels (a1) and (a2), respectively. In the case of Budapest (panel a1), the relative differences of the measured visibility vary between -0.50 and 1.25 and show a right-skewed pattern. That means that in most of the cases (the total number of cases, when any of the two methods detected fog,

is 358), the visibility evaluated from ceilometer data is significantly larger than that of observed by PWVS (274 from 358), and the visibility observed by PWVS is larger only about in one-third of the cases (83 from 358). The highest frequency of the relative difference for the visibility is between -1.25 and -0.50. However, there is a significantly smaller second mode, at about a relative difference of 0.75. The standard deviation (hereafter STD) of the dataset is 0.67. Data from Szeged (panel a2) show a similarly right-skewed pattern. However, the distribution is wider, indicated by a larger STD of 0.84 (panel a2). The relative difference of visibility varies between -2.00 and 1.50, and a large relative difference can be observed in a wider range, between -1.75 and -0.50. Similarly, to the Budapest data, there is a significantly smaller second mode at the positive values of the relative difference, at around 1.25.

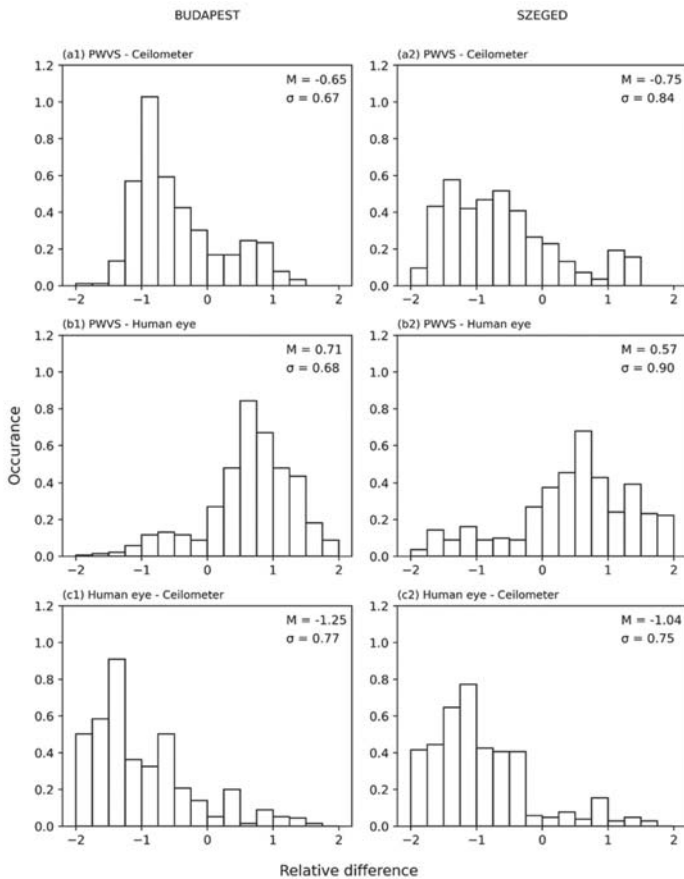


Fig. 1. Relative differences in the 15-minute average visibility values during fog on histograms in Budapest (1) and Szeged (2). (a) differences between PWVS and ceilometer, (b) differences between PWVS and HEM, and (c) differences between HEM and ceilometer. M is the median and σ is the standard deviation.

Fig.2 also shows that both in Budapest (panel a) and Szeged (panel b) there is only a limited number of cases when the ceilometer detected fog, while PWVS did not. The scatter plots in Fig.2 allow us to conclude that there is no correlation between the visibility values evaluated by the two different methods. Scatter plots were created for the other two method pairs, however, valuable information cannot be derived from them.

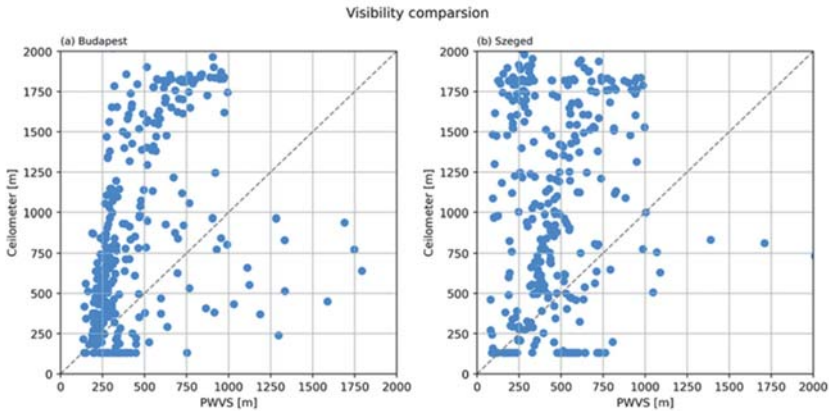


Fig. 2. Relation between visibilities, evaluated from PWVS (x-axis) and ceilometer (y-axis) data at Budapest (panel a) and Szeged (panel b). Gray dashed lines denote the one-to-one relation.

3.2. Comparison of PWVS and HEM

Fig.1 panels b1 and b2 show the comparison of the visibilities detected by PWVS and HEM in Budapest and Szeged, respectively. In Budapest, the data shows a single modal left-skewed distribution, where the relative differences vary between -1.25 and 2.00. The highest value of the peak is between 0.50 and 0.75, while most of the data points spawn between 0 and 1.50. A significantly smaller mode is around -0.75 – -0.50, which is the consequence of a limited number of cases (35) when the PWVS detected fog, while the HEM did not (Table 2, panel b). In Szeged data, there is a single modal left-skewed distribution. Compared to Budapest, the single peak is smaller, but it can be found in the same bin between 0.50 and 0.75. The range where most of the data points can be found is wider spanning between -0.25 and 2.00. The wider distribution is also shown by the larger STD (0.90 compared to 0.68). Panel b of Table 2 shows that the number of cases when HEM detected visibility and PWVS did not is higher than vice versa. However, the difference is less compared to the PWVS-ceilometer comparison. Both the Szeged and Budapest datasets show that the visibility values observed by HEM is significantly smaller than the visibility detected by PWVS.

Table 2. Contingency tables comparing the different methods based on whether fog was detected or not in Budapest (first value) and Szeged (second value). (a) PWVS and ceilometer, (b) PWVS and HEM, and (c) HEM, and ceilometer.

(a) PWVS \ Ceilo	Detected	Not detected	Total
Detected	224 161	120 168	344 329
Not Detected	14 4	1562 1587	1576 1591
Total	238 165	1682 1755	1920 1920

(b) PWVS \ HEM	Detected	Not detected	Total
Detected	309 281	35 48	344 329
Not Detected	111 87	1465 1504	1576 1591
Total	420 368	1500 155	1920 1920

(c) HEM \ Ceilo.	Detected	Not detected	Total
Detected	220 151	200 217	420 368
Not Detected	18 14	1482 1538	1500 1552
Total	238 165	1682 1755	1920 1920

3.3. Comparison of HEM and ceilometer

Panels c of Fig. 1 show the differences in visibility between HEM and ceilometer in Budapest and Szeged. The data from Budapest show a single modal right-skewed distribution, where the highest frequency is between -1.25 and -1.50, while most of the data can be found in the range of -2.00 – 0.50. From the peak to the end of the tail of the distribution, the height of the bins is gradually decreasing, compared to Szeged, where the transition from the peak to the tail is rather sudden. The highest frequency in the Szeged dataset is between -1.50 and -1.00, while most of the values spawn in the range of -2.00 – -0.25. The sudden decrease in the transition from the peak to the tail occurs at -0.25, where the frequency drops from 0.4 to less than 0.1. The STD of the data sets are also similar (0.77 and 0.75). Panel c of Table 2 shows that HEM detected more cases than ceilometer at those times when just one of the methods detected fog. To conclude, the visibility values observed by HEM were lower than those by the ceilometer.

A 2×2 contingency table (Table 2) were prepared to evaluate skill scores for the fog detection. In this analysis, only the data about the fog detection (yes or no) are compared. PWVS detected 344 and 329 foggy time intervals in Budapest and

Szeged, respectively. HEM detected 420 and 368 foggy time intervals in Budapest and Szeged, respectively. Ceilometer detected 238 and 165 foggy time intervals in Budapest and Szeged, respectively. This means that fog was detected for the longest duration by HEM followed by PWVS and ceilometer at both stations. Accordingly, the method pair with the highest number of cases, where both methods detected fog is the PWVS - HEM (309 / 281), followed by the PWVS - ceilometer (224 / 161), and lastly the HEM - ceilometer (220 / 151). *Table 3* shows accuracy attributes of the contingency tables. The trend of the CSI values also follows the previous order. The largest is the PWVS – HEM (0.68 / 0.68), followed by the PWVS - ceilometer (0.63 | 0.48), and the smallest is the HEM – ceilometer (0.50 / 0.40). To conclude, during fog, the observed visibility values differ for the three methods. Calculated visibility from the ceilometer is usually higher than that of from PWVS and HEM, and visibility observed by HEM is usually the lowest. In most cases, the trend of the difference (whether the difference is negative or positive) between the two methods is well defined. This can be also shown by the bias. values (*Table 3*), where the weakest is the PWVS – HEM (0.82 | 0.89). However, the exact reason of the difference is unknown.

Table 3. CSI and bias of the three compared method pairs.

Budapest Szeged	PWVS – Ceilo.	PWVS - HEM	HEM - Ceilo
CSI	0.63 0.48	0.68 0.68	0.50 0.40
bias	1.45 1.99	0.82 0.89	1.76 2.23

3.4. Case study

On November 24, 2020, a radiation fog formed throughout the Carpathian Basin in the early hours and lasted even until late night in some regions of the country.

Fig.3 shows the time evolution of the visibility detected by the 3 different methods in Budapest (panel a) and Szeged (panel b). In Budapest, the fog formation was detected at 03:00 UTC by all the three methods. However, in the case of the ceilometer, the visibility starts to rise at ~14:00 UTC and reaches 1000 m by 15:00 UTC. Until 19:00 UTC it remains close to 1000 m, and after this time it indicates the dissipation of the fog due to the rising of the visibility to 2000 m. The other two methods detected fog dissipation later, at about 22:00 UTC. However, each of the three methods detected fog between 03:00 UTC and 19:00 UTC, the discrepancy for the fog detection occurs in a shorter time interval of 3 hours. Note, that shortly after the fog formed (after 06:00 UTC), when the visibility must have been the smallest, the ceilometer and HEM data agree well. Both methods detected visibility as small as 100 m between 08:00 and 09:00 UTC. Later the visibility detected by the PWVS and HEM agree well, and

the values evaluated from ceilometer data may overestimate the visibility. In the dissipation phase (14:00 UTC–21:00 UTC) the largest difference between the visibility detected by the ceilometer and HEM has a maximum value of 900 m at ~17:50 UTC. However, the trends of visibility evaluated by the three methods are similar. The sudden and significant rise of the visibility in the case of the ceilometer may indicate that using this method for visibility detection is not reasonable in cloudy or clear sky conditions.

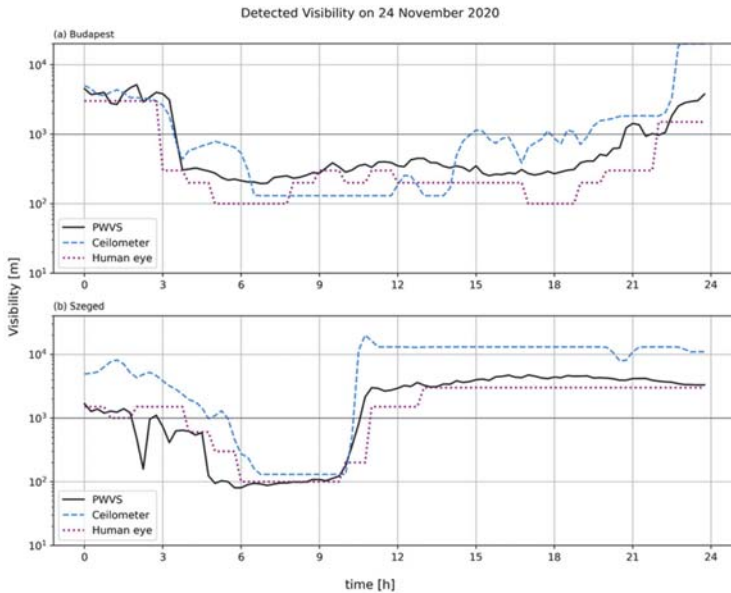


Fig. 3. Time evolution of visibility measured by PWS (solid black line), ceilometer (dashed blue line), and HEM (dotted purple line) in Budapest (a) and Szeged (b).

In Szeged (panel b), the three methods do not agree well in the time period of fog formation, which occurs between 02:00 UTC and 05:00 UTC, while values detected by HEM and PWVS are relatively close to each other during this period. The visibility evaluated from ceilometer data is significantly larger, it decreases from 5000 - 6000 m to 1000 m by 2–3 hours later than the other two methods. However, the coincidence is better in the dissipation period, which occurred at around 10:00 UTC. During the fog (06:00 UTC–10:00 UTC), the visibility evaluated by three methods agree well. Both the ceilometer and the two other methods detect dense fog with visibility of about 150 m and about 100 m, respectively. After the dissipation phase, the visibility values from PWVS and HEM are close to each other, compared to that of from ceilometer, as the later is

constantly between 10,000–20,000 m, while the first varies between 3000–4000 m. This also indicates, that using of the ceilometer for the visibility evaluation is reasonable only in foggy weather and it is not reasonable in the case of the elevated fog or any other cloudy conditions.

4. Conclusion

In this research, horizontal visibility was evaluated from the vertical backscattering profile of the ceilometer, calculated with the Koschmieder formula and the Klett-Fernald algorithm. Visibility values evaluated from the ceilometer data were quantitatively compared to visibility data observed by PWVS and HEM.

Statistical analysis of the visibility data detected during foggy events in Budapest and Szeged station reveals: (i) Considering the fog detection (yes or no), best agreement was found between the PWVS and HEM methods (the CSI index is about 0.67). The largest discrepancy was found between the HEM and ceilometer method (the CSI index is about 0.50). That is these two methods give different results for the occurrence of the fog in about 50% of the data. (ii) Visibility values evaluated by the three variant methods can be significantly different. Statistical analysis of the relative differences reveals that the ceilometer gives the highest visibility values, followed by PWVS and HEM. (iii) The statistical analysis of the relative difference for the visibility and that of the contingency table for the fog detection disclose that the remote sensing technique of PWVS gives a better coincidence with the HEM than the ceilometer does. (iv) The results of the case study suggest that the three methods evaluate similar visibility in dense fog events, and even though the visibility values are different, the temporal trends are similar.

The authors hypothesize that the discrepancy between the different methods is the consequence of the different detection techniques. In the case of the ceilometer, it is supposed that the fog is homogeneous around the sensor. If the structure of the fog is not the same in horizontal and vertical directions, the visibilities that characterize the two directions can be different. While the sampling volume is a few m³ in the case of the ceilometer, the PWVS has a rather small detection volume (few cm³) which can result in differences between the two methods if the fog is inhomogeneous (e.g., large variability in the droplet concentration and/or droplet size).

Acknowledgements: This research was supported by GINOP-2.3.2-15-2016-00055 financed by the Ministry of Finance.

References

- Chan, P.W., 2016: A test of visibility sensors at Hong Kong International Airport. *Weather* 71, 241–246. <https://doi.org/10.1002/wea.2772>
- Cheng, X., Yang, B., Liu, G., Olofsson, T., and Li, H., 2018: A variational approach to atmospheric visibility estimation in the weather of fog and haze. *Sust. Cities Soc.* 39, 215–224. <https://doi.org/10.1016/j.scs.2018.02.001>
- Czarnecki, T., Perlicki, K., and Wilczewski, G., 2014: Atmospheric visibility sensor based on backscattering using correlation coding method. *Opt. Quantum Electr.* 47, 771–778. <https://doi.org/10.1007/s11082-014-9951-x>
- Gandhi et al, 2023: Fog Experiment in Budapest (2020–21). Micrometeorological measurements during foggy situations (submitted into Pure and Applied Geophysics)
- Haefelin, M., Laffineur, Q., Bravo-Aranda, J.-A., Drouin, M.A., Casquero-Vera, J.-A., Dupont, J.-C., and De Backer, H., 2016: Radiation fog formation alerts using attenuated backscatter power from automatic lidars and ceilometers. *Atmos. Measur. Tech.* 9, 5347–5365. <https://doi.org/10.5194/amt-9-5347-2016>
- Hameed, S., Mirza, M.I., Ghauri, B.M., Siddiqui, Z.R., Javed, R., Khan, A.R., Rattigan, O.V., Qureshi, S., and Husain, L., 2000: On the widespread winter fog in northeastern Pakistan and India. *Geophysical Research Letters*, 27, 1891–1894. <https://doi.org/10.1029/1999gl011020>
- Kim, K.W., 2018: The comparison of visibility measurement between image-based visual range, human eye-based visual range, and meteorological optical range. *Atmos. Environ.* 190, 74–86. <https://doi.org/10.1016/j.atmosenv.2018.07.020>
- Kolláth, K. and Kolláth, Z., 2020: On the feasibility of using ceilometer backscatter profile as input data for skyglow simulation. *J. Quantitativ. Spectros. Radiative Trans.* 253, 107158. <https://doi.org/10.1016/j.jqsrt.2020.107158>
- Larson, S.M. and Cass, G.R., 1989: Characteristics of summer midday low-visibility events in the Los Angeles area. *Environ. Sci. amp; Technol.* 23, 281–289. <https://doi.org/10.1021/es00180a003>
- Li, S., Joseph, E., Min, Q., Yin, B., Sakai, R., Payne, M.K., 2017: Remote sensing of PM2.5 during cloudy and nighttime periods using ceilometer backscatter. *Atmos. Measur. Techn.* 10, 2093–2104. <https://doi.org/10.5194/amt-10-2093-2017>
- Molnar, A., Meszaros, E., Imre, K., and Rull, A., 2008: Trends in visibility over Hungary between 1996 and 2002. *Atmos. Environ.* 42, 2621–2629. <https://doi.org/10.1016/j.atmosenv.2007.05.012>
- Münkel, C., Eresmaa, N., Räsänen, J., and Karppinen, A., 2006: Retrieval of mixing height and dust concentration with lidar ceilometer. *Bound.-Lay. Meteorol.* 124, 117–128. <https://doi.org/10.1007/s10546-006-9103-3>
- Muñoz, R.C. and Alcañal, R.I., 2012: Variability of urban aerosols over Santiago, Chile: Comparison of surface PM10 concentrations and remote sensing with ceilometer and lidar. *Aerosol Air Qual. Res.* 12, 8–19. <https://doi.org/10.4209/aaqr.2011.08.0133>
- Nowak, D., Ruffieux, D., Agnew, J.L., and Vuilleumier, L., 2008: Detection of fog and low cloud boundaries with ground-based remote sensing systems. *J. Atmos. Ocean. Technol.* 25, 1357–1368. <https://doi.org/10.1175/2007jtecha950.1>
- Shepard, F.D., 1996: Reduced visibility due to fog on the highway. Transportation Research Board.
- Taillade, F., Belin, E., and Dumont, E., 2008: An analytical model for backscattered luminance in fog: Comparisons with Monte Carlo computations and experimental results. *Measur. Sci. Technol.* 19, 055302. <https://doi.org/10.1088/0957-0233/19/5/055302>
- Wang, J., Liu, X., Yang, X., Lei, M., Ruan, S., Nie, K., Miao, Y., and Liu, J., 2014: Development and evaluation of a new digital photography visiometer system for automated visibility observation. *Atmos. Environ.* 87, 19–25. <https://doi.org/10.1016/j.atmosenv.2013.12.045>
- Wang, R., Gong, J., Wang, Y., Chen, H., Chen, S., and Wang, Q., 2017: Relationship between gross domestic product and accident in china. *J. Safety Stud.* 3, 19. <https://doi.org/10.5296/jss.v3i1.10571>

- Wang, X., Chen, J., Cheng, T., Zhang, R., and Wang, Xinming, 2014: Particle number concentration, size distribution and chemical composition during haze and photochemical smog episodes in Shanghai. *J. Environ. Sci.* 26, 1894–1902. <https://doi.org/10.1016/j.jes.2014.07.003>
- Werner, C., Streicher, J., Leike, I., and Münkler, C., 2006: Visibility and Cloud Lidar, In: Lidar: Range-Resolved Optical Remote Sensing of the Atmosphere. Springer Science & Business, 165–186.
- Zhao, H., Che, H., Zhang, X., Ma, Y., Wang, Yangfeng, Wang, H., and Wang, Yaqiang, 2013: Characteristics of visibility and particulate matter (PM) in an urban area of Northeast China. *Atmos. Pollut. Res.* 4, 427–434. <https://doi.org/10.5094/apr.2013.049>

IDŐJÁRÁS

*Quarterly Journal of the HungaroMet Hungarian Meteorological Service
Vol. 129, No. 1, January – March, 2025, pp. 15–37*

Temporal and spatial analysis of lightning density in Türkiye

**İhsan Çiçek^{1,*}, Necla Türkoğlu¹, Zerrin Demirörs², Edanur Gözet³,
Batuhan Ateş Yılmaz³, and İlker Alan²**

¹*Ankara University, Faculty of Letters, Department of Geography*

²*Türkiye State Meteorological Service*

³*Türkiye State Meteorological Service, 11th Regional Directorate*

**Corresponding Author E-mail: ihsan.cicek@ankara.edu.tr*

(Manuscript received in final form June 25, 2024)

Abstract— In this study, a temporal analysis of lightning density was performed on lightning data obtained from the Türkiye State Meteorological Service (TSMS) for the period 2017–2021, with the analysis encompassing hourly, monthly, seasonal, and annual scales. ArcGIS version 10.4.1 was used. When the annual lightning density was evaluated by regions, the highest values were observed in the Inner Aegean, Marmara, Southwest Anatolia, Western Black Sea, and Eastern Anatolia Regions. The Central Anatolia Region has the lowest lightning density. Lightning density is also the highest in late spring, early summer when the ground temperature and, thus, instability is highest. May and June were determined to have the highest lightning density, whereas December, January, and February had the lowest lightning density. Considering lightning activity hourly, the highest number of lightning strikes occurred at noon, while the lowest number occurred at night and during the morning hours. Upon examining the relationship of lightning with latitude and longitude values, it was concluded that the relationship with latitude values was more significant and positive. Lightning changes as a function of altitude: it increases between 30-150 m and 500-1000 m, while it decreases between 150-500 m and above 1000 m.

Key-words: lightning analysis, lightning density, lightning detection network (LINET), convective storms, thunderstorms, Türkiye

1. Introduction

The electrical discharge resulting from ascending and descending air movements between the ground and the atmosphere is called lightning (*Ackerman and Knox, 2015*). Lightning can be defined as an electric spark of more than 1 km (*Dwyer and Uman, 2013*). Lightning usually occurs as an intercloud (IC), cloud-to-cloud (CC), or cloud-to-ground (CG) phenomenon (*Uman, 1986; K ıçeci and Salamcı 2020*). The cloud-to-cloud lightning event occurs more often than the lightning striking the ground (*Holle and Cooper, 2016*). Positively charged ice crystals gather at the top of the cloud, and negative charges gather at the bottom of the cloud. Lightning is caused by the electric current between positively and negatively charged regions. If electric charges inside clouds are dense enough, they create electric fields that can ionize the air and produce electric sparks that can develop into lightning flashes (*Rupke, 2002; Ackerman and Knox, 2015*).

Approximately 40–100 lightning strikes the Earth's surface every second (*Tinmaker et al., 2019*). Lightning flashes originate especially from cumulonimbus (Cb) clouds (*Rupke, 2002*). Cold air and a thick layer of moisture are needed at the upper levels for the formation of cumulonimbus (Cb) clouds. Cb clouds that cause thunderstorms, occur with the warming of the ground, orographic elevation, and dynamic elevation in frontal systems (*TSMS, 2022a*). Lightning and rainfall are associated with severe storms that can damage agriculture, power grids, property, and human life (*Tinmaker et al., 2017*). Atmospheric instability, sufficient moisture content, and a lifting mechanism to bring the moist air parcel to the level of free convection are the necessary elements for the development of lightning and thunderstorms (*Tinmaker et al., 2010;  ztopal, 2017*).

Lightning is affected by numerous meteorological variables and is very sensitive to changes in surface temperature. As it can be seen in the studies, there is a positive correlation between lightning activity and surface temperature (*Williams, 2005*). The temperature difference formed due to cold air masses on hot land surfaces increases instability and causes deep convection (*Galanaki et al., 2018*). Hence, lightning density on land is higher during the summer months and at noon and evening when the ground temperature is high (*Pinto and Pinto Jr., 2003; Holle and Cooper, 2016*).

Although the lightning event has generally been observed on land, it also occurs in seas, oceans, and coastal areas (*Turman and Edgar, 1982; Orville and Henderson, 1986*). Convection on land is deeper and stronger than convection in the sea, since the land surface warms faster than oceans and seas (*Tinmaker et al., 2019*). Lightning activity over the sea in autumn and winter periods is higher than that over the land, particularly at night (*Manzato et al., 2022*). The seas are colder in the spring than in the autumn. Therefore, stronger vertical atmospheric instability occurs in autumn (*Altaratz et al., 2003*). In the Mediterranean Sea,

September, when sea surface temperatures are the highest, is the period with the most intense lightning activity (*Rivas Soriano and de Pablo, 2002*).

There is a similarity between the spatial and temporal distribution of lightning and that of tornadoes. In the study conducted by *Bayraktar and Çiçek (2022)*, it was determined that 47% of all tornadoes in Türkiye were seen in the Mediterranean Region. In the Mediterranean and Aegean regions, they occur in late autumn and winter; in the Marmara and Black Sea regions, they occur in summer and early autumn; in the inner regions, they usually occur in spring, early summer, and late summer.

The lightning event is often accompanied by hail and heavy rains (*Herring et al., 2018; Williams and Guha, 2019*). Due to global warming, the amount of lightning has increased by 12% for every 1°C increase in temperature. In other words, there is a high correlation between the lightning displacement speed and the convective available potential energy (CAPE) value of precipitation. An unstable air mass is characterized by warm, moist air near the surface and cold, dry air aloft. In these conditions, if an air parcel is forced upward, it will continue to rise on its own. CAPE is a measure of atmospheric instability and is directly related to the maximum possible vertical velocity of the updraft. Thus, higher values of CAPE are associated with intense vertical speed and thunderstorm occurrence. Observed CAPE values during a storm often exceed 1000 J kg⁻¹ and in extreme cases may exceed 5000 J kg⁻¹. However, there are no CAPE thresholds that can be used to determine the thunderstorm occurrence (*Mazarakis et al., 2008; Ziv et al., 2009; Romps et al., 2014; Galanaki et al., 2015*). Sea surface temperature has a significant effect on precipitation (*Reason and Mulenga, 1999*). The increase in precipitation is associated with an increase in the advection of moisture carried from the seas (*Petersen and Rutledge, 1998*). The high temperature difference between cold air currents and warm sea surfaces leads to instability in the atmosphere. The water that evaporates from the warm sea surface forms convective clouds. These clouds can drop large amounts of precipitation in a short time. The terrestrial surface temperatures, sea surface temperatures, and severity of meteorological events increase the summer season (*Bozkurt and Göktürk, 2009*). Studies conducted with long-time data series of sea surface temperatures have proven that if sea surface temperatures increase by 1–2°C, there is an increase in the number of days of lightning events by 20–45 days, (*Yamamoto et al., 2016*). Although high sea surface temperature is not a sufficient factor for convective development, it supports synoptic conditions that may cause deep convection (*Kotroni and Lagouvardos, 2016*). In the studies conducted by *Yavuz et al. (2022)* on convective precipitation in the cold season from the Marmara Region, it was stated that atmospheric contents (such as atmospheric instability, a lifting mechanism, and high moisture content) similar to those of the warm season are required. Lower convective available potential energy (CAPE) values have been observed in winter thundersnows compared to summer convective thunderstorms.

Surface temperature is among the basic elements of climate and is affected by geographical location and landforms (Erol, 2011). This difference in temperature changes can be associated with latitude and altitude. Previous studies have obtained different results; examining the relationship between lightning density and latitude shows that lightning density is higher in the tropical regions (0° – 20° latitudes) than in the temperate regions (20° – 40° latitudes). Lightning density is lower at high latitudes (40° – 60°) (Mackerras and Darveniza, 1994). Considering lightning activity in the terrestrial areas of China, the areas where lightning is densest are located at latitudes of 20 – 30° N, and lightning activity decreases to the north (Xu et al., 2022).

The relationship between altitude and temperature is more significant than the relationship between latitude and temperature (Aydin and Karabulut, 2021). Numerous studies have detected a positive correlation between lightning density and orography. Mountain ranges are places with the highest lightning activity. In these regions, it has been revealed that the effect of topographic elevation, orographic forcing, and the heating of the ground as a result of solar radiation, increases convective activities (Rivas Soriano et al., 2001b; Galanaki et al., 2015; Kotroni and Lagouvardos, 2016; Saha et al., 2017; Xu et al., 2022). Lightning density in terrestrial and mountainous regions is considerably greater than in seas and coasts (Zipser and Lutz, 1994; Rivas Soriano et al., 2001a; Koutroulis et al., 2012; Galanaki et al., 2018). This difference is even greater in terms of convection initiation (CI). In studies performed in the Mediterranean, the areas with the densest lightning are mountainous areas (Montenegro's Dinaric Alps and the high mountains of the Balkans), whereas the areas where lightning is observed the least are arid and semi-arid areas (Galanaki et al., 2018; Xu et al., 2022). The Alps' location closer to the level of free convection (LFC) weakens convective inhibition (CIN) (Manzato et al., 2022). The smaller the CIN, the deeper the convection (Manzato et al., 2022; Kirshbaum et al., 2018). Mountains act as a barrier that provides an important orographic lift mechanism, increasing the transport of incoming air from the sea to the land. In addition, a stronger uplift of clouds near mountains leads to more developed cloud formations (Reynolds et al., 1957; Takahashi, 1984; Altaratz et al., 2003).

Mountains located at mid-latitudes are very sensitive to global warming due to the greenhouse effect (Rangwala and Miller, 2012). The warming rate is higher in areas with higher altitudes (Dhital et al., 2022). In studies carried out in the Mediterranean, June and July are the months with the highest lightning activity (Manzato et al., 2022). Concerning the lightning activity of China, whereas lightning density increased with altitude between 1000–2000 m, it decreased between 0–1000 m and above 2000 m altitude. Ninety percent of lightning activity occurred between May and September (Xu et al., 2022).

Since lightning bolts and flashes cause NO_x production and forest fires, resulting in significant climatic consequences over long-time scales (Pinto JR and Pinto, 2020). Lightning activity is expected to increase in the future (Williams and

Guha, 2019). In a warmer future scenario, there will be more water vapor in the atmosphere to release latent heat during condensation. On a global scale, extreme daily precipitation events are predicted to intensify by approximately 7% for every 1°C of global warming (IPCC, 2021). This leads to expectations of an increase in storm development and lightning flashes. Furthermore, lightning activity in the future will also depend on the vertical air temperature profile in the troposphere (Pinto JR et al, 2013). As Brooks (2013) noted, as climate changes, the magnitude of CAPE and shear is also changing. Given that different combinations of CAPE and shear favor the occurrence of different convective phenomena, therefore, this may provide insight into expected future changes in the distribution and nature of convective hazards. For example, if in the coming days both CAPE and shear increase, tornadoes and hailstorms will likely become more common. If low CAPE - high shear days are more frequent, the number of severe convective wind gust events may increase. Preliminary results from climate projections for Europe indicate that an increase in CAPE and a slight increase in shear is expected in the next 100 years. Because of this, the number of unstable, strongly sheared environments is projected to increase as well. As a result, thunderstorms capable of producing severe and extremely severe phenomena may become more frequent.

The objective of the present study is to conduct the temporal and spatial density analyses (simple density) of lightning and lightning flash events that took place between 2017 and 2021 in Türkiye. In this study, both meteorological parameters (ground temperature, moisture content influenced by the sea) and geographical features (latitude-longitude and altitude) were addressed in the spatial analysis of lightning density. Hourly, monthly, seasonal, and annual periods were evaluated in the temporal analysis of lightning density.

1.1. Lightning tracking systems

Lightning detection and tracking systems began to be used in the world in the 1980s. A lightning system is used in almost all European countries. Some of these are low-frequency (LF, 30–300 kHz), while others are very high-frequency (VHF, 30–300 MHz) systems (Anderson and Klugmann, 2014). The operating frequency range of the system, which began being used in Belgium in 1992, is very high (VHF, 30–300 MHz). The Lightning Detection Network (LINET) system used in Germany performs detection in the 5–100 kHz range, which is very low and low (VLF/LF) frequencies. The Worldwide Lightning Location Network (WWLLN) tracking system is used in the United States. ZEUS detection system is located in Greece, which works in the low frequency range (VLF, 7–15 kHz) (Öztopal, 2017). Lightning detection systems can even monitor lightning events on a global scale. Thus, a reliable lightning database can be created (Lay et al., 2007).

1.2. The lightning detection and tracking system in Türkiye

The lightning detection and tracking system is a remote sensing system that provides meteorological information to detect flash events and make short-term weather forecasts. The lightning detection and tracking system determines the location, type, current intensity, and current direction of lightning. There was a total of 41 passive sensor systems of the lightning detection network LINET installed in Türkiye in 2014, one of which is located in the Turkish Republic of Northern Cyprus. LINET represents a ground-based lightning detection system. LINET sensors consist of electric field sensors and central processing units. The LINET field processor receives signals from the LINET field antenna and the GPS antenna and transmits them to the central processing units. The LINET field antenna is sensitive to electromagnetic waves emitted from lightning. It operates in the VLF range of about 5–100 kHz. The GPS antenna receives signals from GPS satellites (TSMS, 2022a). With this system, it is possible to detect the location, current intensity, and current direction of lightning (from cloud to ground or ground to cloud electrical activity) with an accuracy of 200 m.

3.6. Study area and data

The region between 26–45E and 35–43N, where Türkiye is located, was taken as the study area (Fig. 1). A data set from 2017 to 2021 of the LINET system described in the previous section was used as study data. This data includes the date and time of the lightning, the latitude and longitude of the place where it occurred, the type of events (IC, CC, or CG), and the event's intensity. In the following study sections, all events will be described as lightning, without distinction.



Fig. 1. The Lightning Detection and Tracking System station information

2. Materials and methods

The data utilized in the present study were provided by the Türkiye State Meteorological Service (TSMS). The acquired data cover only cover the time during which events occurred in 2017–2021. Spatially, it involves the latitude and longitude information of the places where the events took place. The coordinate and time information of lightning events was transferred from an MS Excel file to the GIS environment. ArcGIS version 10.4.1 was used as GIS software. The data transferred to the GIS environment was made ready for use in temporal and spatial analysis by creating databases in ArcGIS. The month, day, and time of events were used in the temporal analysis of lightning events, and latitude and longitude information was used in spatial analysis. To conduct spatial density analysis, the data was converted to the ED-1950 Lambert conformal conic projection system.

The aim of the study is to detect and interpret lightning events in terms of time and space. Two tools in ArcGIS 10.4.1 were used to analyze lightning events. These are the point density and total incidence tools. The point density tool counts the vector points within the surrounding pixels and gives them a raster output. Conceptually, a neighbor is defined around the center of each raster cell. The number of points falling in the neighborhood is summed up and divided by the neighbor area. The dot density tool consists of five basic functions: input data, weight value, output data, cell size of the output, and the radius to neighboring points. The purpose of the total incidence tool is to combine multiple points and assign weight values to the combined points (Özlu *et al.*, 2020).

In the study, sea surface temperatures for the period 1970–2022, obtained from TSMS (TSMS, 2022b), and Turkey's monthly average temperature data for the period 1991–2020 were used in the temporal and spatial interpretation of lightning (TSMS, 2024).

3. Results

3.1. Annual average lightning density

Upon examining the annual average lightning density, it was found that the highest values occur in the Inner Aegean, Marmara, Southwest Anatolia, Western Black Sea, and Eastern Anatolia Regions (25–50 lightning km² yr⁻¹). Central Anatolia is the region with the lowest lightning density (0.4–1.6 lightning km² yr⁻¹). It is seen that sufficient moisture content is an essential factor for supporting instability processes.

The Aegean Sea, Mediterranean, Eastern Black Sea, and Southeastern Anatolia are regions where lightning events occur moderately and not very densely (1.6 to 6.5 lightning km² yr⁻¹) (Fig. 2). Denser lightning events occurred in warm seas at low latitudes, such as the Mediterranean and Aegean Seas,

providing evidence of the positive relationship between sea surface temperature and lightning density, compared to seas at higher latitudes.

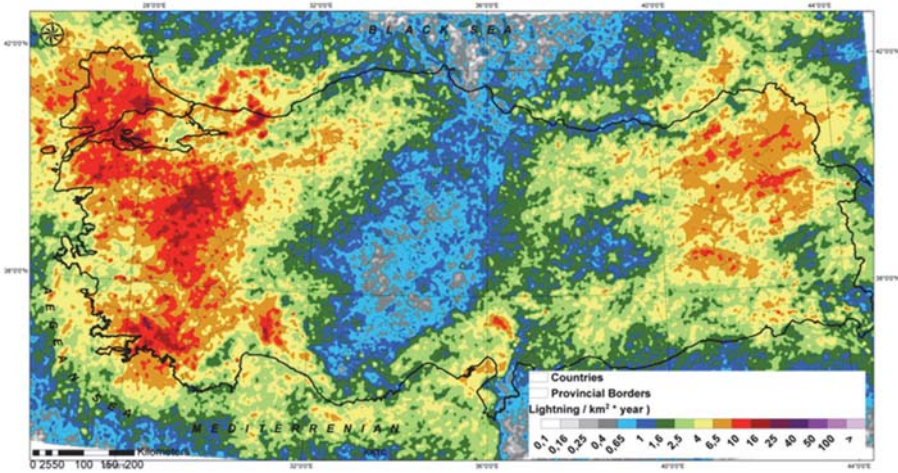


Fig. 2. 5-Yearly average lightning density (2017–2021).

3.2. Seasonal average lightning density

Since the temperature difference between the ground level and the high level of the atmosphere is small in winter, the atmosphere has a more stable structure. lightning density is very low throughout Türkiye. Lightning on land is only observed in areas close to the coasts in the south and west, and in Southeastern Anatolia because of either high levels or a lack of evaporation to support instability during the winter season and the cold land compared to the seas. Lightning occurs more frequently in the Aegean and Mediterranean coastal areas, where temperatures and sea surface temperatures are higher in winter than in Türkiye in general (Fig. 3). While the average sea surface temperature in February for the period of 1970–2022 in the Black Sea is 8.0 °C, it is 15.9 °C in the Mediterranean (Fig. 4). Lightning does not occur on the Black Sea coast as a result of its cold temperature during this period. Concerning the winter averages of lightning events in the last five years, the highest values (4–6 lightning km⁻² yr⁻¹) occurred in the coastal areas of Southwestern Anatolia (Muğla, İzmir, and Aydın provinces) (Fig. 3). The lightning km⁻² yr⁻¹ unit given here expresses the average number of lightning per km² in a year obtained from 5-year data.

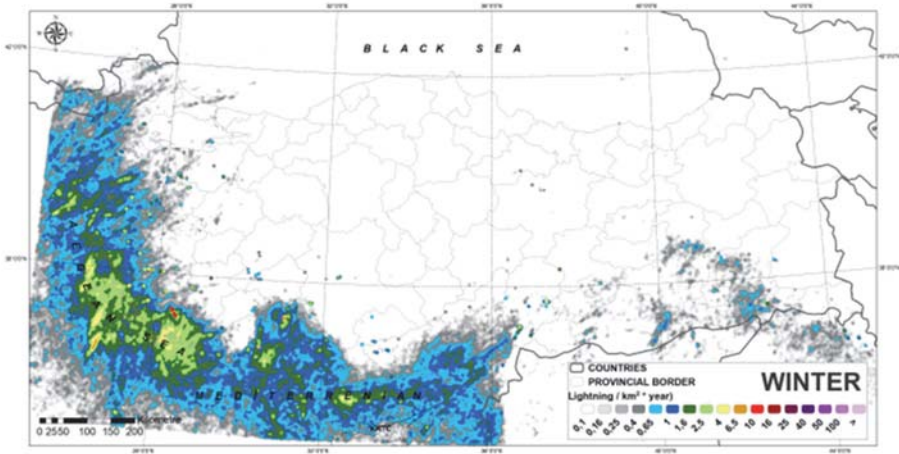


Fig.3. Lightning density during winter (2017–2021).

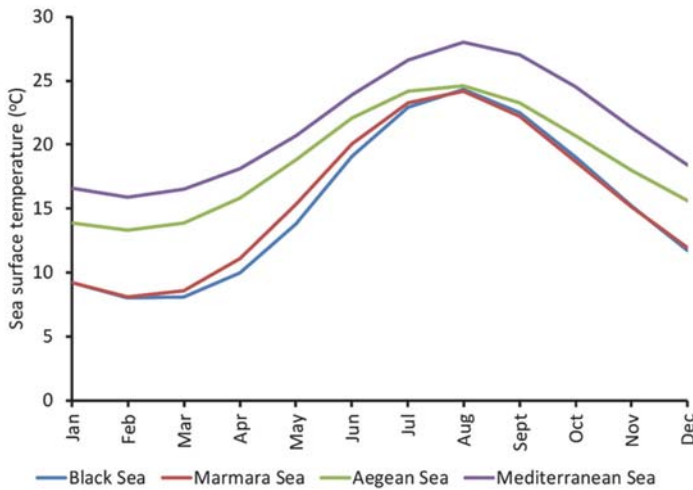


Fig.4. Monthly distribution of sea surface temperature (1970–2022).

Convection is observed with the increasing latent heat transfer as temperatures begin to increase in the spring, and the land warms up faster in the interior of Türkiye. During this season, surface warming, lack of warming in the upper atmosphere, and cold air from the north with jet streams strengthen the instability and increase lightning density. The highest lightning density occurred in the Inner Aegean, western Marmara, and Eastern Anatolia Regions, with a range from 6.5 to 10 lightning events $\text{km}^{-2} \text{yr}^{-1}$, and more lightning events were found here than in other regions (Fig.5).

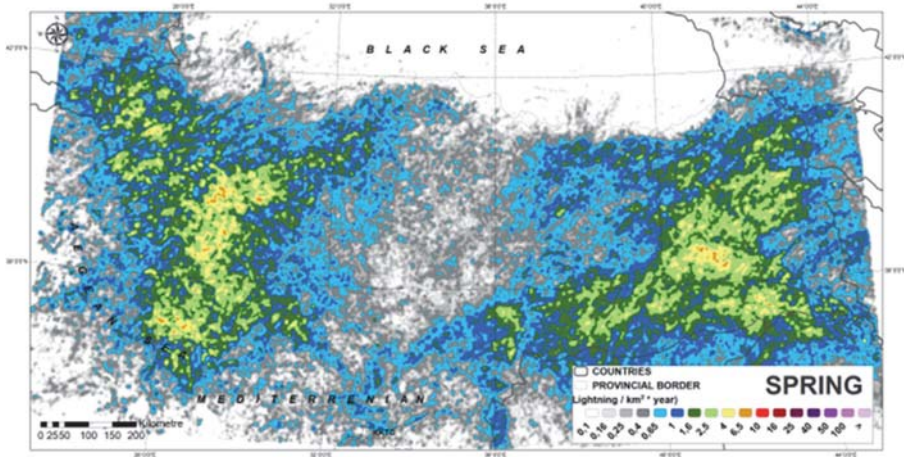


Fig.5. Lightning density during spring (2017–2021).

Summer is the period when instability is the highest, and therefore lightning events are the most frequent. During this period, the Thrace, Western Black Sea, and the inner parts of the Aegean Region are the regions with the highest values (25–40 lightning $\text{km}^{-2} \text{yr}^{-1}$). High values are also observed in the Eastern Anatolia Region and Eastern Black Sea Region. The warming of the Black Sea causes lightning density to shift to the north during this period. The higher lightning density in the western and eastern parts of the Black Sea Region reflects the orographic effect. On the other hand, the very low humidity in the Southeastern and Central Anatolian Regions is the factor influencing the low lightning density (Fig. 6).

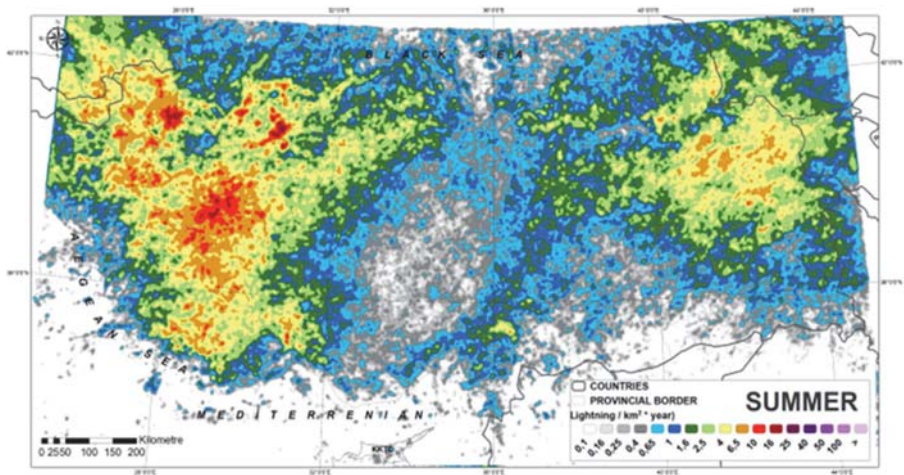


Fig.6. Lightning density during summer (2017–2021).

In autumn, denser lightning events are observed in the Marmara (10–25 lightning km⁻² yr⁻¹) and Southwest Anatolia Regions, on the Mediterranean coasts (4–6.5 lightning km⁻² yr⁻¹), and the Eastern Black Sea with the strong orographic effect (Fig. 7). Due to the rapid cooling of the land, lightning density decreases, especially in the inner regions. Moreover, the cooling of the Black Sea causes a decrease in lightning density on the sea and in the adjacent terrestrial areas (Fig. 4). In the Mediterranean Sea, the sea's warmth strengthens the instability on the sea, and, although the lightning density on the sea and the land close to it decreases, it is higher than in Türkiye in general.

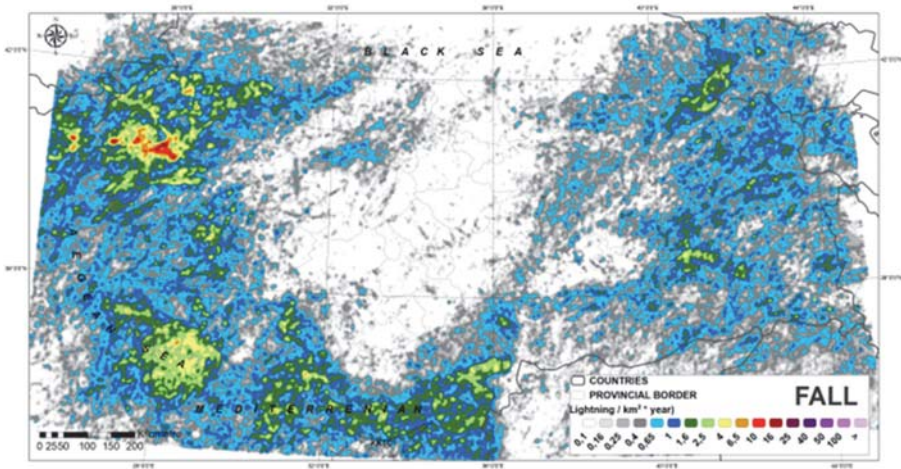


Fig. 7. Lightning density during autumn (2017–2021).

3.3. Monthly average lightning density

When lightning is average monthly, June (29%) and May (18%) are the months with the most lightning. Almost half (47%) of lightning occurs in these two months. December, January, and February are the months with the least lightning (Fig. 8). The annual trend in the number of lightning strikes is related to the annual cycle of surface air temperature. The high surface air temperature during the warm season significantly influences the atmospheric conditions over the land. This single-peak annual lightning density distribution is common at middle latitudes (Rivas Soriano *et al.*, 2001b).

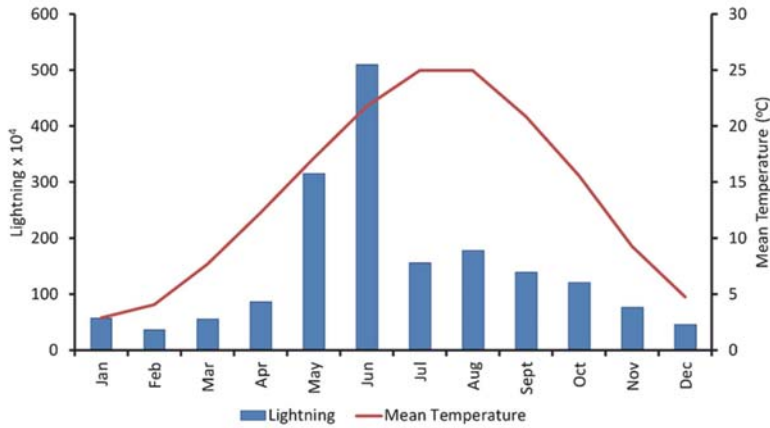


Fig.8. Monthly distribution of lightning (2017–2021) and mean temperature (1991–2020).

It was determined that, considering lightning events by months during the year, lightning events were denser ($2.5\text{--}4$ lightning $\text{km}^{-2} \text{yr}^{-1}$) in the Aegean and Mediterranean coastal regions, particularly in Muğla and its surroundings, in January. In February, lightning events intensified in regions like those affected in January. Average sea surface temperatures in February are lower than those in January. The average sea surface temperature in the Aegean Sea (1970–2022) is 13.9 °C in January and 13.3 °C in February. In the same period, it is 16.6 °C and 15.9 °C in the Mediterranean in January and February, respectively. Hence, relatively fewer lightning events ($0.65\text{--}1.6$ lightning $\text{km}^{-2} \text{yr}^{-1}$) occurred compared to January. The areas where lightning events were experienced also expanded with the increasing temperatures in March. In addition to the Aegean and Mediterranean coasts, lightning events intensified in the Southeast Anatolia Region and the west of the Thrace Region, ($0.4\text{--}1$ lightning $\text{km}^{-2} \text{yr}^{-1}$). In April, with the warming of the Southeastern Anatolia Region, instability increased, and convective activities were supported, which caused an increase in lightning density ($0.65\text{--}1.6$ lightning $\text{km}^{-2} \text{yr}^{-1}$). With the warming of the land in May, lightning density ($2.5\text{--}4$ lightning $\text{km}^{-2} \text{yr}^{-1}$) was observed in the inner parts of the Aegean Region, Marmara, and Eastern Anatolia region (Fig. 8). With the further increase in ground temperatures in June, lightning density in the same regions also increased ($6.5\text{--}16$ lightning $\text{km}^{-2} \text{yr}^{-1}$). In July, lightning density increased over Thrace, Marmara ($6.5\text{--}16$ lightning $\text{km}^{-2} \text{yr}^{-1}$), Central Aegean, Eastern Anatolia, and the Eastern Black Sea Region ($0.65\text{--}1.6$ lightning $\text{km}^{-2} \text{yr}^{-1}$). Whereas lightning density is high in the west of the Muğla - Sinop line and the east of the Trabzon - Hakkari line on the land in July, it is almost absent in the inner regions.

While high pressure is present in the Black Sea, the Azores high pressure in the Mediterranean reflects stable conditions, causing lightning density to decrease significantly. Lightning events occur predominantly in the Western Black Sea (10–16 lightning km⁻² yr⁻¹), the Eastern Black Sea, and Eastern Anatolia (2.5–4 lightning km⁻² yr⁻¹) in August. In the Black Sea Region the average sea surface temperature in the Black Sea Region in August is higher than in July. In the Black Sea, during the period 1970–2022, the average sea surface temperature in July was 22.9 °C, while it was 24.3 °C in August (*Fig. 4*). The increase in lightning density in these regions in August can be associated with the increase in sea surface temperatures and the orographic effect. In September, lightning density is high in the following regions: the Marmara Sea (10–16 lightning km⁻² yr⁻¹), Eastern Black Sea, Mediterranean Region, and Eastern Anatolia Region (0.65–4 lightning km⁻² yr⁻¹). In October, the sea surface temperatures of the Marmara and Eastern Black Seas start to decrease (*Fig. 4*). However, since the sea surface is not cold enough, although lightning density decreases (1.6–4 lightning km⁻² yr⁻¹), it continues to exhibit its effect. Dense lightning events also occurred in Southeastern Anatolia and the Gulf of Iskenderun. It was found that the lightning events observed in the relatively warmer Aegean and Mediterranean coastal regions in November, were concentrated in the surroundings of Muğla and Hatay (1.6–4 lightning km⁻² yr⁻¹). Although lightning events were observed in almost the same regions in December, it can be seen that lightning density decreased relatively (1–2.5 lightning km⁻² yr⁻¹) in comparison with November. Higher sea surface temperatures are associated with higher lightning density in November than in December (*Fig. 9*).

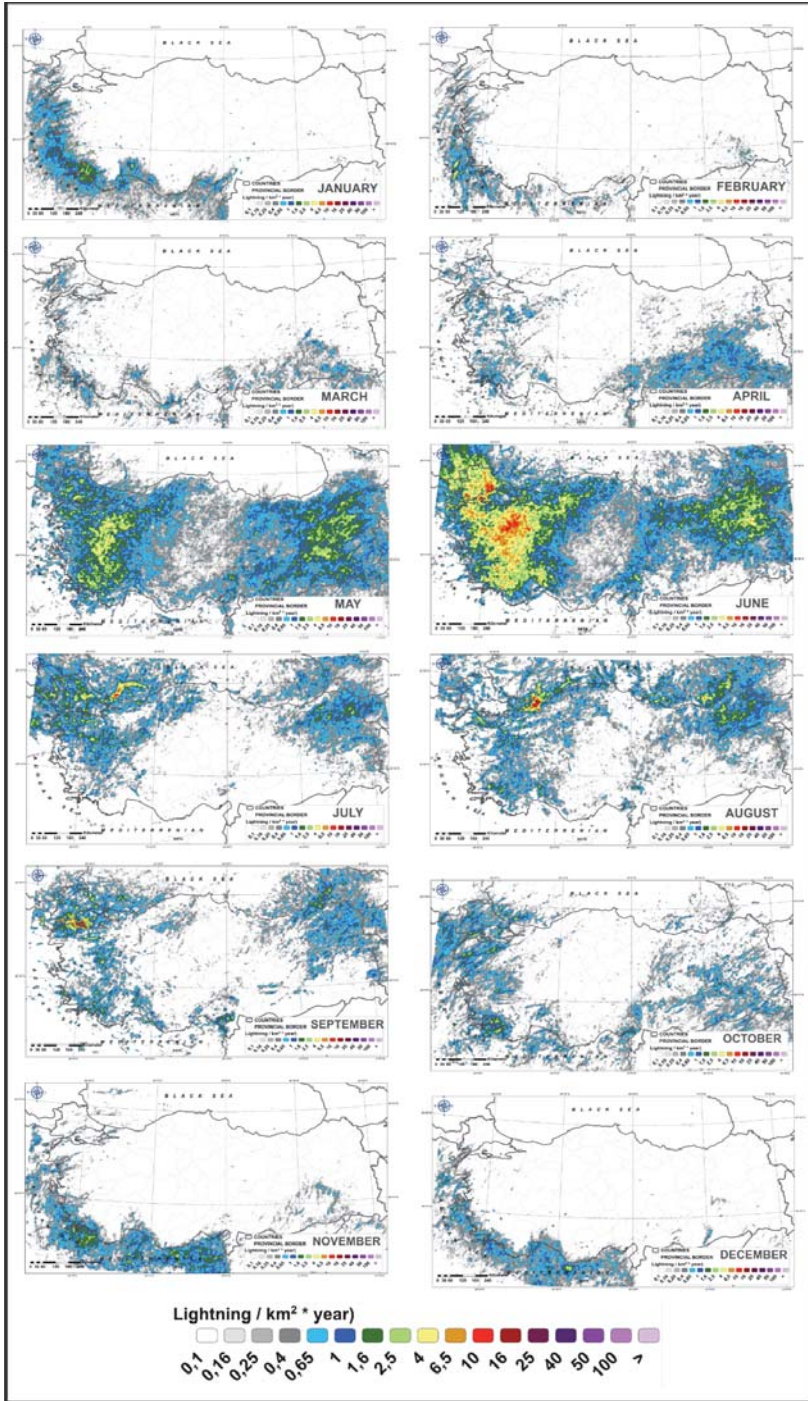


Fig.9. Monthly lightning density (2017–2021).

3.4. Distribution of lightning by the time of day

Upon examining lightning events hourly, the highest number of lightning occurs at noon, whereas the lowest number occurs at night and morning, hours. The period from 11:00 to 15:00 UTC (01:00 to 05:00 national time) is the hottest time of the day. High ground temperature supports convective instability. The period between 19:00–07:00 UTC (22:00–10:00 national time) is when both the ground temperature and instability are at their lowest. Lightning occurs very rarely during this period (Fig.10). While lightning density is low in the morning, it increases rapidly after 09:00 UTC (12:00 national time), peaks at 13:00–14:00 UTC (16:00–17:00 national time), and begins to decrease after 14:00 UTC (17:00 national time). The rate of increase from morning to noon is greater than the downward trend from noon to evening. This asymmetrical trend is associated with the rapid warming of the land, the increase in instability at noon, and the continuation of these unstable conditions in the afternoon. This diurnal trend is consistent with the global daily lightning change, in which the peak of lightning activity occurs at noon, and in the afternoon, following the maximum warming of the soil due to solar radiation in land areas (Galanaki et al., 2015).

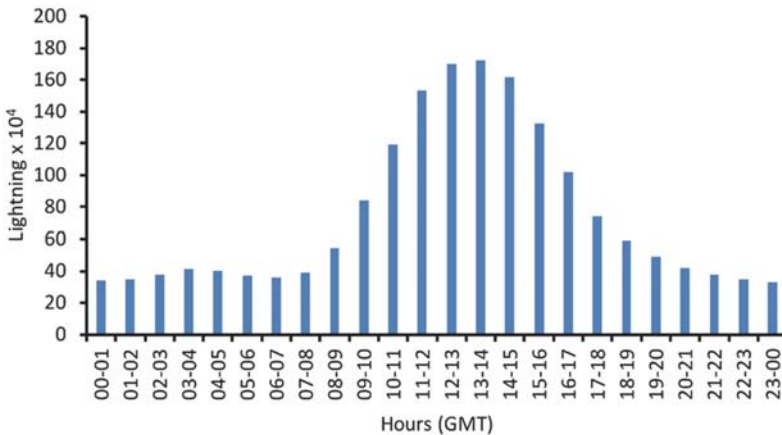


Fig.10. Hourly distribution of lightning (2017–2021).

3.5. The relationship of lightning with latitude and longitude

Considering the relationship between latitude values and lightning density, lightning is positively correlated with latitude, although the correlation is not regular. Lightning intensity increases from the Mediterranean coastline to

approximately the peaks of the Taurus Mountains at approximately 37.5N latitude. Lightning intensity decreases in the continental interior, which is roughly between 37.5N and 39.5N. Lightning intensity increases again in the high parts of the Black Sea Mountains and in the coastal areas towards the north. Lightning intensity decreases again over the cold, Black Sea (Fig. 11).

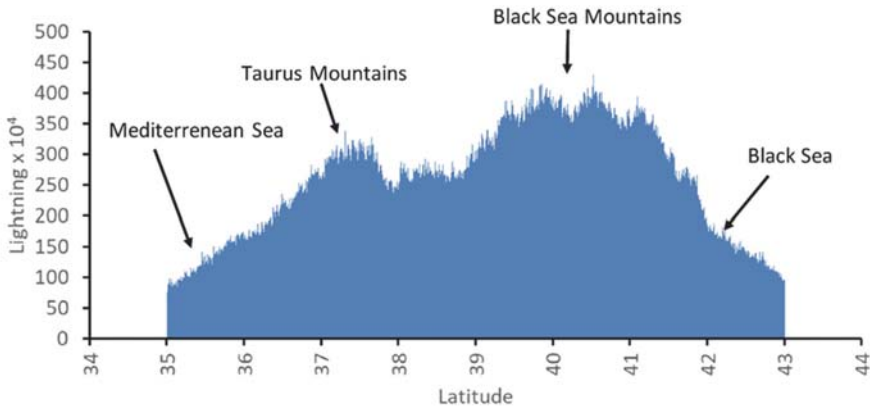


Fig. 11. The relationship between latitude and lightning density (2017–2021).

Concerning the relationship between longitude values and lightning density, the region between 26°E and 32°E longitudes facilitate the movement of the humid air of the Aegean Sea to reach the inner parts due to the east-west direction of the mountains. It is the area with the most intense lightning activity in Türkiye because of the sufficient moisture content and high ground temperature found between these longitudes. Previous studies have proven that mountain ranges and elevated areas support convective activities with the effect of orographic forcing, and high summer temperatures. The area between 39E and 44E longitudes is the region of Türkiye with the highest altitude. Lightning activity is also very high in this area. The region between 32E and 39E longitudes is very deficient in terms of moisture content. This should be related to soil moisture and vegetation. Soil moisture was revealed to increase summer convective precipitation efficiency under weak synoptic-scale forcing due to the presence of large sensible heat fluxes in forest areas. As sensible heat fluxes increase the potential to enhance convection and soil moisture abnormalities, they can change boundary layer properties (Schär *et al.*, 1999). This situation should be effective in reducing lightning density in the interior parts, between 32–39E longitudes with poor vegetation and low soil moisture. The longitudinal distribution is mostly related

to altitude and vegetation. Lightning density increases as altitude increases, from the low parts in the west to Inner West Anatolia. Lightning density decreases in Central Anatolia because of altitude and insufficient humidity, while lightning density increases with altitude toward Eastern Anatolia (Fig.12).

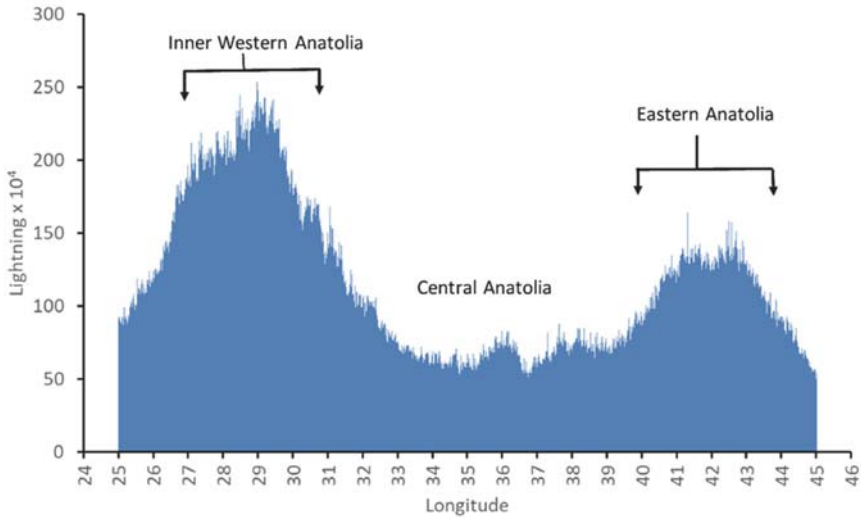


Fig.12. The relationship between longitude and lightning (2017–2021).

3.6. Relationship between lightning and altitude

The relationship between altitude and lightning is examined in two different ways in the present section. Approximately 4×10^6 lightning events were recorded at sea level between 2017 and 2021. Of lightning strikes, 22.5% ($\approx 9 \times 10^5$ lightning strikes) occurred over the sea. Considering the relationship between altitude and lightning, it becomes difficult to see the trend across different altitudes when sea level is included (Fig. 13a). For this reason, the lightning occurring over the sea was subtracted from the total number of lightning strikes, and hence, the relationship between lightning and the elevation in the terrestrial area was predicted. When the relationship is examined without including lightning at sea level, it is seen that lightning increases as a function of altitude between 30–150

m, and 500–1000 m, and decreases as a function of altitude between 150–500 m and above 1000 m. Lightning activity is negligible at 3000 m and above (*Fig. 13b*).

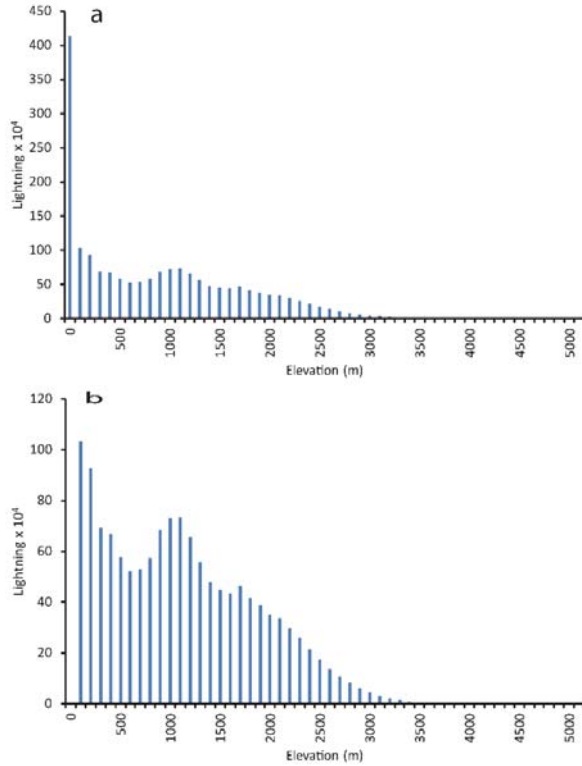


Fig. 13. The relationship between lightning and altitude between 2017 and 2021 (a) when sea level is included, (b) when sea level is not included.

4. Discussion and conclusion

In the present study, the annual, monthly, seasonal, and hourly densities of lightning data for 5 years (2017–2021) were calculated. Considering the annual lightning density by regions, the highest values were observed in the Inner Aegean, Marmara, Southwestern Anatolia, Western Black Sea, and Eastern Anatolia Regions. Lightning density in these regions is related to their proximity to the sea, orography, and vegetation type. It was determined that the high level of low-pressure activity on the sea in the Mediterranean basin, especially during the cold period, increases lightning density in the sea and coastal areas. Additionally, the topography and forests increase lightning density with forest influences particularly notable in the warm period (*Kotroni and Lagouvardos,*

2008; Galanaki et al., 2015; Xu et al., 2022). The Central Anatolia Region is the region with the lowest lightning density. Poor vegetation cover and low soil moisture are factors that should be taken into consideration in this situation. A study from Greece found that lightning efficiency on bare ground surfaces was very low throughout the year, with the lowest values in the summer months (Kotroni and Lagouvardos, 2008). Furthermore, low soil moisture in the inner parts weakens convective development (Schär et al., 1999). The Aegean Sea, the Mediterranean, the Eastern Black Sea, and the Southeastern Anatolia Region are regions where lightning events occur moderately.

Considering the seasonal lightning density, a relatively higher density of lightning was observed in spring with the warming of the land in comparison with autumn. Although the overall atmosphere is more stable during the winter season, the Aegean and Mediterranean Seas experience a higher frequency of lightning, which, despite being among periods of lowest overall lightning activity, still experiences significant lightning density is the highest in summer, when the surface temperature and, accordingly, instability is the highest. Terrestrial convection is higher in spring and summer. Therefore, denser lightning events occur over the seas in autumn, while the lightning density is higher over the Inner Aegean and Eastern Anatolia Regions during autumn. In winter, it is concentrated in this area because the Mediterranean is warmer. Whereas the dynamic high-pressure system dominating the summer months in the Mediterranean prevents convection and reduces lightning density despite the warm sea surface, the warming of the Black Sea in summer causes lightning density to increase during this period. Summer is the season with the lowest lightning density in the Mediterranean and the highest lightning density in the Black Sea. Upon examining lightning activity hourly, lightning density is the highest at noon and the lowest at night and in the morning hours. These findings are consistent with the results of the study conducted by Holt et al. (2001) and Defer et al. (2005). Lightning activity in Europe occurs predominantly over land during summer, while during winter, thunderstorms are usually located over the Mediterranean Sea. During spring, the geographical distribution of lightning activity is more spread, while during autumn, the lightning is mainly observed over the sea (Holt et al., 2001; Defer et al., 2005).

The monthly variation of lightning follows a course with a single maximum, and 29% of the annual lightning strikes occur in June, and 18% in May. Of the annual number of lightning strikes, 47% occur in these two months. Increased lightning activity in late spring and early summer is consistent with the annual temperature trend at mid-latitudes. These findings are similar to the monthly distribution of lightning strikes in the Iberian Peninsula by Rivas Soriano et al. (2001b). On the Iberian Peninsula, the monthly variation shows a single peak: about 79% of all lightning events were observed between the months May and September. The number of lightning occurrences increases from April to June, and the sharp decrease after October marks the end of the storm period. This

single-peak distribution is related to the annual cycle for the surface air temperature. The high surface air temperature during the warm season supplies an appropriate thermodynamic atmospheric background for convection (*Rivas Soriano et al.*, 2001b). According to lightning climatology studies for parts of western and central Europe, thunderstorm high season falls in summertime and extends from May to August with a peak in July. However, some thunderstorms also occur in the transitional months: March/April and September/October. They are the least likely during wintertime from November to February (*Taszarek et al.*, 2017).

Altaratz et al. (2003) carried out a study in the Eastern Mediterranean, and contrary to what is known, the annual average lightning density is higher over the sea than on land. Larger frequencies of ground flashes were detected over the sea than over land during the study period. This is probably due to the large heat and humidity fluxes from the sea surface, which destabilize the colder air above and drive cloud convection. The annual distribution shows that during midwinter (December–January–February), there is higher flash density over the sea, while during autumn and spring, the flash density is similar over the sea and terrestrial regions. However, lightning events on seas in Türkiye over a 5-year period constitute about 22.5% of all lightning, which is consistent with the study by *Altaratz et al.* (2003). It supports the findings of *Williams and Stanfill* (2002) and *Kotroni and Lagouvardos* (2008), indicating that the difference in thermal properties of land compared to sea surfaces explains why considerably more lightning is observed on land than on sea.

Concerning the relationship between altitude and lightning, while lightning increases with altitude in the ranges of 30–150 m and 500–1000 m, it decreases in the ranges of 150–500 m and above 1000 m. This result is consistent with the findings of the lightning activity study in China by *Xu et al.* (2022) and *Galanaki et al.* (2015), indicating that 67% of lightning occurs at altitudes lower than 600 m in winter.

Upon examining the relationship between latitude and longitude values and lightning, a more significant result was obtained regarding latitude. There is a positive relationship between latitude and lightning. Considering the relationship between longitude values and lightning, it can be interpreted that there is a significant decrease in lightning activity, at longitudes 30–35E, in the Central Anatolia Region, where humidity is low. Lightning activity increases as the degree of longitude increases with sufficient moisture content in terrestrial areas together with the orographic effect.

Availability Statement: The data that supports the findings of this study are available from TSMS. Restrictions apply to the availability of these data, which were used under license for this study. Data are available from the authors with the permission of TSMS.

References

- Ackerman S.A. and Knox J.A., 2015: Meteorology: Understanding the Atmosphere. 4th Edition, Jones & Bartlett Learning, Burlington, 244–271.
- Altaratz O., Levin Z., Yair Y., and Ziv B., 2003: Lightning activity over land and sea on the Eastern coast of the Mediterranean. *Month. Weather Rev.* 131, 2060–2070.
[https://doi.org/10.1175/1520-0493\(2003\)131<2060:LAOLAS>2.0.CO;2](https://doi.org/10.1175/1520-0493(2003)131<2060:LAOLAS>2.0.CO;2)
- Anderson G. and Klugmann D., 2014: A European lightning density analysis using 5 years of ATDnet data. *Nat. Hazards Earth Syst. Sci.* 14, 815–829. <https://doi.org/10.5194/nhess-14-815-2014>
- Aydın K. and Karabulut M., 2021: Temperature relationships with elevation and latitude in Turkey. *J. Soc. Sci.* 53, 501–519. <https://doi.org/10.29228/SOBIDER.51986>
- Bayraktar Ö.S. and Çiçek, İ., 2022: Türkiye’de hortum olayları. *J. Soc. Humanities Sci. Res.* 9(86), 1604–1616. <http://dx.doi.org/10.26450/jshsr.3202>
- Bozkurt D. and Göktürk O.M., 2009 Artan deniz suyu sıcaklıkları yağmur ve rüzgârı hırçınlaştırırken aşırı yağışlar, seller, fırtınalar *Bilim ve Teknik*, 55–57.
<https://services.tubitak.gov.tr/edergi/yazi.pdf;jsessionid=dCK1nYJMtkWV6qeWh2DmyvdY?drgiKodu=4&cilt=42&sayi=646&sayfa=54&yaziid=28542>
- Brooks, H.E., 2013: Severe thunderstorms and climate change. *Atmos. Res.* 123, 129–138.
<https://doi.org/10.1016/j.atmosres.2012.04.002>
- Defer E., Lagouvardos H., and Kotroni V., 2005: Lightning activity in the eastern Mediterranean region. *J. Geophys. Res.* 110, D24210, <https://doi.org/10.1029/2004JD005710>
- Dhital Y., Tang J., Pokharel A., Tang G., and Rai M., 2022: Impact of aerosol concentration on elevation-dependent warming pattern in the mountains of Nepal. *Atmos. Sci. Lett.* 23(10).
<https://doi.org/10.1002/asl.1101>
- Dwyer J.R. and Uman M.A., 2013: The physics of lightning. *Physics Rep.* 534, 147–241.
<http://doi.org/10.1016/j.physrep.2013.09.004>
- Erol O., 2011: Genel Klimatoloji (10th Edition). Çantay Press, İstanbul ISBN: 9789757206316
- Herring S.C., Christidis N., Hoell A., Kossin J.P., Schreck III C.J., and Scott P.A., 2018: Explaining extreme event of 2016 from a climate perspective. *Bull. Amer. Meteorol. Soc.* 99(1)-S1-S6.
<http://doi.org/10.1175/BAMS-D-17-0284.1>
- Holle R.L. and Cooper M.A. 2016: Lightning occurrence and social vulnerability, In: (Ed. Coleman J.S.M.) Atmospheric Hazards, Case Studies in Modeling, Communication, and Societal Impact. Published by ExLi4EvA, 3–19, ISBN-10 9789535125150
- Galanaki V., Vassiliki K., Konstantinos L., and Athanassios A., 2015: A ten-year analysis of lightning activity over the Eastern Mediterranean. *Atmos. Res.* 166, 213–222,
<https://doi.org/10.1016/j.atmosres.2015.07.008>
- Galanaki E., Lagouvardos K., Kotronia V., Flaounasa E., and Argirioub A., 2018: Thunderstorm climatology in the Mediterranean using cloud-to-ground lightning observations. *Atmos. Res.* 207.136–144. <https://doi.org/10.1016/j.atmosres.2018.03.004>
- Holt M.A., Hardaker P.J., and McLelland G.P., 2001: A lightning climatology for Europe and the UK, 1990–99, *Weather* 56, 290–296.
- IPCC, 2021: Climate Change 2021: The Physical Science Basis. Contribution of Working Group I to the Sixth Assessment Report of the Intergovernmental Panel on Climate Change [Masson-Delmotte, V., P. Zhai, A. Pirani, S.L. Connors, C. Péan, S. Berger, N. Caud, Y. Chen, L. Goldfarb, M.I. Gomis, M. Huang, K. Leitzell, E. Lonnoy, J.B.R. Matthews, T.K. Maycock, T. Waterfield, O. Yelekçi, R. Yu, and B. Zhou (eds.)]. Cambridge University Press, Cambridge, United Kingdom and New York, NY, USA, In press. <http://doi.org/10.1017/9781009157896>
- Kiçeci E.C., and Salamcı E., 2020: Aircraft–lightning interaction. *Eur. J. Sci Technol*, Special Issue, 177–187. <http://doi.org/10.31590/ejosat.araconf23>
- Kirshbaum D.J., Adler B., Kalthoff N., Barthlott C., and Serafin S., 2018: Moist orographic convection: Physical mechanisms and links to surface-exchange processes. *Atmosphere* 9, 80.
<https://doi.org/10.3390/atmos9030080>
- Kotroni V. and Lagouvardos K., 2008: Lightning occurrence in relation with elevation, terrain slope, and vegetation cover in the Mediterranean. *J. Geophys. Res.* 113, D21118,
<http://doi.org/10.1029/2008JD010605>

- Kotroni V. and Lagouvardos K., 2016: Lightning in the Mediterranean and its relation with sea-surface temperature. *Environ. Res. Lett.* 11(3). <http://dx.doi.org/10.1088/1748-9326/11/3/034006>
- Koutroulis A.G., Grillakis M.G., Tsanis I.K., Kotroni V., and Lagouvardos, K., 2012: Lightning activity, rainfall and flash flooding – occasional or interrelated events? A case study in the island of Crete. *Nat. Hazards Earth Syst. Sci.* 12, 881–891. <https://doi.org/10.5194/nhess-12-881-2012>
- Lay E.H., Jacobson A.R., Holzworth R.H., Rodger C.J., and Dowden R.L., 2007: Local time variation in land/ocean lightning flash density as measured by the world wide lightning location network. *J. Geophys. Res.* 112, D13111. <https://doi.org/10.1029/2006JD007944>
- Mackerras D. and Darveniza M., 1994: Latitudinal variation of lightning occurrence characteristics. *J. Geophys. Res.* 99, 10,813–10,821. <https://doi.org/10.1029/94JD00018>
- Manzato A., Serafin S., Miglietta M.M., Kirshbaum D., and Schulz W., 2022: A Pan-Alpine climatology of lightning and convective initiation. *Month. Weather Rev.* 150, 2213–2230, <https://doi.org/10.1175/MWR-D-21-0149.1>
- Mazarakis N., Kotroni V., Lagouvardos K., and Argiriou A., 2008: Storms and lightning activity in Greece during the warm periods of 2003–06. *J. Appl. Meteorol. Climatol.* 47, 3089–3098, <https://doi.org/10.1175/2008JAMC1798.1>
- Orville R.E. and Henderson R.W., 1986: Global distribution of midnight lightning: September 1977 to August 1978. *Month. Weather Rev.* 114, 2640–2653. [https://doi.org/10.1175/1520-0493\(1986\)114<2640:GDOMLS>2.0.CO;2](https://doi.org/10.1175/1520-0493(1986)114<2640:GDOMLS>2.0.CO;2)
- Öztopal, A., 2017: Türkiye'nin yıldırım ve şimşek gözlemlerinin incelenmesi *Dokuz Eylül Üniversitesi Mühendislik Fakültesi Fen ve Mühendislik Dergisi.* 19 (56), 304–313. <https://doi.org/10.21205/deufmd.2017195634>
- Özlu T., Haybat H. and Zerenöglu H., 2020: Trafik kazalarının zamansal ve mekânsal incelenmesi: Eskişehir şehir örneği. *Int. J. Geogr. Geogr. Educat. (IGGE)* 43, 136–158. <https://doi.org/10.32003/igge.746447>
- Petersen W.A. and Rutledge S.A., 1998: On the relationship between cloud-to-ground lightning and convective rainfall. *J. Geophys. Res.* 103, D112, 14025–14040. <https://doi.org/10.1029/97JD02064>
- Pinto I.R.C.A., and Pinto Jr O., 2003: Cloud to-ground lightning distribution in Brazil. *J. Atmos. Solar-Terrest. Phys.* 65, 733–737. [https://doi.org/10.1016/S1364-6826\(03\)00076-2](https://doi.org/10.1016/S1364-6826(03)00076-2)
- Pinto Jr O., Pinto I.R.C.A., and Neto O., 2013: Lightning enhancement in the Amazon region due to urban activity. *Amer. J. Climate Change* 2(4), 270–274. <http://doi.org/10.4236/ajcc.2013.24026>
- Pinto Jr O. and Pinto I.R.C.A., 2020 Lightning changes in response to global warming in Rio de Janeiro, Brazil. *Amer. J. Climate Change* 9(3), 266–273. <https://doi.org/10.4236/ajcc.2020.93017>
- Rangwala, I. and Miller, J.R., 2012: Climate change in mountains: a review of elevation-dependent warming and its possible causes. *Climatic Change* 114, 527–547. <https://doi.org/10.1007/s10584-012-0419-3>
- Reason C.J.C. and Mulenga H., 1999: Relations between South African rainfall and SST anomalies in the southwest India Ocean. *Int. J. Climatol.* 19, 1651–1673. [https://doi.org/10.1002/\(SICI\)1097-0088\(199912\)19:15<1651::AID-JOC439>3.0.CO;2-U](https://doi.org/10.1002/(SICI)1097-0088(199912)19:15<1651::AID-JOC439>3.0.CO;2-U)
- Reynolds S.E., Brook M., and Gourley M.F., 1957: Thunderstorms charge separation. *J. Atmos. Sci.* 14, 426–436. [https://doi.org/10.1175/1520-0469\(1957\)014<0426:TCS>2.0.CO;2](https://doi.org/10.1175/1520-0469(1957)014<0426:TCS>2.0.CO;2)
- Rivas Soriano L., de Pablo F., Diez E.G., 2001a: Relationship between convective precipitation and cloud-to-ground lightning in the Iberian Peninsula. *Monthly Weather Review*, 129:12, 2998–3003. [https://doi.org/10.1175/1520-0493\(2001\)129%3C2998:RBCPAC%3E2.0.CO;2](https://doi.org/10.1175/1520-0493(2001)129%3C2998:RBCPAC%3E2.0.CO;2)
- Rivas Soriano L., de Pablo F., Diez, E.G., 2001b: Cloud-to-ground lightning activity in the Iberian Peninsula: 1992–94. *Journal of Geophysical Research*, 106:D11, 11,891–11,901. <https://doi.org/10.1029/2001JD900055>
- Rivas Soriano L. and de Pablo F., 2002: Maritime cloud-to-ground lightning: The western Mediterranean Sea. *J. Geophys. Res.* 107, D21. <https://doi.org/10.1029/2002JD00221>
- Romps D.M., Seeley J.T., Vollaro D. and Molinari J., 2014: Projected increase in lightning strikes in the United States due to global warming. *Science* 346, 851–854. <https://doi.org/10.1126/science.1259100>
- Rupke E., 2002: Lightning direct effects handbook. Lightning Technologies Inc., AGATE-WP3.1-031027-043-Design Guideline <https://agate.niar.wichita.edu/Lightning/AGATE-Handbook-Rev-E.pdf>

- Saha U., Siingh D., Kamra A.K., Galanaki E., Maitra A., Singh R.P., Singh A.K., Chakraborty S., and Singh R., 2017: On the association of lightning activity and projected change in climate. *Atmos. Res.* 183, 173–190. <https://doi.org/10.1016/j.atmosres.2016.09.001>
- Schär C., Lüthi D., Beyerle U., and Heise E., 1999: The soil–precipitation feedback: a process study with a regional climate model. *J. Climate* 12, 722–741. [https://doi.org/10.1175/1520-0442\(1999\)012<0722:TSPFAP>2.0.CO;2](https://doi.org/10.1175/1520-0442(1999)012<0722:TSPFAP>2.0.CO;2)
- Takahashi T., 1984: Thunderstorm electrification—A numerical study. *J. Atmos. Sci.* 41, 2541–2558. [https://doi.org/10.1175/1520-0469\(1984\)041<2541:TENS>2.0.CO;2](https://doi.org/10.1175/1520-0469(1984)041<2541:TENS>2.0.CO;2)
- Taszarek M., Brooks H.E., and Czernecki B., 2017: Sounding-Derived Parameters Associated with Convective Hazards in Europe. *Month. Weather Rev.* 145, 1511–1528. <https://doi.org/10.1175/MWR-D-16-0384.1>
- Tinnaker M.I.R., Ali K., and Beig G., 2010: Relationship between lightning activity over Peninsular India and sea surface temperature. *J. Appl. Meteorol. Climatol.* 49, 828–835. <https://doi.org/10.1175/2009JAMC2199.1>
- Tinnaker M.I.R., Aslam M.Y., and Chate D.M., 2017: Association of rainfall and stability index with lightning parameter over the Indo-Gangetic Plains. *Amer. J. Climate Change* 6, 443–454. <https://doi.org/10.4236/ajcc.2017.63023>
- Tinnaker M.I.R., Ghude S.D., and Chate D.M., 2019: Land-sea contrasts for climatic lightning activity over Indian region. *Theor. Appl. Climatol.* 138, 931–940. <https://doi.org/10.1007/s00704-019-02862-4>
- TSMS (Türkiye State Meteorological Service), 2022a: <https://www.mgm.gov.tr/genel/meteorolojiyegir.aspx?s=17> accessed October 25 2022
- TSMS (Türkiye State Meteorological Service), 2022b: <https://www.mgm.gov.tr/veridegerlendirme/il-ve-ilceler-istatistik.aspx?k=K> accessed February 02 2024
- TSMS (Türkiye State Meteorological Service), 2024: <https://www.mgm.gov.tr/veridegerlendirme/sicaklik-analizi.aspx>
- Turman B.N. and Edgar B.C., 1982: Global lightning distributions at dawn and dusk. *J. Geophys. Res.* 87, 1191–1206. <https://doi.org/10.1029/JC087iC02p01191>
- Uman M.A., 1986: All About Lightning. Dover Publications N.Y. 99:173; ISBN- 2-486-25237-x
- Williams E., 2005: Lightning and climate: a review. *Atmos. Res.* 76, 272–287. <https://doi.org/10.1016/j.atmosres.2004.11.014>
- Williams E. and Guha A., 2019: Lightning and climate change. In Proceedings of the International Seminar on Lightning Protection. São Paulo: Institute of Energy and Environment of the University of São Paulo ISBN: 9781728118925
- Williams E. and Stanfill S., 2002: The physical origin of the land-ocean contrast in lightning activity. *Comptes Rendus Physique* 3, 1277–1292. [https://doi.org/10.1016/S1631-0705\(02\)01407-X](https://doi.org/10.1016/S1631-0705(02)01407-X)
- Xu M., Qie X., Pang W., Shi G., Liang L., Sun Z., Yuan Z., Zhu K., and Zhao P., 2022: Lightning climatology across the Chinese continent from 2010 to 2020. *Atmos. Res.* 275. <https://doi.org/10.1016/j.atmosres.2022.106251>
- Yamamoto K., Nakashima T., Sumi S., and Ametani A., 2016: About 100 years survey of the surface temperatures of Japan sea and lightning days along the coast. 33rd International Conference on Lightning Protection (ICLP). <https://doi.org/10.1109/ICLP.2016.7791346>
- Yavuz V., Lupo A.R., Fox N.I., and Deniz A., 2022: A long-term analysis of thundersnow events over the Marmara Region, Turkey. *Nat. Hazards* 114, 367–387. <https://doi.org/10.1007/s11069-022-05393-w>
- Zipser E.J. and Lutz K.R., 1994: The Vertical profile of radar reflectivity of convective cells: A strong indicator of storm intensity and lightning probability? *Month. Weather Rev.* 122, 1751–1759. [https://doi.org/10.1175/1520-0493\(1994\)122<1751:TVPORR>2.0.CO;2](https://doi.org/10.1175/1520-0493(1994)122<1751:TVPORR>2.0.CO;2)
- Ziv B., Saaroni H., Yair Y., Ganot M., Baharad A., and Isasrachi D., 2009: Atmospheric factors governing winter thunderstorms in the coastal region of the eastern Mediterranean. *Theor. Appl. Climatol.* 95, 301–310. <https://doi.org/10.1007/s00704-008-0008-6>

IDŐJÁRÁS

*Quarterly Journal of the HungaroMet Hungarian Meteorological Service
Vol. 129, No. 1, January – March, 2025, pp. 39–51*

An observational study of a long-lived monsoon depression over the South China Sea

Pak-wai Chan¹ and Junyi He²

¹*Hong Kong Observatory, Hong Kong, China*

²*City University of Hong Kong, Hong Kong, China*

** Corresponding Author E-mail: pwchan@hko.gov.hk*

(Manuscript received in final form January 8, 2024)

Abstract— In general, there would be one monsoon depression affecting the South China Sea every summer. Such depressions are relatively short-lived and mostly last for a few days. In early June 2023, there was a relatively long-lived monsoon depression over the South China Sea with a lifespan of around 10 days. The paper documents the life of this monsoon depression, including the meteorological observations. This depression is found to have the typical structure of a monsoon depression, namely, very weak winds near the center and higher wind speed with intense convection associated with a burst of southwest monsoon in its periphery. The strong southwest monsoon was also observed as a boundary layer jet in the upper air observations. The study is unique from the perspective that there are more meteorological observations over the northern part of the South China Sea, including the weather buoys and oil platforms, which provide unprecedented meteorological observations of the depression. It is hoped that this paper could stimulate further studies of monsoon depressions in this region in the future.

Key-words: monsoon depression, meteorological observations, numerical weather prediction models, China

1. Introduction

The coast of southern China is often affected by tropical cyclones. For instance, for Hong Kong which is situated at the Pearl River Estuary, there are on average around 4 to 7 tropical cyclones affecting the place in every year. Timely monitoring of low pressure areas which may develop into a tropical cyclone is of utmost importance for ensuring the safety of the city.

Apart from tropical cyclones, Hong Kong may also be affected by monsoon depressions in the summer. This kind of depression has not yet developed into a tropical cyclone. It normally has a rather large center with very weak winds (say 2.5 to 5 m/s), whereas the outer region has intense convective developments and much strong winds (which are mostly related to the southwest monsoon over the South China Sea). Monsoon depressions may also bring about unsettled weather to the south China coastal areas.

According to *Hurley and Boos (2014)*, there are on average about 0.5 to 1.0 monsoon depressions affecting the coast of southern China every summer. In general, they are relatively short-lived, with a lifespan in the order of a few days only. They may develop over the South China Sea, or enter this ocean from the northwest Pacific.

The Hong Kong Observatory has published a number of articles in its website to educate the public about the difference between monsoon depression and tropical cyclone (including <https://www.hko.gov.hk/en/blog/00000142.htm> and <https://www.hko.gov.hk/en/blog/00000149.htm>). In the scientific literature, the term monsoon depression is mainly used for cyclones over the Bay of Bengal and Indian subcontinent (such as https://glossary.ametsoc.org/wiki/Monsoon_depression). There have been a number of scientific papers, though limited, to study the monsoon depression in that region. The climatology of Indian monsoon depressions has been discussed in *Pottapinjara et al. (2014)*, *Rastogi et al. (2018)*, *Karmakar et al. (2021)*, and *Ray and Sil (2023)*, and the long-term trends in the number of them have been statistically analyzed in *Krishnamurti et al. (2013)*, *Cohen and Boos (2014)*, and *Vishnu et al. (2016)*. Several important aspects related to Indian monsoon depressions, such as barotropic growth (*Diaz and Boos, 2019a, 2019b; Suhas and Boos, 2023*), westward drift (*Boos et al., 2015; Hunt and Parker, 2016*), and precipitation (*Hunt et al., 2016; Murthy and Boos, 2019*), have been investigated. The influence of horizontal resolution (*Hunt and Turner, 2017*), cloud microphysics (*Hazra and Pattnaik, 2021*), and data assimilation (*Lodh et al., 2022; Vinodkumar et al., 2009*) on the mesoscale simulations of them have also been assessed.

2. A case study of a monsoon depression

In the first half of June 2023, there was a relatively long-lived monsoon depression over the South China Sea and southern China. It had a life of around 10 days, and the numerical weather prediction (NWP) models once forecasted that it might develop into a stronger system (possibly a tropical cyclone) affecting the Pearl River Estuary. As such, the weather services in the region conducted very close monitoring of its movement and development. Eventually, it remained as a rather weak system throughout its whole life and dissipated over the seas near Taiwan. With the availability of more weather observations nowadays, such as the buoys and oil platforms over the South China Sea, global lightning location system, etc., there are unprecedented observations of this system throughout its whole life. Though its impact on the coastal areas is not significant, its long life and the available weather observations worth to be documented for reference by weather forecasters in this part of the world in the future. This is the novelty of this observational study, and it is hoped that the study could stimulate similar analysis, especially statistical analysis, of tropical depressions in the South China Sea in the future.

2.1. Overview of the monsoon depression

The locations of the monsoon depression at various stages of its life are given in *Fig. 1*. Please note that, as shown in the later figures of this paper, the location of the depression is rather hard to pinpoint as it remains as a relatively weak system, and as such the locations are indicative only. However, the general trend of the movement of the depression is still rather clearly shown in this figure.



Fig. 1. The track and location of the monsoon depression under study in this paper for its whole lifespan. The locations of the radiosonde stations which have been included in the study are marked by red triangles.

The monsoon depression first appeared in the central part of the South China Sea. It then generally moved in the direction of the Hainan Island and entered the Beibu Wan. It further moved north and made landfall over the southwestern part of China, and lingered over that area for a couple of days. Afterwards it moved into the Hainan Island again.

The threat of the monsoon depression over south China coastal areas was closely monitored and assessed when this depression moved into and across the northern part of the South China Sea in an east-northeast direction. The depression remained at a distance of more than 200 km from Hong Kong, and thus turned out to have rather limited impact on the Pearl River Estuary. Finally, it touched upon the southern tip of Taiwan, moved into the northwest Pacific and dissipated.

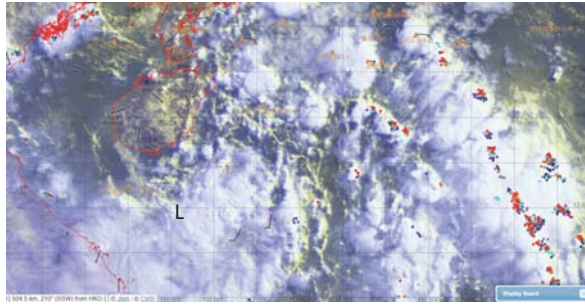
2.2. Surface, satellite, and lightning observations

The observations at four stages of the life of the monsoon depression are documented here using surface wind observations, weather satellite imageries, and lightning location area. *Fig. 2(a)* refers to the time when the depression was about to make landfall over Hainan Island. The convective clouds associated with the depression were rather loosely organized. The surface winds were generally rather weak, only about 2.5 to 5 m/s from the available observation. The most significant convective development appeared at the northeastern part of the South China Sea, where the southwest monsoon over the southern flank of the monsoon depression converged with the western flank of the subtropical ridge. There was north-northwest to south-southeast oriented cloud band over there with frequent lightning.

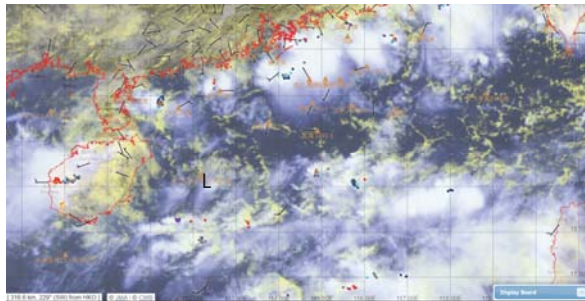
Fig. 2(b) refers to the time when the depression entered the Hainan Island the second time and was about leave the Island to enter the northern part of the South China Sea. Since the depression was over the land, the associated convective development was very weak, and it was once thought that the depression was about to dissipate. The winds near the center of the depression were extremely weak, generally less than 2.5 m/s.

In *Fig. 2(c)*, the monsoon depression was crossing the northern part of the South China Sea, and it was closest to Hong Kong. The surface wind observations, though rather weak, clearly depicted that there was a close circulation, and the convective development (west-east oriented cloud band with frequent lightning activity) appeared in the southern part of the system. The southwest monsoon remained rather weak, as shown in the surface observations, and this is consistent with the NWP analysis and forecast (not shown).

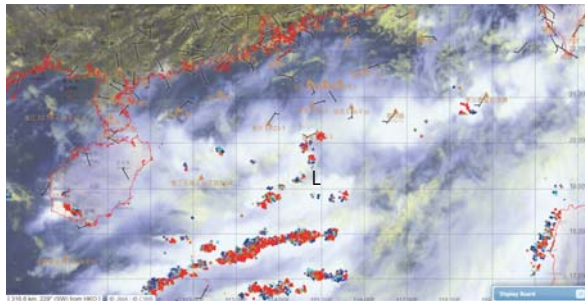
The monsoon depression continued to track east-northeastwards towards Taiwan, as shown in *Fig. 2(d)*. Consistent with NWP model forecast (not shown), there was a burst of southwest monsoonal flow at that time, and a ship observation recorded southwesterly winds of around 18 m/s (red wind barb in *Fig. 2(d)*).



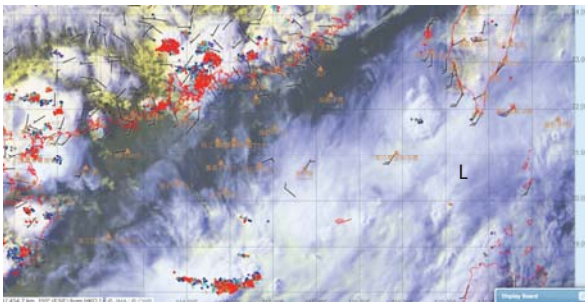
(a) 07:30 UTC, June 6, 2023



(b) 10:40 UTC, June 11, 2023



(c) 13:30 UTC, June 12, 2023



(d) 16:30 UTC, June 13, 2023

Fig. 2. Meteorological observations of the monsoon depression at four instances of its life, including surface wind observations (wind barbs), satellite imageries, and lightning location information (colored dots). Indicative location of the depression is marked as “L”.

There were rather significant convective cloud bands to the southwest of the system with frequent lightning activity. There were frequent discussions among the weather forecasters on the need to upgrade the system into a tropical depression by that time. However, as the system was about to make landfall over Taiwan, the upgrade was withheld, and eventually the monsoon depression, when located to the east of Taiwan, was submerged into a surface trough of low pressure and could no longer to be identified independently. This is taken to be the end of the life of the monsoon depression. On the whole, the monsoon depression lasted for 10 days.

Apart from surface wind observations, there are additional measurements of the surface pressure. Two instances of the surface pressure distributions are given in *Fig. 3*. *Fig.3(a)* refers to the time when the monsoon depression was located at the northeastern corner of Hainan Island and was about to enter the northern part of the South China Sea. The surface pressure near the center of the depression was found to be around 1001.5 hPa. When the depression was rather close to Hong Kong, as shown in *Fig. 3(b)*, it was found to have a pressure of around 1000.7 hPa near the center. It appears that, throughout the whole life, the monsoon depression had a lowest pressure of around 1000 hPa near its centre.



(a) 10:40 UTC, June 11, 2023



(b) 13:30 UTC, June 12, 2023

Fig. 3. Surface observations at two time instances of the lifespan of the monsoon depression. They include wind barbs, temperature (black), dew point (red), and pressure (013 refers to 1001.3 hPa, etc.). The indicative location of the monsoon depression is given by “L”.

2.3. Radar observations

As the convective developments near the center of the monsoon depression were rather weak, the weather radar imageries of the system did not show the typical radar echoes in association with the spiral rain bands. Two instances of the radar pictures are shown in *Fig. 4*.

In *Fig. 4(a)*, when the monsoon depression just left the Hainan Island, there were only isolated radar echoes near the center of the system. The echoes did not take a band shape, and they did not appear to be circulating from the radar picture animations (not shown).

When located at around 200 km to the south-southwest of Hong Kong, the monsoon depression had rather weak and isolated radar echoes near its center (*Fig.4(b)*). On the other hand, the convective developments associated with the southwest monsoon, the south and east of the system appeared to be much more intense, consistently with satellite imagery and lightning location information.

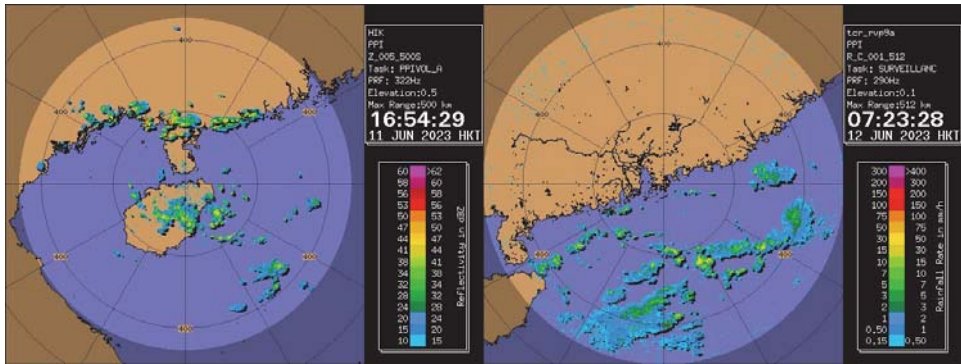


Fig. 4. Weather radar imageries of the monsoon depression with indicative location “L”.
(a) 16:54 UTC, June 11, 2023, for Haikou radar (b) 07:23 UTC, June 12, 2023, for Hong Kong radar

2.4. Upper air observations

Regular radiosonde data are available from a number of stations within 300 km from the center of the monsoon depression, and they provide some information, though rather limited, about the upper air situation in association with the depression. The stations include Xisha, Haikou, and Dongsha, and their locations are given in *Fig. 1*.

For upper-air winds, only Xisha and Haikou are considered as the vertical resolution of the available radiosonde, data from Dongsha are rather coarse. For Xisha (*Fig. 5(a)*), the wind direction changed from northeasterly to southeasterly and then southerly, with the passage of the monsoon depression over this station. The boundary layer winds remained rather weak, consistently with the surface

observations. When turning to southerly, the mid-tropospheric flow (around 4 km) showed a jet, reaching around 15 m/s. This might be related to the mid-level southwest monsoon.

For Haikou (*Fig. 5(b)*), one notable feature was the low-level jet (below 2 km) on June 11-13, 2023, though the wind speed was not particularly high (around 6 to 13 m/s). The jet feature was rather apparent. More specifically, for southwest monsoon at 00 UTC, June 13, 2023, the jet feature was the most significant, and the boundary layer wind speed reached the maximum of around 13 m/s.

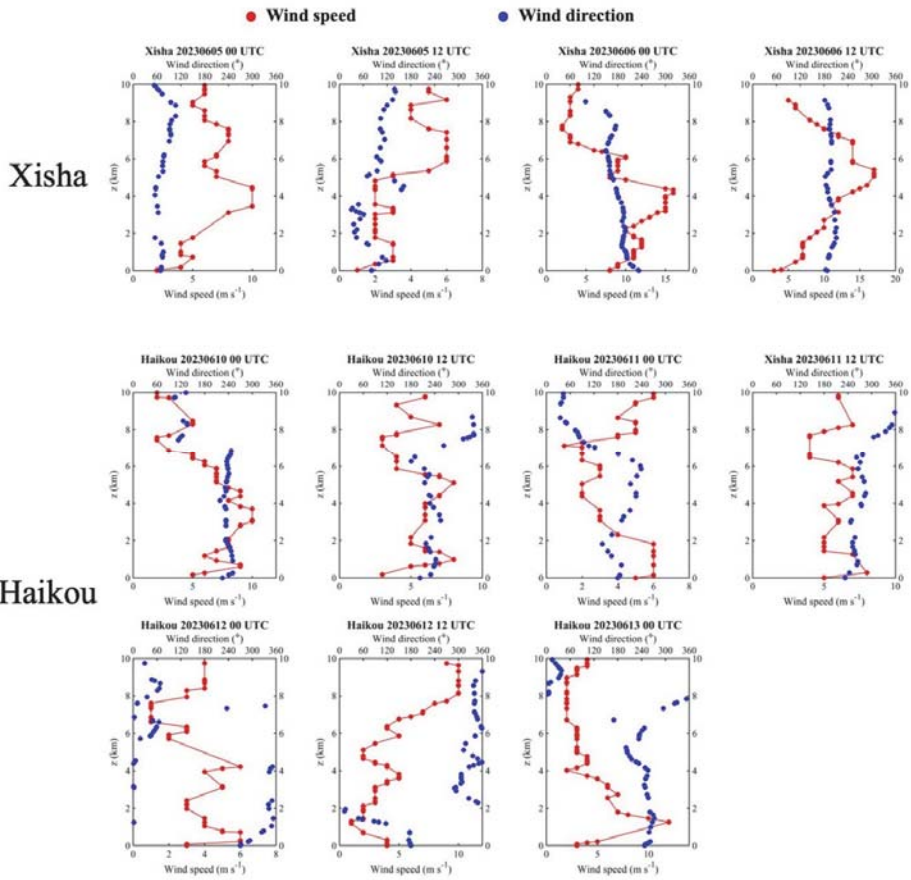


Fig. 5. Radiosonde observations of Xisha and Haikou for wind speed and wind direction.

The thermodynamic features of the upper-air soundings from the three stations are shown in *Fig. 6*. In general, the boundary layers of the three stations (below 2 km) were rather unstable, shown in the relatively sharp decrease of equivalent potential temperature with height. A previous study of dropsonde data of tropical cyclones (*He et al., 2022*) suggests that, in such conditions, there could be chance of intensification of the cyclonic system. As such, from the available observations, the thermodynamic conditions of the atmosphere did favor the further development of the system.

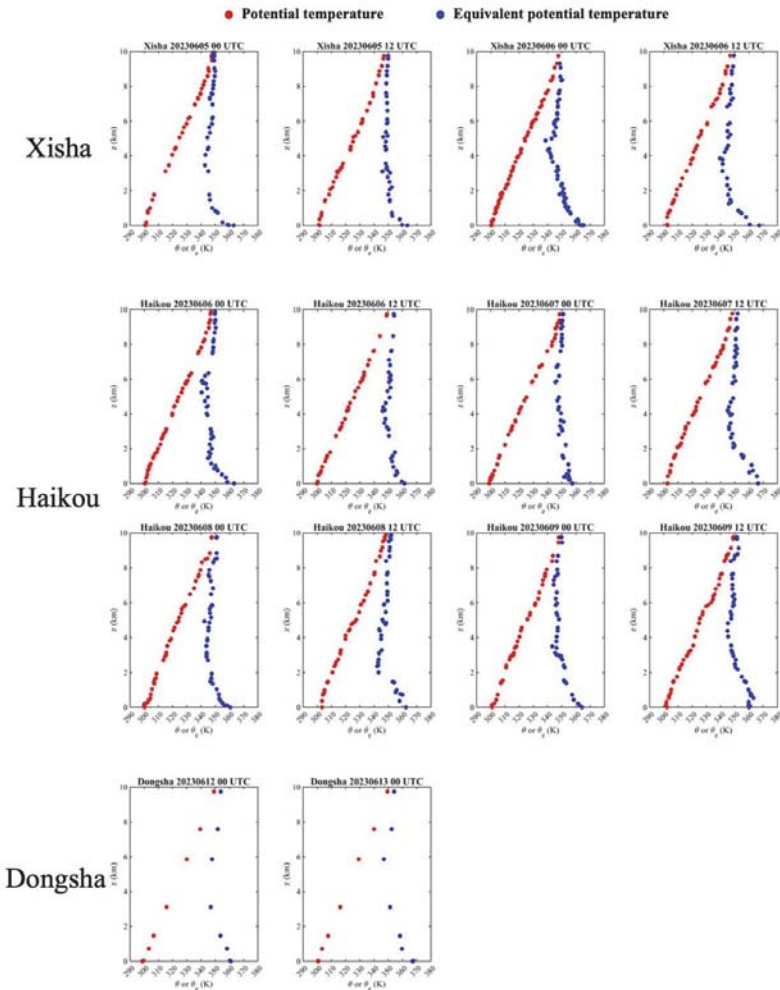


Fig. 6. Radiosonde observations of Xisha, Haikou, and Dongsha for potential temperature and equivalent potential temperature.

2.5. Performance of numerical weather prediction models

The NWP models in general capture the weak system quite well, which may be related to the improved data assimilation system and higher spatial resolution of the model. Here we take the ensemble system ECEPS of the European Centre of Medium-Range Weather Forecasts as an example. Ensemble tracks of the three stages of the system are shown in Fig. 7. The model ensemble forecasts are shown as black curves. They are in generally consistent with the actual locations of the monsoon depression in Fig. 1. The ECEPS forecasts are all 120-hour forecasts in the figure.

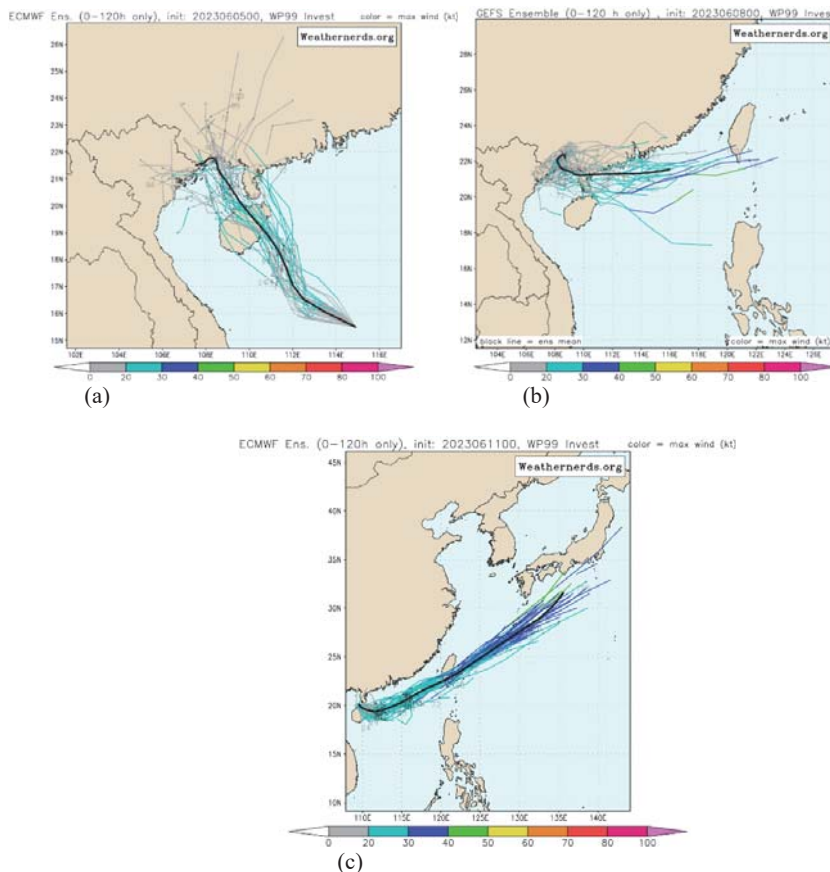
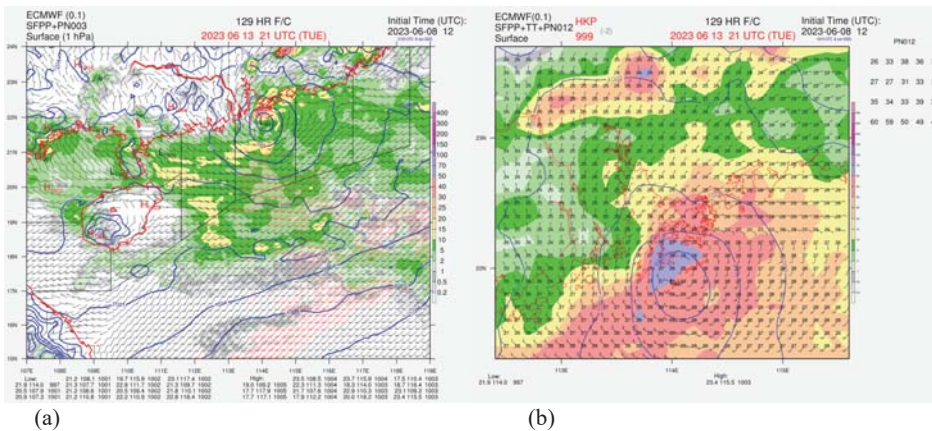


Fig. 7. ECEPS tracks of the monsoon depression for three model runs. Copyright: Weathernerds

However, there might be some limitations in the forecasts of the deterministic model of the ECMWF about the location and, especially, the intensity of the system. *Fig. 8* shows the deterministic forecast with the initial time of 12 UTC, June 8, 2023, with a forecast time of 129 hours. The ECEPS model once forecasted that the system could be extremely close to Hong Kong, with deepening of central pressure to around 997 hPa. As such, it was expected to bring about significant rain to Hong Kong (up to 60 mm of rain in 12 hours). Because of that, the Hong Kong Observatory once issued the message that the system would be closely monitored, and there might be a need of issuing tropical cyclone warning signal if the system further developed into a tropical cyclone and moved close to Hong Kong. This turned out to be a bust forecast. The performance of the NWP model is documented here for future reference by the model developers and weather forecasters.



(a) (b)
Fig. 8. 129-hour forecast of the ECMWF’s deterministic model initialized at 12 UTC, June 8, 2023. (a) surface forecast for wind, pressure, and rainfall. (b) zoom in of (a) around Hong Kong.

The ECEPS and the deterministic model are considered this paper because they are considered to be operationally the most accurate systems for tropical cyclones. It is shown in the verification webpages of tropical cyclones of ECMWF, e.g., about the number of typhoons in each year over the last 20 years in the western North Pacific, the error in the annual number of typhoons is in the order of 3, and the correlation between the predicted and the actual number of typhoons are very high. At least in the Atlantic Ocean (e.g., in the study https://iacweb.ethz.ch/doc/publications/TC_MasterThesis.pdf, which has been accessed on January 6, 2024), the track errors are verified to be rather small so

that the model is considered to be skilful. However, the monsoon depression in the present study is rather weak. It could be difficult for global models to capture the intensity of tropical cyclones well due to a number of limitations, the major one being the cumulus parameterization (*Wang and Tan, 2023*). As such, it is not surprising that the present modeling systems are not satisfactory for a rather weak monsoon depression.

3. Conclusions

The life of a weak monsoon depression is documented in this paper. It has a lifespan of around 10 days and, to the knowledge of the author, it is a rather long lived monsoon depression in this part of the world. Thermodynamically speaking, there could be chance for the system to further intensify into a tropical cyclone. This is supported by ECMWF model forecasts. There is also a burst of southwest monsoon that could feed more energy and moisture into the system. The sea surface temperature was also favorable, which was measured to be around 28 to 29 °Celsius in Hong Kong. The monsoon depression failed to develop further at the end, probably because of the rather weak horizontal shear, particularly the northern flank of the system (very weak easterly winds).

There are more weather observations in the northern part of the South China Sea, which provide unprecedented observations of the weak systems for the first time. It is hoped that this documentation of the monsoon depression would stimulate more studies of this kind of system in this part of the world.

References

- Boos, W.R., Hurley, J.V., and Murthy, V.S., 2015: Adiabatic westward drift of Indian monsoon depressions. Quart. J. Roy. Meteorol. Soc. 141(689), 1035–1048. <https://doi.org/10.1002/qj.2454>*
- Cohen, N.Y., and Boos, W.R., 2014: Has the number of Indian summer monsoon depressions decreased over the last 30 years? Geophys. Res. Lett. 41(22), 7846–7853. <https://doi.org/10.1002/2014gl061895>*
- Diaz, M. and Boos, W.R., 2019a: Barotropic growth of monsoon depressions. Quarterly Journal of the Royal Meteorological Society, 145(719), 824–844. <https://doi.org/10.1002/qj.3467>*
- Diaz, M. and Boos, W.R., 2019b: Monsoon depression amplification by moist barotropic instability in a vertically sheared environment. Quart. J. Roy. Meteorol. Soc. 145(723), 2666–2684. <https://doi.org/10.1002/qj.3585>*
- Hazra, V. and Pattnaik, S., 2021: Influence of cloud microphysical parameterization on the characteristics of monsoon depressions over the Indian region. Int. J. Climatol. 41, 6415–6432. <https://doi.org/https://doi.org/10.1002/joc.7203>*
- He, J.Y., Hon, K.K., Chan, P.W., and Li, Q.S., 2022: Dropsonde observations and numerical simulations for intensifying and weakening tropical cyclones over the northern part of the South China Sea. Weather 77, 332–338.*
- Hunt, K.M.R. and Parker, D.J., 2016: The movement of Indian monsoon depressions by interaction with image vortices near the Himalayan wall. Quart. J. Roy. Meteorol. Soc. 142(698), 2224–2229. <https://doi.org/10.1002/qj.2812>*

- Hunt, K.M.R. and Turner, A.G., 2017: The effect of horizontal resolution on Indian monsoon depressions in the Met Office NWP model. *Quart. J. Roy. Meteorol. Soc.* 143(705), 1756–1771. <https://doi.org/10.1002/qj.3030>
- Hunt, K.M.R., Turner, A.G., and Parker, D.E., 2016: The spatiotemporal structure of precipitation in Indian monsoon depressions. *Quart. J. Roy. Meteorol. Soc.* 142(701), 3195–3210. <https://doi.org/10.1002/qj.2901>
- Hurley, J.V., and Boos, W.R., 2014. A global climatology of monsoon low-pressure systems. *Quart. J. Roy. Meteorol. Soc.* 141(689), 1049–1064. <https://doi.org/10.1002/qj.2447>
- Karmakar, N., Boos, W.R., and Misra, V., 2021: Influence of Intraseasonal Variability on the Development of Monsoon Depressions. *Geophys. Res. Lett.* 48(2). <https://doi.org/10.1029/2020gl090425>
- Krishnamurti, T.N., Martin, A., Krishnamurti, R., Simon, A., Thomas, A., and Kumar, V., 2013: Impacts of enhanced CCN on the organization of convection and recent reduced counts of monsoon depressions. *Climate Dynam.* 41, 117–134. <https://doi.org/10.1007/s00382-012-1638-z>
- Lodh, A., Routray, A., Dutta, D., George, J.P., and Mitra, A.K., 2022: Improving the prediction of monsoon depressions by assimilating ASCAT soil moisture in NCUM-R modeling system. *Atmos. Res.* 272. <https://doi.org/10.1016/j.atmosres.2022.106130>
- Murthy, V.S. and Boos, W.R., 2019: Quasigeostrophic Controls on Precipitating Ascent in Monsoon Depressions. *J. Atmos. Sci.* 77, 1213–1232. <https://doi.org/10.1175/jas-d-19-0202.1>
- Pottapinjara, V., Girishkumar, M.S., Ravichandran, M., and Murtugudde, R., 2014: Influence of the Atlantic zonal mode on monsoon depressions in the Bay of Bengal during boreal summer. *J. Geophys. Res.: Atmospheres*, 119, 6456–6469. <https://doi.org/10.1002/2014jd021494>
- Rastogi, D., Ashfaq, M., Leung, L.R., Ghosh, S., Saha, A., Hodges, K., and Evans, K., 2018: Characteristics of Bay of Bengal Monsoon Depressions in the 21st Century. *Geophys. Res. Lett.* 45, 6637–6645. <https://doi.org/10.1029/2018gl078756>
- Ray, A. and Sil, S., 2022: Monsoon depressions and air-sea interactions during different phases of monsoon intraseasonal oscillation. *Climate Dynam.* 60, 851–866. <https://doi.org/10.1007/s00382-022-06352-8>
- Suhas, D.L. and Boos, W.R., 2023: Monsoon Depression Amplification by Horizontal Shear and Humidity Gradients: A Shallow Water Perspective. *J. Atmos. Sci.* 80, 633–647. <https://doi.org/10.1175/jas-d-22-0146.1>
- Vinodkumar, Chandrasekar, A., Alapaty, K., and Niyogi, D., 2009: Assessment of Data Assimilation Approaches for the Simulation of a Monsoon Depression Over the Indian Monsoon Region. *Bound-Lay. Meteorol.* 133, 343–366. <https://doi.org/10.1007/s10546-009-9426-y>
- Vishnu, S., Francis, P.A., Shenoi, S.S.C., and Ramakrishna, S.S.V.S., 2016: On the decreasing trend of the number of monsoon depressions in the Bay of Bengal. *Environ. Res. Lett.* 11, 1–12. <https://doi.org/10.1088/1748-9326/11/1/014011>
- Wang X. and Tan X.M., 2023: On the Combination of Physical Parameterization Schemes for Tropical Cyclone Track and Intensity Forecasts in the Context of Uncertainty. *J. Adv. Modell. Earth Syst.* 15, e2022MS003381

IDŐJÁRÁS

*Quarterly Journal of the HungaroMet Hungarian Meteorological Service
Vol. 129, No. 1, January – March, 2025, pp. 53–68*

Assessment of climate change impact on temperature and rainfall trend in the Setifian High Plains of Algeria

Nour Elhouda Maria Chellil^{1,2,*} and Sabah Chermat^{1,3}

¹ *Laboratory Urban Project, City and Territory*

² *Department of Plant Biology and Ecology, Faculty of Nature and Life Sciences
Setif 1 University - Ferhat Abbas. El Bez, Setif, 19000, Algeria*

³ *Department of pharmacy, Faculty of Medicine, Setif 1 University
Ferhat Abbas. El Bez, Setif, 19000, Algeria*

**Corresponding Author E-mail: maria.chellil@univ-setif.dz*

(Manuscript received in final form January 20, 2024)

Abstract— Within the scope of the global climate change, monitoring and assessment of meteorological parameters gain growing importance. Hence, the analysis of long-term climate series having either increasing or decreasing trend, makes relevance to the weather patterns, and often provides further prediction of extreme meteorological events in the near future.

In this perspective, this research purposes to investigate and interpret temperature and rainfall trends as well as the effect of climate change in three main districts from the Setifian High Plains region, namely, Setif, Ain Oulmene, and Boutaleb. Meteorological data were extracted from the TerraClimate dataset available at the Google Earth Engine platform over a 42-year-long period (from 1980 to 2021). Mann-Kendall, Spearman's rho, and Şen's trend tests were used to assess the trend, while Pettitt's test was applied to detect the change point in time series data. The Theil-Sen approach was used to estimate the slope magnitude in the series. Results showed significant increasing trends in the minimum, maximum, and average temperatures over time for all the three stations. The magnitude of the upward trend in temperature data was found to be at the rate of 0.023 to 0.03 °C per year for all stations. Pettitt's test found the year 1998 as a change point both for the maximum and average annual temperatures for all stations, while the year 2013 was detected as a change point in the minimum temperature for Ain Oulmene and Boutaleb stations. However, rainfall showed non-significant decreasing trends at 5% significance level for all stations.

This study concludes that there is an increase in climate variability over the sampling period, which reveal the necessity of adopting the suitable adaptation strategies for facing the impact of climate change.

Key-words: Algeria, climate change, change point, Pettitt's test, rainfall, semi-arid, Şen's trend test, temperature, trend analysis

1. Introduction

In our era, it is inevitable to talk about enormous, chronic environmental problems and challenges without addressing climate change. It is usually described as a phenomenon that has plagued our planet, often by directly or indirectly affecting ecosystems, cropping systems, lives, and livelihood of the society (*Sharma et al.*, 2021). In last decades, global warming became dominant, and it can be felt in different parts of the globe due to the new technologies' increased contribution to greenhouse gas emissions in the atmosphere. This situation could get worse, because of the deterioration of the normal behavior of the hydrological and meteorological parameters, particularly in terms of rainfall patterns and temperature. Various researches from different parts of the world found, that there are less rains and more elevated mean temperatures in average as a result of climate change. These changes will in turn lead to various weather events such as droughts, storms, floods, and heat waves (*Riedy*, 2016) either seeing at the global or regional scales. Therefore, due to changes in the water cycle and increased demands on water resources, the majority of people today experience food and water insecurity, especially in areas that are dry or semi-arid and have extremely erratic, inadequate, and unexpected rainfall events.

The Mediterranean area is one of the most responsive regions to global climate change (*Giorgi*, 2006), due to its location between the arid-warm climate of North Africa and the rainy, temperate climate of central Europe (*Giorgi and Lionello*, 2008). Based on global climate projections, the Mediterranean region's temperature will increase from 2 °C to 3 °C by 2050 and from 3 °C to 5 °C by 2100 (IPCC, 2007). Like the most countries of the Mediterranean Basin, Algeria has threatened, over time, by numerous meteorological hazards, and it tends to be more vulnerable to the impacts of climate change, because most parts of the country fall under arid and semi-arid climates. A study on analysis of drought showed that the northern part of Algeria will experience more dry periods, and the probability of occurrence of extreme events will increase from 0.2650 in 2005 to 0.5756 in 2041 (*Lazri et al.*, 2015). In this context, several studies across the northeast part of Algeria concluded, that arid and semi-arid zones have experienced a larger number of drought events with a significant warming, while the humid and sub-humid locations received more precipitation events (*Merabti et al.*, 2017; *Beldjazia et al.*, 2019).

In the Setifian High Plains region, where the climate is typically semi-arid, the climate change is on the rise due to its sensitive location, which conceives of the transition and interaction between the country's humid north and dry south climates. Considering the impact of climate change and other factors such as population growing, industrial and agro-pastoral activities, water deficit and land degradation are already in a critical level in this region. As per *Rouabhi* (2017), the performance of precipitation during the period 1991–2011 became slightly different and spatially more heterogeneous in the Setif region. Hence, a study of

projecting future climate established by *Bouregaa and Fenni (2014)* found, that there will be a consistent increase in seasonal temperatures until 2075, despite the rainfall models' predictions of large seasonal variations. Since the issues related to the climate change effects on the Setifian High Plains area are less investigated, such identification and monitoring studies spanning past, present, and future times are crucial. For this reason, the assessment of local weather should receive particular interests for better understanding of the risks and challenges associated with the climate variation in this region.

One of the most essential tools of recognizing whether there is a rise, fall, or no change in meteorological variables is to examine their historical time series, especially with application of effective trend identification tests. Typically, numerous trend tests exist, which can be categorized according to the parametric or nonparametric methods. Furthermore, parametric trend tests are more powerful than nonparametric ones (*Shadmani et al., 2012*). However, unlike the nonparametric trend methods that do not consider any assumption, the normal distribution should be followed when obtaining data for the parametric trend testing. In this context, a large number of scientists have targeted temperature and rainfall trends worldwide, employing various statistical techniques (*Alemu and Dioha, 2020; Ragatoa et al., 2018; Sharma et al., 2021; Yacoub and Tayfour, 2019; Patel and Mehta, 2023, Panwar et al., 2018; Deb and Sil, 2019*).

The Mann-Kendall (MK test) and the Spearman's rho test (SR test) are two nonparametric tests commonly used to detect upward or downward trends in series of hydrometeorological and environmental data. These tests can deal with non-normal data, missing values, seasonality, censoring (detection limits), and serial dependence (*Hirsch and Slack, 1984*).

The Sen's detection trend test is an innovative trend analysis method, which is performed to detect the trend in the time series, especially in terms of low, medium, and high values of the data. This method is valid independently of the sample size, serial correlation structure of the time, and non-normal probability distribution functions (*Şen, 2012*).

The Theil-Sen approach is another nonparametric test used for the detection of trends in time series analysis. It is also used to compute the linear rate of change (slope) (*Hirsch et al., 1982*). The Pettitt's test method (*Pettitt, 1979*) is usually employed to detect an abrupt change or a step change in time records.

The overall objective of this research is to clearly investigate the trend analysis of temperature and rainfall in the Setifian High Plains region focusing on three main districts: Setif, Ain Oulmene, and Boutaleb over a 42-year-long period through application of different nonparametric approaches. The MK test, the SR test, and the Şen's trend test were applied as a first attempt to identify the trends in the time series. Thereafter, the Theil-Sen approach was used to estimate the trend magnitude, while the Pettitt's test was used to detect the breaking year or the change point in the time series data. Moreover, this work aims to monitor the evolution of local climate for better looking at the effects of the climate change in

the study area. Indeed, the results obtained were a function of help for local populations and decision makers to achieve the suitable adaptations strategies in the field of sustainable development to face climate change.

2. Study area and data used

2.1. Study area

The Setifian High Plains region is located in the northeastern part of Algeria, which lies in the administrative area of the Setif province between 35° to 36° 9' N and 5° to 6° E (*Fig. 1*). Geographically, it is limited to the north by the Babor mountain chain and to the south by the El Hodna mountain chain with an area of about 4076.62 km². The region has a continental semi-arid climate. The annual rainfall of the region is varying from 443.31 mm to 334.44 mm from the north to the south, respectively. The hot season lasts for almost five months in the year, in which it starts from May and end up in September. The region has long been a favorable territory for agro-pastoral activities, which constitute high importance for the country by ensuring food security. As shown in *Fig. 1*, three pilot districts from the Setifian High Plains region, namely Setif (station 1), Ain Oulmene (station 2), and Boutaleb (station 3) were considered to this study. The geographical location of stations with corresponding mean values for the metrological variables are summarized in *Table 1*. The annual average of rainfall (1980–2021) in the study area varies from 334.44 mm in Boutaleb station to 360.82 mm in Ain Oulmene station, while Setif station receives the most of rainfall with an average of 443.31 mm. The mean annual values of minimum and maximum temperatures for the selected stations range from 8.61 °C to 8.83 °C and from 20.62°C to 20.85°C, respectively, while the mean annual value of average temperature is found to vary between 14.71 °C to 14.81°C.

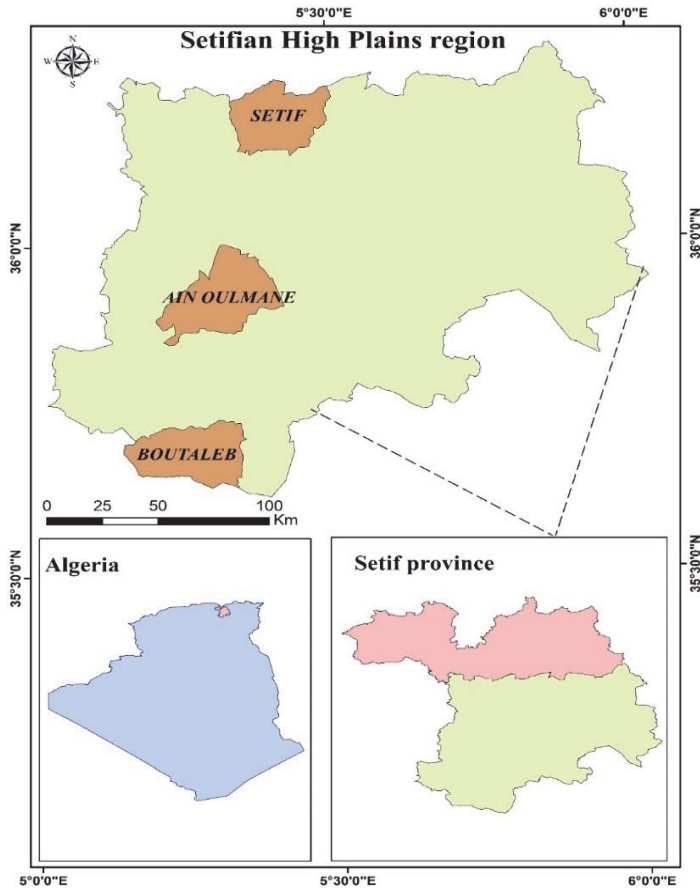


Fig. 1. Location of the study area.

Table 1. Geographic coordinates of the stations with their annual mean values for the meteorological variables for the period 1980-2021.

District	Lat (°N)	Long (°E)	Alt (m)	P (mm)	T _{min} (°C)	T _{max} (°C)	T _{avg} (°C)
Setif (station 1)	36.15	5.43	948-1224	443.31	8.79	20.62	14.71
Ain Oulmene (station 2)	35.90	5.28	900-1272	360.82	8.83	20.79	14.81
Boutaleb (station 3)	35.66	5.32	680-1767	334.44	8.61	20.85	14.73

2.2. Data used

To study the situation, trend of monthly series of temperature and rainfall data ranging from 1980 to 2021 (42 years) were collected from the TerraClimate dataset available for downscaling at the Google Earth Engine platform. This dataset of a high-spatial resolution ($1/24^\circ$, ~ 4 km) is derived from the combination of the high spatial resolution of the WorldClim dataset and the high temporal resolution of other sources such as the Climate Research Unit global climate dataset (CRU Ts4.0), and the Japanese 55-year Reanalysis (JRA-55) (Abatzoglou *et al.*, 2018). It allows obtaining for global terrestrial surfaces monthly climate and climatic water balance data of various elements (rainfall, maximum and minimum temperatures, wind speed, evapotranspiration, and solar radiation). The selected data are of good quality having continuous record since 1958, which make it well suited for climatic and hydrological studies (Salhi *et al.*, 2019; Kessabi *et al.*, 2021; Khan *et al.*, 2020).

Further, to understand the possible impact of the climate change on regimes, characteristics, and variability for different climatic components, a regional-scale research is particularly important. Thus, rainfall as well as minimum and maximum temperature data were used as key meteorological elements in the current investigation, to find annual trends and monitor changes over the time period. The mean monthly data of rainfall is extracted for the years 1980–2021 (42 years), whereas the monthly average temperature is computed by using averaging function for available data of minimum and maximum temperatures in the corresponding month.

3. Methodology

Trend analysis is one of the most frequently performed techniques to give an idea about the variation in the meteorological parameters attributable to the potential climate change effects. In this study, different methods are adopted for computing the annual time series trends of temperature and rainfall data over a 42-year-long period (1980–2021). Firstly, the statistical Mann-Kendall (MK) and Spearman's rho (SR) tests, besides the graphical approach of Şen's test are useful to identify the existence of trend, whether it is rising or falling. Next, the Theil-Sen method (Theil, 1950; Sen, 1968) is employed to find the proper slope magnitude. Finally, the Pettitt's test is applied to detect the change point in the time series (Pettitt, 1979).

A brief description of the methods adopted for the analysis is presented as follows.

3.1. Mann–Kendall test

This is a well-known nonparametric test that was developed by *Mann* (1945) and *Kendall* (1975). It is also performed to statistically detect monotonic upward or downward trends in a series of climate data. The MK test is based on two hypotheses; the null hypothesis (H_0) expresses the no existence of trend, which means the data are identically distributed, while the alternative hypothesis (H_1) elucidates that the variable follows a significant rising or declining trend in time (*Shadmani et al.*, 2012).

Let x_1, x_2, \dots, x_n represent n data points where x_j represents the data point at time j . Then the Mann-Kendall statistic (S) is calculated as:

$$S = \sum_{k=1}^{n-1} \sum_{j=k+1}^n \text{sgn} (x_j - x_k) , \quad (1)$$

where the sign function is given as:

$$\text{sgn} (x_j - x_k) = \begin{cases} +1 & \text{if } x_j > x_k \\ 0 & \text{if } x_j = x_k \\ -1 & \text{if } x_j < x_k \end{cases} . \quad (2)$$

x_j and x_k refer to the sequential data values of the time series, n is the data set record length. In case where n is superior than 10, S is calculated by the original variance of S as

$$\text{Var} (S) = \frac{n(n-1)(2n+5) - \sum_{i=1}^p t_i(t_i-1)(2t_i+5)}{18} , \quad (3)$$

where p is the number of tied groups and t_i is the number of data points in the p^{th} group.

A very high positive value of S represents an indicator of an increasing trend, while a very low negative value signifies a trend of decreasing performance over time. However, for statically quantify the significance of trend, it is necessary to compare the significance level α with the computed probability P value. If P value tends to be less than 5%, it denotes significant trend, while, the reverse is true if P value is greater than 5%, and this indicates the absence of trend in the data.

3.2. Spearman's rho test

The Spearman's rho (SR) test is another rank-based nonparametric statistical test that can also be used to detect monotonic trend in time series (*Yue et al.*, 2002). Charles Spearman initially proposed it in 1904, nevertheless, this test is widely used to check the validity of one of the two traditional hypotheses. The null hypothesis (H_0) is that all the data in the time series are independent and identically distributed, while the alternative hypothesis (H_1) is that increasing or

decreasing trend exists (Shadmani et al., 2012). The SR statistic (D) is given by the following formula:

$$D = 1 - \frac{6 \sum_{i=1}^n (R_i - i)^2}{n(n^2 - 1)}, \quad (4)$$

where R_i is the rank of the i th observation X_i in the time series and n is the sample size. According to the SR statistic, positive D values indicate upward trends, while negative values indicate downward trends in the time series. At the significance level of 5%, if $P \leq 0.05$, then the existence of trend is considered statically significant.

3.3. Şen's trend test

This innovative approach developed by Şen (2012) aims for extracting trend graphically. First, in order to evaluate trend in meteorological variables, time series are divided into two equal halves, and then they are independently ranked in ascending (or descending) order (Wu and Qian, 2017). In practical applications, a scatter of points along the 1:1 (45°) straight-line implies no trend, and accordingly, any plot appearance above (below) this line reveals increasing (decreasing) trends (Şen, 2012). To make a detailed interpretation, the scatter diagram is split into three verbal clusters as low, medium, and high data values (Pastagia and Mehta, 2022).

3.4. Theil-Sen approach

This approach (Theil, 1950; Sen, 1968) is commonly used to provide the magnitude of the slope (change per unit time) after the trend detection has been assessed by both the MK and SR tests within the time series. It is another nonparametric method based on the median slope, which can be calculated as:

$$\beta = \text{median} \left[\frac{X_j - X_i}{j - i} \right] \quad \text{for all } i < j, \quad (5)$$

where X_i and X_j denote the sequential data values of the time series in the years i and j , and β is the estimated magnitude of the trend slope in the data series.

3.5. Pettitt's test

As a typical nonparametric approach to study change point problems, the Pettitt's test method (Pettitt, 1979) has been widely used to detect an abrupt change or a step change in the mean value of the distribution of hydrometeorological variables (Xie et al., 2013). When a sequence of random variables with n sample size is divided into two samples (X_1, X_2, \dots, X_t) and ($X_{t+1}, X_{t+2}, \dots, X_n$), then the sudden

change point in record is assumed to occur at time t . The test statistic U_t can be generated as:

$$U_t = \sum_{i=1}^t \sum_{j=i+1}^n \text{sgn}(x_i - x_j), \quad (6)$$

where the sign function is given as:

$$\text{sgn}(x) = \begin{cases} +1 & \text{if } x > 0 \\ 0 & \text{if } x = 0 \\ -1 & \text{if } x < 0 \end{cases}. \quad (7)$$

The maximum probable and significant change point $|U_t|$, affected mostly at time t , is approximately evaluated by the following formula:

$$P(t) = 2 \exp\left(\frac{-6U_t^2}{n^2 + n^3}\right). \quad (8)$$

Note that if p value is inferior to the significance level $\alpha = 0.05$, the alternative hypothesis is accepted, and a statically significant change point exists at the time t .

In this research, the statistical significance of trends and their breakpoints in time series analyzed by the MK, SR, and Pettitt's tests are conducted utilizing the *trend* package in the *Rstudio* software, while the *ggplot2* package was used to plot the graphs of Şen's trend.

4. Results and discussions

4.1. Temperature trends

MK, SR, and Şen tests were used to assess the trends for minimum, maximum, and average annual temperatures, while Pettitt's test was applied to detect the change point in time series of each stations data from 1980 to 2021. The summary of practical results is presented in *Table 2*.

It is clear from *Table 2*, that the analysis of annual temperatures shows a positive trend for the three stations. The MK and SR tests indicate similar results revealing that a significant increasing trend exists consistently for the minimum, maximum, and average annual temperatures with $P \leq 0.05$ at all the three stations.

Beside the identification of the existence of trends by the MK and SR tests, the Theil-Sen approach may also conducted to estimate the magnitude of the slope (change per unit time). As given in *Table 2*, the slope of the significant increasing trend in the average annual temperature ranged from 0.025 °C/year at Setif to

0.027°C/year at Ain Oulmene, and 0.028 °C/year at Boutaleb. This result is somehow agree with that of *Boudiaf et al. (2020)*, who reported that the annual average temperature across the Setif region having a rising trend at a slope equals to 0.03. Our findings are also in accordance with the world situation, where the global surface temperature trend is about 0.02 ± 0.01 °C/year, while in the Mediterranean region, the trend is about 0.03°C/year (UNEP, 2020).

Table 2. Temperature analysis results detected by the MK, SR, Theil-Sen, and Pettitt’s tests at the 5% significance level.

Station	Annual temperature	MK (S)	P value	SR (D)	P value	Trend	B (rate of increase) (°C/year) 1980-2021	Pettitt’s test (change point)	B (rate of increase) (°C/year) 1980-2000	B (rate of increase) (°C/year) 2001-2021
Setif	T _{min}	335	0.000*	0.511	0.001*	Rising	0.023	—	0.036	0.046
	T _{max}	347	0.000*	0.559	0.000*	Rising	0.025	1998*	0.047	0.030
	T _{avg}	347	0.000*	0.553	0.000*	Rising	0.025	1998*	0.041	0.037
Ain Oulmene	T _{min}	345	0.000*	0.528	0.000*	Rising	0.023	2013*	0.035	0.056
	T _{max}	363	0.000*	0.576	0.000*	Rising	0.028	1998*	0.048	0.035
	T _{avg}	359	0.000*	0.560	0.000*	Rising	0.027	1998*	0.041	0.047
Boutaleb	T _{min}	335	0.000*	0.512	0.001*	Rising	0.025	2013*	0.036	0.062
	T _{max}	381	0.000*	0.604	0.000*	Rising	0.030	1998*	0.048	0.038
	T _{avg}	369	0.000*	0.570	0.000*	Rising	0.028	1998*	0.041	0.047

* Trends statistically significant at the 5% significance level

Similar significant increasing tendencies were seen in the annual maximum and minimum temperatures. The annual maximum temperature varied with the rates of 0.025 °C/year, 0.028 °C/year and 0.03 °C/year at stations Setif, Ain Oulmene, and Boutaleb, respectively. The same trend was seen in the annual minimum temperature, which varied between the rates of 0.023 °C/year at both Setif and Ain Oulmene stations to 0.025 °C/year at Boutaleb. It is clear from the results, that the observed rise in the annual average temperature is more influenced by the maximum than the minimum temperature. In general, the temperature increase results of this study are partially in agreement with the tendencies found by *Rouabhi et al. (2018)*, stating that the annual minimum temperature records the highest raise compared to the annual maximum temperature within the study period (1981–2015).

Moreover, the Sen's slope values calculated in two periods: 1980–2000 and 2001–2021 showed the increase of the average temperature in the first period (1980–2000) for Setif compared to Ain Oulmene and Boutaleb, where the rise is remarkable in the last period (2001–2021). Ultimately, these spatiotemporal variabilities of temperatures seem to indicate the potential evolution of the distribution of bioclimates in this territory, sometimes with the shift of a bioclimatic stage (*Djellouli et al., 2020*).

Based on the Pettitt's method for detecting the sudden changes in the annual temperatures (minimum, maximum, and average), our results show that it can be found two significant change points, which were detected in 1998 for both the maximum and average annual temperatures at all stations. Whereas the time change point for the minimum annual temperature is noticed in the year 2013, except for Ain Oulmene and Boutaleb stations (*Table 2*). This suggests that the maximum temperature reflects on a quick variability under climate change effect, while the minimum and average temperature are affected tardier. It should be also noted that the two breaking years that occurred in 1998 and 2013 are in conformity with the extent of the global warming trend. Meteorological specialists have determined that 2013 and 1998 are ranked as the fifth and eighth hottest years on record since 1880 (NOAA, 2017).

In terms of the evaluation of low, medium, and high values of the annual temperatures (minimum, maximum, and average), the Sen trend graphs reveal that all the three stations exhibited similar temperature variabilities. Hence, via the layout of the scatter point that is well concentrated above the line, an upward trend is clearly determined. It is also observed that the medium clusters have much higher distribution and tend to increase more than the low and high clusters (*Fig. 2*).

The overall interpretation for the results discussed above is that the impact of climate change appears more influential and earlier detectable at Boutaleb station followed by Ain Oulmene and Setif stations. This can be explained by the geographic position of Boutaleb, which is located in the extreme southern part of the study region in confrontation with the warmly Sirocco wind coming from the Sahara, especially during the summer and autumn periods. Consequently, this situation calls for more drought events and a hotter climate in the entire Setifian High Plains region.

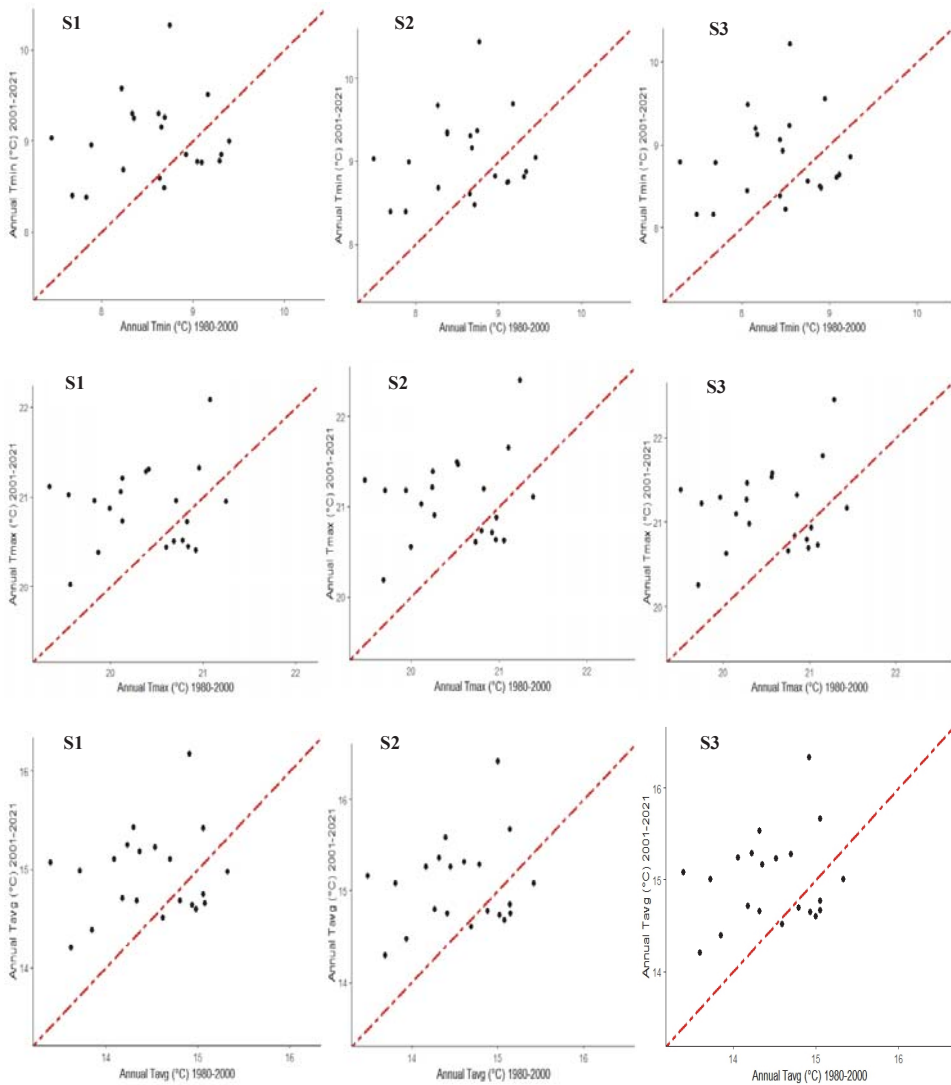


Fig. 2. Annual minimum, maximum and average temperatures (°C) at Setif (S1), Ain Oulmene (S2), and Boutaleb (S3) stations by Şen's trend test in the period of 1980-2021.

4.2. Rainfall trends

Trend analysis of the annual rainfall was carried out on the time series of the three main stations of Setif, Ain Oulmene, and Boutaleb. It is clear from the results presented in *Table 3*, that the MK and SR tests show the same results at all the

stations by detecting non-significant decreasing trends during the investigated period (1980–2021).

Correspondingly, an overall trendless is observed through the data group behaviors in the Şen graphs. As it is shown in Fig. 3, for all three stations, the scatter point distributes on both sides of the 1:1 line. This plot appearance implies that the increasing and decreasing tendencies occurred within the same time clearly indicating a non-monotonic trend in rainfall. *Boudiaf et al. (2021)* also reported that rainfall in Setif region has a decreasing trend during the period 1982–2019.

Investigating of changes in climate variables reflects that higher temperatures and reduced amount of rainfall will increase the risk in water availability inducing a significant vulnerability in the Setifian High Plains region by progressively modifying its bioclimatic stage from semi-arid to arid.

Table 3. Rainfall analysis results detected by the MK, SR, Theil-Sen, and Pettitt’s tests at the 5% significance level.

Station	MK (S)	P value	SR (D)	P value	Trend	B (rate of increase (mm/year))	Pettitt’s test (change point)
Setif	-61	0.516	-0.101	0.525	Falling	—	—
Ain Oulmene	-57	0.544	-0.089	0.5735	Falling	—	—
Boutaleb	-59	0.530	-0.084	0.5982	Falling	—	—

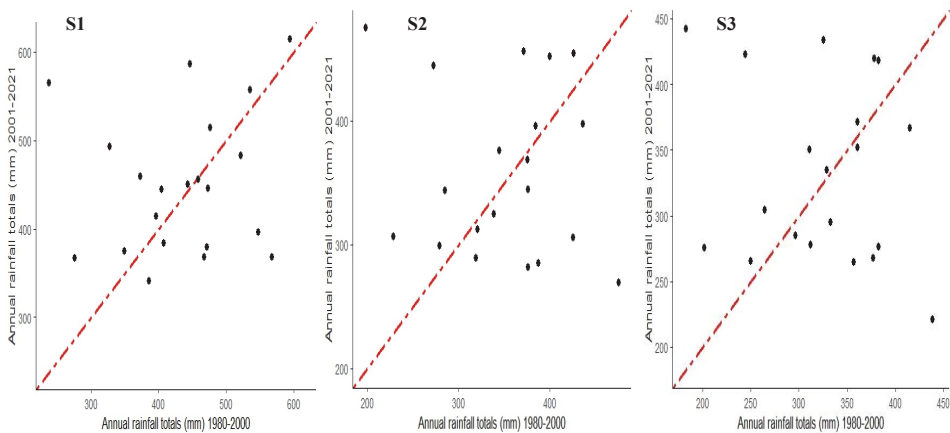


Fig. 3. Annual rainfall (mm) at Setif (S1), Ain Oulmene (S2), and Boutaleb (S3) stations by Şen’s trend test from 1980 to 2021.

5. Conclusions

In the present research, we performed a trend analysis of temperature and rainfall under climate change over the Setifian High Plains region in Algeria, focusing on three major stations: Setif, Ain Oulmene, and Boutaleb. Based on a 42-year-long period (1980–2021), the annual temperature and rainfall time series were assessed by utilizing various nonparametric trend detection methods. It can be concluded that the overall significant increase trends of the temperature led to demonstrate the changes in temperature during last 42 years. Consequently, the annual average temperature is slightly increasing between 0.025 and 0.028 °C/year inducing a warming and more drought events in the region, which also falls under a semi-arid climate. For maximum and average annual temperatures, all the stations detect the year 1998 as an abrupt change, while the minimum temperature detects the year 2013 as change point particularly at Ain Oulmene and Boutaleb stations. Besides this, a declining trend appears in the annual rainfall time series also, for all stations, but it is not statistically significant. Therefore, increasing temperature and decreasing rainfall are already a major trouble that can affect the environment and threaten natural life.

Our findings of this study highlight the climatic variation in the whole studied region induced by the global trend of climate change. Furthermore, this contribution would serve as a useful guide for more effective monitoring and analysis on the effects of climate change, especially in semi-arid and arid climates, in order to help adopting suitable adaptation strategies and development decisions to face climate change.

References

- Abatzoglou, J.T., Dobrowski, S.Z., Parks, S.A., and Hegewisch, K.C., 2018: TerraClimate, a high-resolution global dataset of monthly climate and climatic water balance from 1958–2015. *Scientific Data* 5(170191), 1–12. <https://doi.org/10.1038/sdata.2017.191>
- Alemu, Z.A. and Dioha, M.O., 2020: Climate change and trend analysis of temperature: the case of Addis Ababa, Ethiopia. *Environ. Syst. Res.* 9(27), 1–15. <https://doi.org/10.1186/s40068-020-00190-5>
- Beldjazia, A., Missaoui, K., and Allatou, D., 2019: Thermal Disturbances and their Impact on Vegetation Productivity in Natural Reserve of Beni Salah (North East of Algeria) from 1986 to 2015. *World J. Environ. Biosci.* 8(1), 81–91.
- Boudiaf, B., Dabanli, I., Boutaghane, H., and Şen, Z., 2020: Temperature and Precipitation Risk Assessment Under Climate Change Effect in Northeast Algeria. *Earth Syst. Environ.* 4, 1–14. <https://doi.org/10.1007/s41748-019-00136-7>
- Boudiaf, B., Şen, Z., and Boutaghane, H., 2021: Climate change impact on rainfall in north-eastern Algeria using innovative trend analyses (ITA). *Arabian J. Geosci.* 14(511), 1–18. <https://doi.org/10.1007/s12517-021-06644-z>
- Bouregaa, T. and Fenni, M., 2014: Assessment of inter-seasonal temperature and precipitation changes under global warming over Setif high plains region, vulnerability and adaptation. *World J. Sci. Technol. Sustain. Develop.* 11, 304–314. <https://doi.org/10.1108/wjstsd-05-2014-0005>

- Deb, S. and Sil, B.S., 2019: Climate change study for the meteorological variables in the Barak River basin in North-East India. *Urban Climate* 30, 100530. <https://doi.org/10.1016/j.uclim.2019.100530>
- Djellouli, Y., Louail, A., Messner, F., Missaoooui, K., and Gharzouli, R., 2020: The natural ecosystems of eastern Algeria facing the risk of climate change. *Geo-Eco-Trop* 44, 609-621.
- Giorgi, F., 2006: Climate change hot-spots. *Geophys. Res. Lett.* 33(8), 1–4. <https://doi.org/10.1029/2006GL025734>.
- Giorgi, F. and Lionello, P., 2008. Climate change projections for the Mediterranean region. *Global Planet. Change* 63(2–3), 90–104. <https://doi.org/10.1016/j.gloplacha.2007.09.005>
- Hirsch, R.M., Slack, J.R., and Smith, R.A., 1982: Techniques of trend analysis for monthly water quality data. *Water Resour. Res.* 18, 107–121. <https://doi.org/10.1029/WR018i001p00107>
- Hirsch, R.M. and Slack, J.R., 1984: A nonparametric trend test for seasonal data with serial dependence. *Water Resour. Res.* 20, 727–732. <http://dx.doi.org/10.1029/WR020i006p00727>
- IPCC, 2007: Climate Change: The Physical Science Basis. Contribution of Working Group I to the Fourth Assessment Report of the Intergovernmental Panel on Climate Change. Cambridge University Press, 996. [online] <https://www.ipcc.ch/report/ar4/wg1/> Accessed on 26/11/ 2023.
- Kendall, M.G., 1975: Rank Correlation Methods. *J. Inst. Actuaries* 75(1), 140–141. <https://doi.org/10.1017/S0020268100013019>
- Khan, R., Gilani, H., Iqbal, N., and Shahid, I., 2020: Satellite-based (2000-2015) drought hazard assessment with indices, mapping, and monitoring of Potohar plateau, Punjab, Pakistan. *Environ. Earth Sci.s* 79(1), 1–18. <https://doi.org/10.1007/s12665-019-8751-9>
- Kessabi, R., Hanchane, M., and Belmahi, M., 2021: Estimation of climatic drought indices according to TerraClimate data and those from measurement stations (case of five station in the Fez-Meknes region). Proceedings of Climate change, earthly potentialities and environmental justice Conference, 163–181.
- Lazri, M., Ameur, S., Brucker, J. M., Lahdir, M., and Sehad, M., 2015: Analysis of drought areas in northern Algeria using Markov chains. *J. Earth Syst. Sci.* 124(1), 61–70. <https://doi.org/10.1007/s12040-014-0500-6>
- Mann, H.B., 1945: Nonparametric Tests Against Trend. *Econometrica: J. Econometric Soc.* 13, 245–259. <https://doi.org/10.2307/1907187>
- Merabti, A., Meddi, M., Martins, D., and Pereira, L., 2017: Comparing SPI and RDI applied at local scale as influenced by climate. *Water Resour. Manage.* 32, 1071–1085. <https://doi.org/10.1007/s11269-017-1855-7>.
- NOAA, 2017: Monthly Global Climate Report for Annual 2016. [online] <https://www.ncei.noaa.gov/access/monitoring/monthly-report/global/201613> Accessed on 20/11/2023.
- Panwar, M., Agarwal, A., and Devadas, V., 2018: Analyzing land surface temperature trends using non-parametric approach: A case of Delhi, India. *Urban Climate* 24, 19–25. <https://doi.org/10.1016/j.uclim.2018.01.003>
- Pastagia, J. and Mehta, D., 2022: Application of innovative trend analysis on rainfall time series over Rajsamand district of Rajasthan state. *Water Supply* 22, 7189–7196. <https://doi.org/10.2166/ws.2022.276>
- Patel, S. and Mehta, D., 2023: Statistical analysis of climate change over Hanumangarh district. *J. Water Climate Change* 14, 2029–2041. <https://doi.org/10.2166/wcc.2023.227>
- Pettitt, A.N., 1979: A non-parametric Approach to the Change-point Problem. *Applied Statistics* 28(2), 126–135. <https://doi.org/10.2307/2346729>
- Ragatoa, D.S., Ogunjobi, K.O., Okhimamhe, A.A., Francis, S.D., and Adet, L., 2018: A Trend Analysis of Temperature in Selected Stations in Nigeria Using Three Different Approaches. *Open Access Library J.* 5(e4371), 1–18. <https://doi.org/10.4236/oalib.1104371>
- Riedy, C., 2016: Climate Change. In: (Ed.:Ritzer G.) *The Blackwell Encyclopedia of Sociology*. John Wiley and Sons, 1-8. <https://doi.org/10.1002/9781405165518.wbeos0737>
- Rouabhi, A., 2017: Spatiotemporal characterization of the annual rainfall in Setif region-Algeria. *Agricult. J.* 8(1), 31–38.
- Rouabhi, A., Kebiche, M., Hafsi, M., and Monneveux, P., 2018: Climate change during the last century in Sétif province, Algeria. *Agricult. J.* 8(2), 61–75.

- Salhi, A., Martin-Vide, J., Benhamrouche, A., Benabdelouahab, S., Himi, M., Benabdelouahab, T., and Casas Ponsati, A., 2019: Rainfall distribution and trends of the daily precipitation concentration index in northern Morocco: a need for an adaptive environmental policy. *SN Appl. Sci.* 1(277), 1–15. <https://doi.org/10.1007/s42452-019-0290-1>
- Sen, P.K., 1968: Estimates of the Regression Coefficient Based on Kendall's Tau. *J. Amer. Stat. Assoc.* 63(324), 1379–1389. <https://doi.org/10.1080/01621459.1968.10480934>
- Şen, Z., 2012: Innovative Trend Analysis Methodology. *J. Hydrol.Engin.* 17, 1042–1046. [https://doi.org/10.1061/\(ASCE\)HE.1943-5584.0000556](https://doi.org/10.1061/(ASCE)HE.1943-5584.0000556)
- Shadmani, M., Marofi, S., and Roknian, M., 2012: Trend Analysis in Reference Evapotranspiration Using Mann-Kendall and Spearman's Rho Tests in Arid Regions of Iran. *Water Resour. Manage.* 26(1), 211–224. <https://doi.org/10.1007/s11269-011-9913-z>
- Sharma, S.K., Sharma, D.P., Sharma, M.K., Gaur, K., and Manohar, P., 2021: Trend Analysis of Temperature and Rainfall of Rajasthan, India. *J. Probability Stat.* 2021, 1–7. <https://doi.org/10.1155/2021/6296709>
- Theil, H., 1950: A rank-invariant method of linear and polynomial regression analysis. In: (Eds. Raj B. and Koerts J.) *Advanced Studies in Theoretical and Applied Econometric*. Vol. 23. Spring Dordrecht, 345-381. https://doi.org/10.1007/978-94-011-2546-8_20
- UNEP, 2020: SoDE State of the Environment and Development in the Mediterranean. Plan Bleu Regional Activity Centre. Marseille, France. [online] Accessed on 04/10/2023. <https://www.unep.org/resources/report/state-environment-and-development-mediterranean>
- Wu, H., and Qian, H., 2017: Innovative trend analysis of annual and seasonal rainfall and extreme values in Shaanxi, China, since the 1950s. *Int. J. Climatol.* 37, 2582–2592. <https://doi.org/10.1002/joc.4866>
- Xie, H., Li, D., and Xiong, L., 2013: Exploring the ability of the Pettitt method for detecting change point by Monte Carlo simulation. *Stoch. Environ. Res. Risk Assess.* 28, 1643–1655. <https://doi.org/10.1007/s00477-013-0814-y>
- Yacoub, E. and Tayfour, G., 2019: Trend analysis of temperature and precipitation in Trarza region of Mauritania. *J. Water Climate Change* 10, 484–493. <https://doi.org/10.2166/wcc.2018.007>
- Yue, S., Pilon, P., and Cavadias, G., 2002: Power of the Mann-Kendall and Spearman'S rho tests for detecting monotonic trends in hydrological series. *J. Hydrology.* 259(1–4), 254–271. [https://doi.org/10.1016/S0022-1694\(01\)00594-7](https://doi.org/10.1016/S0022-1694(01)00594-7)

IDOJÁRÁS

*Quarterly Journal of the HungaroMet Hungarian Meteorological Service
Vol. 129, No. 1, January – March, 2025, pp. 69–87*

Assessment of hydroclimatic trends in Southeast Europe – Examples from two adjacent countries (Bosnia & Herzegovina and Serbia)

Ana Milanović Pešić^{1,2}, Dejana Jakovljević^{1,*}, Vesna Rajčević³, and
Slobodan Gnjato³

¹ *Geographical Institute “Jovan Cvijić” Serbian Academy of Sciences and Arts,
Djure Jakšića 9, 11000 Belgrade, Serbia*

² *L. N. Gumilyov Eurasian National University, Faculty of Natural Sciences, Department of
Physical and Economic Geography, Kazhymukan Street 13, 100008 Astana, Kazakhstan*

³ *University of Banja Luka, Faculty of Natural Sciences and Mathematics,
Mladena Stojanovića 2, 78000 Banja Luka,
Republic of Srpska, Bosnia and Herzegovina*

**Corresponding author. E-mail: d.jakovljevic@gi.sanu.ac.rs*

(Manuscript received in final form March 4, 2024)

Abstract— Water quantity is often analyzed throughout mean annual and seasonal discharges in various studies worldwide. This paper aims to present water discharge trends in the lower parts of the Una, Sana, and Vrbanja rivers in Bosnia and Herzegovina and the largest Serbian national river Velika Morava and its tributaries Jasenica and Resava rivers in Serbia for the period 1961–2020. Also, the paper examines air temperature and precipitation trends and their connection with discharge trends. Mann-Kendall test was applied for the determination of trends in air temperature, precipitation, and discharges; the Sen's nonparametric estimator was utilized for establishing the magnitude of the trend, while the t-test was used for determining the statistical significance of the trend. In order to determine possible changes, two periods were observed: 1961–1990 and 1991–2020. Results showed statistically insignificant changes in discharges and precipitation trends on annual and seasonal levels. On the other hand, a significant air temperature increase was recorded in the period 1991–2020, with the highest increase during the summer. The most significant increase was observed in Banja Luka due to urban heat island effect in this city.

Key-words: air temperature, discharge, precipitation, trends, Bosnia and Herzegovina, Serbia

1. Introduction

Water resources, including their quality, quantity, and availability, are vital in all aspects of life, human activities, and development. Considering their significance, knowledge of water resources, as well as water-related disasters, such as floods and droughts, is important for adequate water resources management.

Water quantity is often analyzed throughout mean annual and seasonal discharges. Discharges are usually studied regarding their dependence on recent climate change and variability. Opinions about their possible impacts are divided. While some studies found changes in climate elements (precipitation and air temperature) in recent years and their impacts on water quantity (*Zhong et al.*, 2021; *Rajčević and Mislicki-Tomić*, 2021), the other ones considered climate variability as an influence of cyclicity (*Arrieta-Pastrana et al.*, 2022), with no or insignificant changes in long-term period (*Balistrocchi et al.*, 2021).

Discharges are directly dependent on climatic elements, especially precipitation and air temperature. Previous studies researched trends of precipitation, air temperatures, and discharges, as well as their correlation. Researches have been done around the world: *Shrestha et al.* (2021) in Canada; *Xu et al.* (2021) in the Amu Darya River Basin in Central Asia; *Dissanayaka and Rajapakse* (2019) in the Kelani River basin in Sri Lanka; *Orkodjo et al.* (2022) in the Omo-Gibe basin in Ethiopia.

Many studies analyzed the connection between precipitation and discharge trends: *Zhong et al.* (2021) in the Yellow River basin in China; *Swain et al.* (2021) in the Brahmani and Baitarani River basins in India; *Manzano and Barkdoll* (2022) in Michigan; *Mallakpour et al.* (2018) in California; *Silva et al.* (2019) in Brazil; *Cuevas et al.* (2019) in Chile; *Talchabhadel et al.* (2021) in the west Rapti River basin in Nepal; *Maledé et al.* (2022) in the Birr River watershed in Ethiopia; *Balistrocchi et al.* (2021) in the Central Italian Alps.

Air temperature and discharge trends have also been the subject of various studies: *Ouyang et al.* (2017) in the Lower Mississippi River Alluvial Valley; *Jiang et al.* (2007) in the Tarim River basin in China; *Shahgedanova et al.* (2018) in the northern Tien Shan in Kazakhstan; *Singh et al.* (2010) in the Gangotri Glacier basin in Western Himalayas in India.

Climate change significantly influences the river regime in Bosnia and Herzegovina. The consequences are increase in occurrence of extremely dry periods and heavy rains, which cause floods (*Crnogorac and Rajčević*, 2019). However, a few researchers studied the impact of climate change on discharges in Bosnia and Herzegovina. In recent periods, annual and seasonal trends were analyzed in the lower parts of the Vrbas River from 1961–2016 (*Gnjato et al.*, 2019) and in the Sana River from 1961–2014 (*Gnjato*, 2018). Results showed a negative correlation between annual discharges and air temperature, while the connection between discharges and precipitation was positive. According to *Gnjato et al.* (2021), an analysis of annual and seasonal trends of climatic and

hydrological elements in the Sava River basin in Bosnia and Herzegovina shows a warming tendency in all seasons, while the precipitation trends are insignificant. *Rajčević and Mislicki-Tomić (2021)* emphasised air temperature increase in the Vrbanja River basin in the period 1961–2015, while the precipitation trends are negative. A statistically significant positive correlation is recorded between discharges and precipitation and a negative and insignificant correlation between discharges and air temperature. According to *Imamović and Trožić-Borovac (2013)*, a negative discharge trend is obtained for eight hydrological stations on the Bosnia River in the period 1961–1990.

In Serbia, mean annual and seasonal discharges were analyzed on 94 hydrological stations in the period 1961–2010 (*Kovačević-Majkić and Urošev, 2014*). *Dimkić (2018)* found a correlation between precipitation and discharge trends in the following periods: 1946–2006, 1946–2016, and 2007–2016. *Dorđević et al. (2020)* forecasted negative impacts of a decrease in precipitation and increased air temperatures on the discharge regime for the periods 2011–2040, 2041–2070, and 2071–2100, comparing with the control period 1971–2000. Annual discharge trends were also analyzed for Jablanica and Toplica rivers from 1950 to 2012 (*Gocić et al, 2016*), Zapadna Morava River basin in the period 1965–2014 (*Langović et al., 2017*), Velika Morava River (*Manojlović et al., 2016*) in the period 1967–2007. Air temperature trends were examined for Šumadija region in the period 1961–2010 (*Milanović Pešić and Milovanović, 2016*). *Milentijević et al. (2020)* analyzed air temperature and precipitation trends for Mačva region in the period 1945–2015. *Plavšić et al. (2016)* examined precipitation changes for Belgrade station (1923–2014), Loznica station (1952–2014), and Valjevo station (1949–2014). *Milanović Pešić (2015)* found that maximum values in precipitation in May and June in the Šumadija region are not in line with maximum discharges which occur in February and March due to increased evapotranspiration in May and June. During the period 1961–2015, the lowest discharges of the Šumadija rivers were recorded in August and September (*Milanović Pešić, 2019*). *Leščešen et al. (2022)* found decreasing discharges of Sava River on Sremska Mitrovica station for the period 1928–2017 as the consequence of decreasing precipitation and increasing temperature. *Haddeland et al. (2013)* projected the effects of changes in air temperature and precipitation on discharges in the Kolubara River basin and the Toplica River basin for the periods 2001–2030 and 2071–2100, compared with the control period 1961–1990. *Martić Bursać et al. (2022)* analyzed changes in air temperatures, precipitation, and discharges in Toplica River valley in the following periods: 1957–2018, 1957–1987, and 1988–2018. *Langović et al. (2023)* found significant cyclicality of mean annual discharges in the South (Južna) Morava River, from 1924 to 2021, which was mainly influenced by variation in the precipitation.

This paper aims to present a trend analysis of mean annual and seasonal discharges for selected rivers in Bosnia and Herzegovina and Serbia for the period 1961–2020. It examined whether the changes in discharges exist, whether they

occur on the annual or seasonal level, whether the changes are significant, and on what level of confidence. As discharges directly depend on climatic elements, the correlation between discharge trends in rivers with a natural regime and trends in precipitation and air temperatures in their basins was analyzed. This paper's primary objective is to explore the impact of recent climate change and variability on discharge trends in this region of Europe. One of the goals of this study is to determine whether river basins with significant changes exist in the study area, which is important for sustainable water resources management establishing.

2. Study area

The study area covers three rivers in central Serbia and Bosnia and Herzegovina, in the Republika Srpska (Fig. 1, Table 1). On the territory of Serbia, the largest national river Velika Morava and its tributaries, Jasenica River and Resava River, while in Bosnia and Herzegovina, the lower parts of the Una River, Sana River, and Vrbanja River were analyzed (Table 1).

Rivers with a natural regime with no or minor hydromorphological alteration were chosen in this study, making them more suitable for studying the connection between climate variables and discharges. There are no built dams on the selected rivers, and existing meanders were cut only on the Velika Morava in the 60s and 70s of the 20th century, in order to straighten the riverbed and minimize floods caused by the formation of ice barriers (Gavrilović and Dukić, 2014).

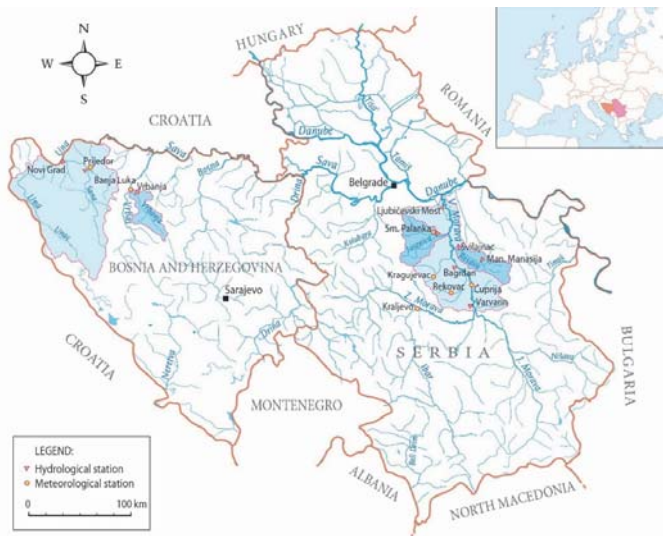


Fig. 1. The study area.

Table 1. Morphometric data of rivers. L: length of the river, F: surface of the river basin, I: total fall of the river, It: mean fall of the river.

	River	River Basin	L (km)	F (km ²)	Elevation of the source (m a.s.l.)	Elevation of the mouth (m a.s.l.)	I (m)	It (‰)
Bosnia and Herzegovina	Una	Sava	212	9980	376	94	2812	1.32
	Sana	Una	146	3782	440	116	324	2.21
	Vrbanja	Vrbas	96	804	1515	147	1368	14.24
Serbia	Velika Morava	Danube	175	6814	130.3	71	60	0.34
	Jasenica	Velika Morava	73	1417	705	92	613	8.43
	Resava	Velika Morava	66	681	668	93	575	8.78

The prevailing climate of the study area is moderate continental climate. According to the Köppen climate classification, this region belongs to the following types: Cfa – moderately warm and humid climate with hot summer, Cfb – moderately warm and humid climate with warm summer, and Dfb – moderately cold and humid climate with warm summer (Milovanović *et al.*, 2017). The region is influenced by the North Atlantic circulation and continental polar masses from northern Europe and western Siberia. The river basins are located in the middle of the temperate zone, in the area of frequent and intensive exchanges of tropical and polar air masses. According to Bajić and Trbić (2016), two action centers of atmospheric circulation impact climate features: the Azores anticyclone, which causes stable weather conditions and hot weather during the summer and the Icelandic cyclone, which brings precipitation. Precipitation increase is in correlation with high altitudes (Rajčević and Crnogorac, 2011).

In this study, data from 3 hydrological stations in Bosnia and Herzegovina and 6 hydrological stations in Serbia were used for hydrological analyses, and data from 2 meteorological stations in Bosnia and Herzegovina and 5 meteorological stations in Serbia were used for the analysis of air temperature and precipitation (Fig. 1).

3. Data and methods

For the rivers in Bosnia and Herzegovina, annual and seasonal discharges in the period 1961–2020 were calculated by using the data on mean monthly discharges from Novi Grad, Prijedor, and Vrbanja hydrological stations, located in the lower parts of the Una River, Sana River, and Vrbanja River, respectively. The selection of these three hydrological stations is a result of the non-existence of continuous long-term measurements at most rivers of Bosnia and Herzegovina. The analysis of annual and seasonal discharges on the rivers in Serbia for the same observation

period was made based on data on mean monthly discharges from hydrological stations Varvarin, Bagrdan, and Ljubičevski Most on the Velika Morava River, Smederevska Palanka on the Jasenica River, and Manasija and Svilajnac on the Resava River.

Analysis of the climatological dataset in the period 1961–2020 was performed based on mean monthly values of air temperatures and precipitation retrieved from two meteorological stations (Prijedor and Banja Luka) in Bosnia and Herzegovina and five meteorological stations (Ćuprija, Kragujevac, Kraljevo, Rekovac, and Smederevska Palanka) in Serbia. All hydrological and climatological data were acquired from the Republic Hydrometeorological Institute – Republic of Srpska (<https://rhmzrs.com/>) and the Republic Hydrometeorological Service of Serbia (<https://www.hidmet.gov.rs/>).

For determining monotonic positive/negative hydroclimatic trends in this study, a sixty-year time series of annual and seasonal values were submitted to the nonparametric Mann-Kendall (MK) test and the nonparametric Sen's estimator of the slope. The Mann-Kendall test is often used to examine trends in a data series. This test was proposed by *Mann* (1945) and further developed by *Kendall*. It is related to the Kendall's correlation coefficient (*Kendall*, 1975). It was further improved by *Hirsch et al.* (1982, 1984), who included seasonality. In addition, *Gilbert* (1987), *Helsel and Hirsch* (1992), and *Helsel et al.* (2020) later studied and improved this test. This test is used to statistically assess whether or not there is a linear monotonic upward or downward trend in the given time series data. There are three alternative hypotheses: there is no trend in the series, there is a negative trend, or there is a positive trend. The Mann-Kendall test analyses the differences between later-measured data and earlier-measured data. Each later measured value is compared with all values measured earlier, resulting in a total of $n(n-1)/2$ possible data pairs, where n is the total number of observations (*Helsel et al.*, 2020). The advantages of using the MK test are that it does not require the normal distribution of the data, not affected by missing data, irregular spacing of time points of measurements, and length of the time series. The limitation of the MK test is the tendency to give more negative results for shorter data series (*Helsel and Hirsch*, 1992).

If a significant trend for data series is found, the rate of change can be calculated using the Sen's slope estimator (*Helsel and Hirsch*, 1992). According to *Salmi et al.* (2002), this test is very convenient when a monotonic trend (without seasonal or cyclic variations) exists in the data. The Sen's method is very useful in slope estimation and shows changes in units per time. Also, it is not sensitive to errors and outliers.

The t-test is a widely used statistical test for comparing data of two groups. It is often used to examine whether the difference between the two groups is statistically significant or not. This test is usually applied when data sets follow a normal distribution. This test is called Student's t-test, after William Sealy Gosset,

who first published it in English in 1908 in the scientific journal *Biometrika* under the pseudonym "Student" (*Student*, 1908).

In this study, the MK test is used to identify a trend in the time series. At the same time, the Sen's nonparametric estimator is utilized to establish the trend's magnitude. The statistical significance of the identified trends was determined at the 99% ($p \leq 0.01$) and 95% ($0.01 < p \leq 0.05$) levels. Furthermore, to verify hydroclimatic trends in the studied river basins, mean annual and seasonal climatic and discharge values in two 30-year periods (1961–1990 and 1991–2020) were analyzed and compared. The t-test was applied to estimate the significance of distribution differences between the two periods.

For the calculations in this study, the Mann-Kendall test and the Sen slope incorporated in Excel 2010 software were used, as well as the t-test within the SPSS Statistics 20 software.

4. Results and discussion

4.1. Discharges

Rivers of various sizes and mean annual discharges are selected for this study, including two rivers with mean annual discharges above 200 m³/s, two rivers with mean annual discharges above 10 m³/s and three rivers with mean annual discharges below 10 m³/s (*Table 2*). The mean annual and monthly values of discharge and their MK trend values at the selected stations in the period 1961–2020 are presented in *Tables 2* and *3*, respectively. The lowest discharge was observed in the summer season in all three rivers in Bosnia and Herzegovina and at the most upstream station in Velika Morava River (Varvarin), while it was observed in the autumn season at the other two stations on the Velika Morava, as well as on the other analyzed rivers. The highest discharges were registered in the spring season at all rivers (*Table 2*). It could be addressed that the same values of multi-annual discharges are recorded during the winter and spring seasons on the Resava River (Manasija).

In the period 1961–2020, mean annual discharges showed a weak and negative trend change that has low significance or is not statistically significant on all rivers (*Table 3*). A moderate significant negative trend ($p \leq 0.05$) is recorded only at Varvarin (-0.94 m³/s/year). Similar results have been obtained for the same stations in Serbia in the previous studies. *Manojlović et al.* (2016) confirmed no statistically significant trend at Ljubičevski Most in the period 1967–2007. *Milanović Pešić* (2019) found low significant negative trends for the Ljubičevski Most and Bagrdan and trends with no statistical significance for other stations in the period 1961–2015. *Kovačević-Majkić* and *Urošev* (2014) also obtained the trends with no statistical significance in the period 1961–2010. *Gnjato et al.* (2021) found that negative discharge trends are recorded on the Sana and Vrbanja rivers.

Table 2 Annual and seasonal mean discharges at the selected hydrological stations in 1961–2020, 1991–2020, and 1961–1990 and differences between 1991–2020 and 1961–1990 (m³/s)

	Period	Year	Winter	Spring	Summer	Autumn
Bosnia and Herzegovina	Novi Grad – Una					
	1961–2020	217.7	266.8	311.7	121.0	171.1
	1961–1990	219.7	269.4	315.2	131.4	161.3
	1991–2020	215.7	264.0	308.1	110.6	180.8
	difference	-4.0	-5.4	-7.1	-20.8	19.5
	Prijedor – Sana					
	1961–2020	79.0	97.0	119.3	41.3	58.1
	1961–1990	81.6	98.2	122.5	47.7	57.5
	1991–2020	76.4	95.7	116.0	35.0	58.7
	difference	-5.2	-2.5	-6.5	-12.7	1.2
	Vrbanja – Vrbanja					
	1961–2020	15.6	19.1	23.8	10.3	9.1
1961–1990	16.4	21.0	24.2	11.1	9.4	
1991–2020	14.7	17.2	23.4	9.5	8.8	
difference	-1.7	-3.8	-0.8	-1.6	-0.6	
Serbia	Varvarin – Velika Morava					
	1961–2020	198.3	221.91	343.24	131.30	96.64
	1961–1990	212.29	243.60	360.82	143.87	100.84
	1991–2020	184.26	200.22	325.66	118.72	92.44
	difference	-28.03	-43.38	-35.16	-25.15	-8.4
	Bagrdan – Velika Morava					
	1961–2020	211.7	234.19	368.94	142.42	101.87
	1961–1990	223.29	256.90	381.05	154.91	107.07
	1991–2020	200.43	215.65	356.34	130.90	98.82
	difference	-22.86	-41.25	-24.71	-24.01	-8.25
	Ljubičevski Most – Velika Morava					
	1961–2020	229.0	252.26	396.18	159.85	109.21
	1961–1990	237.47	267.58	403.55	169.81	108.96
	1991–2020	221.28	236.94	388.82	149.90	109.47
	difference	-16.19	-30.64	-14.73	-19.91	0.51
	Manasija – Resava					
	1961–2020	3.56	6.43	6.43	2.79	1.48
	1961–1990	3.88	3.67	7.05	3.31	1.50
	1991–2020	3.24	3.42	5.81	2.28	1.46
	difference	-0.64	-0.25	-1.24	-1.03	-0.04
	Svilajnac – Resava					
	1961–2020	4.73	4.89	8.46	3.68	1.85
	1961–1990	5.05	4.92	8.93	4.32	1.98
	1991–2020	4.40	4.86	7.98	3.04	1.72
difference	-0.65	-0.06	-0.95	-1.28	-0.26	
Smederevska Palanka – Jasenica						
1961–2020	1.80	2.00	3.23	1.42	0.65	
1961–1990	1.72	2.16	3.35	1.52	0.64	
1991–2020	1.65	1.85	3.11	1.22	0.59	
difference	-0.07	-0.31	-0.24	-0.3	-0.05	

Table 3. Trends in annual and seasonal mean discharges at the selected hydrological stations in 1961–2020

	Station	River	Year	Winter	Spring	Summer	Autumn
Bosnia and Herzegovina	Novi Grad	Una	-0.48	-0.86	-0.03	-0.65	-0.14
	Prijedor	Sana	-0.27	-0.30	-0.05	-0.38	-0.14
	Vrbanja	Vrbanja	-0.07	-0.21	-0.02	<i>-0.09</i>	-0.07
	Varvarin	Velika	<i>-0.938</i>	-1.051	-1.529	-0.259	-0.068
	Bagrdan	Morava					
		Velika	-0.728	-0.851	-1.003	-0.026	0.042
Serbia	Ljubičevski Most	Velika	-0.494	-0.564	-0.668	-0.060	0.248
		Morava					
	Manasija	Resava	-0.015	-0.003	-0.028	-0.014	0.003
	Svilajnac	Resava	-0.010	-0.004	-0.012	-0.020	0.000
	Smed. Palanka	Jasenica	-0.009	-0.013	0.002	-0.008	-0.005

Statistical significance: $p \leq 0.01$ and $p \leq 0.05$

The comparative analyses of mean annual discharges between two 30-year periods displayed an insignificant decrease in 1991–2020 compared to the period 1961–1990 at all analyzed hydrological stations in Bosnia and Herzegovina and Serbia (Table 2). Mean discharges also changed towards lower values in winter, spring, and summer in the period 1991–2020, while the highest decrease was observed in the summer and winter seasons. An insignificant increase in the period 1991–2020 compared to the period 1961–1990 was observed in the autumn season at Novi Grad, Prijedor, and Ljubičevski Most (Table 2).

At the seasonal level, mainly decreasing trends were detected throughout the year in the period 1961–2020. The highest negative tendency was primarily observed in winter in the rivers of Bosnia and Herzegovina and in spring and winter in the rivers of Serbia. The exceptions are Prijedor and Svilajnac, with the highest negative trend in summer. A significant negative trend ($p \leq 0.01$) is recorded on Prijedor ($-0.38 \text{ m}^3/\text{s}/\text{year}$) during the summer and at Vrbanja ($-0.21 \text{ m}^3/\text{s}/\text{year}$) in winter; a moderate significant negative trend ($p \leq 0.05$) is recorded at Vrbanja ($-0.09 \text{ m}^3/\text{s}/\text{year}$) in summer. Negative discharge trends in all seasons on Sana River in the period 1961–2014 are also confirmed by *Gnjato* (2018), while on Vrbas River, the most expressed ones were in winter and spring for the period 1961–2016 (*Gnjato et al.*, 2019). On other stations, negative trends are low significant or not statistically significant. A positive trend, which is not statistically significant, is obtained on some rivers in Serbia in spring or autumn (Table 3).

Applying the t-test, it was determined that the changes in discharges between two 30-year periods generally are not statistically significant. The moderate significance decrease ($p \leq 0.05$) in discharge was determined at Prijedor

(- 12.8 m³/s) in the summer period (1991–2020), as well as at Varvarin (-28.8 m³/s) and Svilajnac (-0.65 m³/s) in the same period on annual level.

4.2. Climatic variables

Mean seasonal and annual air temperatures and precipitation at the meteorological stations in selected river basins during the period 1961–2020 are presented in *Table 4*, while their seasonal and annual trend values are given in *Table 5*. It is calculated that the mean annual air temperatures are about 11°C at all stations.

Table 4. Annual and seasonal mean temperatures (°C) at the selected meteorological stations in 1961–2020, 1991–2020, and 1961–1990 and differences between 1991–2020 and 1961–1990

		Period	Year	Winter	Spring	Summer	Autumn	
		Prijedor						
Bosnia and Herzegovina		1961–2020	11.2	1.1	11.5	20.8	11.4	
		1961–1990	10.7	0.5	11.0	20.0	11.1	
		1991–2020	11.7	1.7	12.0	21.6	11.6	
		difference	1	<i>1.2</i>	1.0	1.6	0.5	
	Banja Luka							
		1961–2020	11.3	1.5	11.5	20.7	11.4	
		1961–1990	10.6	0.8	10.9	19.7	10.9	
		1991–2020	12	2.2	12.1	21.8	11.9	
	difference	1.4	1.4	1.2	2.1	1.0		
		Čuprija						
	1961–2020	11.3	1.1	11.5	20.8	11.5		
	1961–1990	10.8	0.7	11.2	19.9	11.1		
	1991–2020	11.7	1.5	11.8	21.6	11.8		
	difference	0.9	<i>0.8</i>	<i>0.6</i>	1.7	<i>0.7</i>		
		Kragujevac						
	1961–2020	11.6	1.7	11.6	20.9	11.9		
	1961–1990	11	1.3	11.2	19.9	11.5		
	1991–2020	12.1	2.2	12.0	21.9	12.3		
	difference	1.1	0.9	<i>0.8</i>	2.0	<i>0.8</i>		
		Kraljevo						
Serbia		1961–2020	11.5	1.4	11.7	20.9	11.8	
		1961–1990	11.1	1.1	11.5	20.1	11.6	
		1991–2020	11.9	1.8	12	21.7	12.1	
		difference	0.8	<i>0.7</i>	0.5	1.6	0.5	
	Rekovac							
		1961–2020	10.8	0	11.0	20.0	11.0	
		1961–1990	10.3	0.6	10.6	19.3	10.6	
		1991–2020	11.3	1.4	11.4	20.8	11.4	
	difference	1.0	<i>0.8</i>	<i>0.8</i>	1.5	<i>0.8</i>		
		Smederevska Palanka						
	1961–2020	11.6	1.5	11.7	21.1	11.7		
	1961–1990	11.0	1.1	11.4	20.2	11.3		
	1991–2020	12.1	2.0	12.1	22.0	12.1		
	difference	1.1	0.9	<i>0.7</i>	1.8	<i>0.8</i>		

Statistical significance: $p \leq 0.01$ and $p \leq 0.05$

The comparative analyses of mean annual and seasonal air temperature between two 30-year periods showed a significant increase in the period 1991–2020 (Table 4), confirming the warming tendency. Mean air temperature has the lowest increase in Kraljevo (0.8 °C) and the highest one in Banja Luka (1.4 °C). The highest increase is obtained for mean summer temperatures at all stations and ranges from 1.5 °C in Rekovac to 2.1 °C in Banja Luka. This could be explained by the fact that Rekovac is a small settlement surrounded by forest, which causes a slight increase in temperature. The lowest increase in mean seasonal temperatures is obtained for autumn at most stations ranging from 0.5 °C (Prijedor and Kraljevo) to 1 °C (Banja Luka). The highest increase in mean annual and seasonal temperatures in Banja Luka could be explained by the fact that it is a town with a lot of urban surfaces, which contributes to an increase in air temperature and to the effect of an urban heat island, typical for cities (Milovanović *et al.*, 2020).

Obtained results calculated by the MK test have shown a significant increase in air temperature at all analyzed meteorological stations in the 1991–2020 period (Table 5). Very significant ($p \leq 0.001$) air temperature increase was obtained on the annual level for all stations, from 0.03 °C/year in Kraljevo (Serbia) to 0.05 °C/year in Prijedor and Banja Luka (Bosna and Hercegovina). The highest air temperature increases were obtained for the summer period at all stations (0.04 to 0.06 °C/year), while significant, moderate, and very significant increases were obtained in other seasons with the lowest rates in autumn (0.015 to 0.04 °C/year). Seasonally, the highest temperature increase was determined at Banja Luka, Prijedor, and Kragujevac in summer. An increase in air temperature that is not statistically significant was obtained only at Kraljevo in spring and autumn. Obtained results are in line with the previous studies for the same stations in Serbia in the period 1961–2010 (Milanović Pešić and Milovanović, 2016; Crnogorac and Rajcevic, 2019; Gnjato, 2018, 2021; Rajčević and Mislicki-Tomić, 2021).

Table 5. Trends in annual and seasonal mean air temperature at the selected meteorological stations in 1961–2020

Station		Year	Winter	Spring	Summer	Autumn
Bosnia and Herzegovina	Prijedor	0.05	0.04	0.04	0.06	0.02
	Banja Luka	0.05	0.05	0.04	0.06	0.04
Serbia	Čuprija	0.031	0.032	0.024	0.048	0.018
	Kragujevac	0.036	0.037	0.026	0.049	0.020
	Kraljevo	0.030	0.032	0.021	0.042	0.015
	Rekovac	0.034	0.032	0.028	0.044	0.018
	Smed. Palanka	0.033	0.036	0.026	0.048	0.019

Statistical significance: $p \leq 0.001$, $p \leq 0.01$, and $p \leq 0.05$

Mean annual precipitation (*Table 6*) ranges from 619.6 mm (Rekovac) to 1036 mm (Banja Luka). The highest precipitation is recorded in the summer due to heavy rains in the summer months, especially in June; the mean summer precipitation ranges from 182.1 mm (Rekovac) to 278 mm (Banja Luka).

Table 6. Annual and seasonal mean precipitation (p - mm) at the selected meteorological stations in 1961–2020, 1991–2020, and 1961–1990 and differences between 1991–2020 and 1961–1990

		Period	Annual	Winter	Spring	Summer	Autumn
		Prijedor					
Bosnia and Herzegovina	1961–2020	943	198	233	245	267	
	1961–1990	928	194	234	261	239	
	1991–2020	958	202	233	228	295	
	difference	30	8	-1	-33	56	
	Banja Luka						
	1961–2020	1036	227	267	278	264	
	1961–1990	1028	221	262	299	246	
	1991–2020	1043	234	271	257	282	
difference	15	13	9	-42	36		
		Čuprija					
	1961–2020	667.0	150.4	181.5	186.4	148.7	
	1961–1990	648.3	144.0	175.5	191.4	137.4	
	1991–2020	685.7	156.7	187.6	181.4	160.0	
	difference	37.4	12.7	12.1	-10	22.6	
		Kragujevac					
	1961–2020	642.2	128.3	169.7	202.5	141.7	
	1961–1990	632.5	127.4	168.1	205.9	131.1	
	1991–2020	651.9	129.3	171.2	199.0	152.4	
	difference	19.4	1.9	3.1	-6.9	21.3	
Serbia	Kraljevo						
	1961–2020	753.4	154.5	204.7	227.2	167.1	
	1961–1990	754.8	163.8	201.0	228.0	162.0	
	1991–2020	752.0	145.2	208.3	226.3	172.3	
	difference	-2.8	-18.6	7.3	-1.7	10.3	
	Rekovac						
	1961–2020	619.6	136.7	163.6	182.1	137.3	
	1961–1990	654.1	142.1	173.4	199.3	139.4	
1991–2020	605.3	135.8	159.2	170.5	139.8		
difference	-48.8	-6.3	-14.2	-28.8	0.4		
		Smederevska Palanka					
	1961–2020	652.0	136.8	166.8	198.8	149.6	
	1961–1990	635.0	133.5	166.3	196.4	138.7	
	1991–2020	669.1	140.0	167.3	201.2	160.5	
	difference	34.1	6.5	1.0	4.8	21.8	

Statistical significance: $p \leq 0.01$ and $p \leq 0.05$

A mild increase in the precipitation amount is recorded at the five stations in the period 1991–2020 compared with the period 1961–1990 (*Table 6*). The decline in mean precipitation amount is recorded in Rekovac (-48.8 mm) and Kraljevo (-2.8 mm) stations. According to obtained results presented in *Table 7*,

changes in seasonal precipitation amounts are negligible. In the period 1991–2020, mean seasonal precipitation amounts increased at most stations compared with the period 1961–1990 during the winter, spring, and autumn. During the summer, the decline in precipitation amount is recorded at all stations except Smederevska Palanka. It could be explained by the intense precipitation on the Rudnik Mountain and the lower part of the Jasenica River basin at the beginning of July 1999. For example, on July 10, 1999, meteorological station Smederevska Palanka recorded 66.5 mm of precipitation, while the mean July precipitation in 1961–1990 amounted to 58.7 mm (*Milanović Pešić*, 2015). This caused floods that covered all left and some right tributaries of Velika Morava, and the Šumadija region suffered the most severe damage (*Gavrilović et al.*, 2012). Results in the Vrbanja River basin show a negative mean annual precipitation trend with a decreasing tendency of -4.33 mm per decade for the period 1961–2015 (*Rajčević and Mislicki-Tomić*, 2021).

Opposite to air temperature, precipitation trends displayed negligible positive or negative tendencies on annual and seasonal levels. Observing the annual values, an increase in precipitation was obtained at five stations and a decrease at two stations. Statistically low significant increase in precipitation is obtained only in Smederevska Palanka (1.84 mm/year). During the spring and autumn seasons, negligible increase in precipitation is recorded at all stations except Rekovac. In winter, an increase is recorded in the precipitation at most stations, while in summer, an increase is recorded at three stations and a decline at four stations (*Table 7*). No one of those trends is statistically significant.

Table 7. Trends in annual and seasonal mean precipitations at the selected meteorological stations in 1961–2020

	Station	Year	Winter	Spring	Summer	Autumn
Bosnia and Herzegovina	Prijedor	0.7	0.1	0.2	-1.1	1.3
	Banja Luka	-1.2	0.03	0.2	-1.5	0.4
Serbia	Ćuprija	1.68	0.48	0.61	-0.07	0.62
	Kragujevac	1.19	0.16	0.14	0.06	0.56
	Kraljevo	0.34	-0.52	0.40	0.32	0.18
	Rekovac	-1.00	-0.23	-0.69	-0.81	-0.30
	Smed. Palanka	1.84	0.27	0.39	0.37	0.64

Statistical significance: $p \leq 0.01$ and $p \leq 0.05$

Comparison of differences between mean annual and seasonal precipitations in two observation periods using the t-test confirmed insignificant changes. Only

a significant ($p \leq 0.01$) increase relative to the period 1961–1990 was observed at Prijedor in autumn.

The obtained results indicate that in all analyzed rivers, there is a decrease in discharges on annual and seasonal levels (winter, spring, and summer). During autumn, a decrease is recorded at Novi Grad, Prijedor, Vrbanja, and Smederevska Palanka stations and an increase at Bagrdan, Ljubičevski Most, and Manasija stations (Table 3). However, these changes are mostly not statistically significant. At all stations, there is a significant increase in mean annual and summer temperatures, while statistically significant increases are obtained for other seasons. In the observed period, the annual precipitation increased at most stations, but it is not statistically significant. At the seasonal level, an increase in precipitation can be observed at all stations during autumn, at most during winter and spring. In contrast, a decrease in precipitation during summer is recorded at almost all stations. According to the results, the increase in annual and seasonal amounts of precipitation at certain stations did not cause an increase in discharges, so it seems that decreasing discharges are mainly the consequence of increasing air temperature (increasing evaporation), which is consistent with the results of other studies of the region.

These findings are in line with the findings for other rivers in this region. *Blöschl et al.* (2019) reported that decreasing discharges in the Balkan Region mainly result from decreasing precipitation and increasing evaporation (due to higher temperatures). *Dimkić and Despotović* (2012) found an inversely proportional correlation between mean annual air temperatures and mean annual discharges on selected hydrological stations in Serbia. They indicate that the changes in air temperature are crucial for precipitation and discharge changes. *Leščešen et al.* (2022) found a statistically insignificant decrease in discharges on the Sava River in the period 1928–2017, which was the consequence of insignificant decreasing precipitation and increasing temperatures. *Gnjato et al.* (2019) concluded that discharge in rivers of Bosnia and Herzegovina displayed a negative tendency in all seasons, but these changes were weak and statistically insignificant. The discharges showed a significant positive correlation with precipitation (especially in summer) and a primarily significant and negative connection with air temperature. *Martić Bursać et al.* (2022) indicated that although precipitation plays a dominant role in year-to-year discharge variability, the effect of air temperature on total annual discharge may become more critical during multiyear droughts. In addition, *Martić Bursać et al.* (2022) found a statistically significant decrease trend in discharges on the Toplica River in the period 1975–1994. In the same period, total precipitation in the river basin increases significantly, so the cause of this decline is a significant increase in air temperature, especially during the summer, that led to an increase in evaporation.

5. Conclusion

This study aimed to present annual and seasonal trends of the hydroclimatic elements (discharge, air temperature, and precipitation) in the lower parts of the Una, Sana, and Vrbanja River basins in Bosnia and Herzegovina and Velika Morava, Jasenica, and Resava River basins in Serbia for the period 1961–2020. In order to show possible changes in these trends, the period 1961–2020 is divided into two parts, 1961–1990 and 1991–2020, which are compared.

The following results have been obtained:

The highest discharges were recorded in spring at all stations. In contrast, the lowest ones were recorded in summer at the stations in Bosnia and Herzegovina and some stations in Serbia and in autumn at other ones in Serbia. With no statistical significance, a decline in mean annual discharges is recorded on all rivers. At the seasonal level, the highest negative tendency is recorded in winter in rivers in Bosnia and Herzegovina and in summer in rivers in Serbia. However, comparing two 30-year periods, as well as the entire period, these changes are not statistically significant.

The highest precipitation is recorded during the summer season as a consequence of heavy rains in the summer months at all stations. Precipitation trends displayed negligible positive or negative tendencies on annual and seasonal levels, with no statistical significance, which is in line with the discharge trends.

Significant increase in air temperature at annual and seasonal levels is recorded at all stations in the period 1991–2020, compared with the period 1961–1990. The highest increase is recorded during the summer season at all stations. The station with the most significant increase in air temperature, both on annual and seasonal levels, is Banja Luka, which could be explained by the presence of large urban surfaces in this town.

The obtained results showed increasing trends in air temperature throughout the year, whereas precipitation displayed mainly insignificant trends. In line with the observed climatic trends, discharges showed negative trends that were mainly insignificant.

The exact impacts of climate change on the water cycle are hard to predict. However, based on the results of this study, it can be concluded that the decrease in discharges on the analyzed rivers (although not statistically significant) is caused mainly by a significant increase in air temperature both at annual and seasonal levels. Increasing air temperature and precipitation variability can lead to water deficiency (especially in small river basins) and cause negative natural and economic implications.

This study represents an attempt to provide detailed hydroclimatic analysis for selected river basins in Bosnia and Herzegovina and Serbia as a base for future research. The obtained results confirm that climatic variable changes affect the discharge regimes over the study area. In addition, the link between trends in air temperature, precipitation, and discharges is very important in the further

assessment of the water resources quantity. Despite the small number of hydrological and meteorological stations in these river basins, which is partly a limitation of this study, the obtained values and the observed changes can be helpful to decision-makers in the development of more efficient water management. We consider that the continuation of the research should be directed toward expanding the research on other rivers with the natural regimes in this region to contribute a complete picture of discharge, precipitation, and air temperature trends.

Acknowledgements: Research by Dr. Ana Milanović Pešić and Dr. Dejana Jakovljević was supported by the Ministry of Science, Technological Development and Innovation of the Republic of Serbia (Contract No. 451-03-136/2025-03/200172).

The authors would like to thank colleague Dr. Milovan Milivojević from the Geographical Institute “Jovan Cvijić” SASA for his advice and assistance in creating the map.

References

- Arrieta-Pastrana, A., Saba, M., and Alcázar, A.P., 2022: Analysis of Climate Variability in a Time Series of Precipitation and Temperature Data: A Case Study in Cartagena de Indias, Colombia. *Water* 14(9), 1378. <https://doi.org/10.3390/w14091378>
- Bajić, D. and Trbić, G., 2016: Klimatski atlas Bosne i Hercegovine, Temperature i padavine. (Climatological Atlas of Bosnia and Herzegovina, Temperature and Precipitation). University of Banja Luka, Faculty of Natural Sciences and Mathematics, Banja Luka, Republic of Srpska, Bosnia and Herzegovina http://www.unfccc.ba/klimatski_atlas/index.html (assessed 22 January 2023) (in Serbian)
- Balisticchi, M., Tomirotti, M., Muraca, A., and Ranzi, R., 2021: Hydroclimatic variability and land Cover transformations in the Central Italian Alps. *Water* 13(7), 963. <https://doi.org/10.3390/w13070963>
- Blöschl, G., Hall, J., Viglione, A., Perdigão, R.A.P., Parajka, J., Merz, B., Lun, D., Arheimer, B., Aronica, G.T., Bilbashi, A., Boháč, M., Bonacci, O., Borga, M., Čanjevac, I., Castellarin, A., Chirico, G.B., Claps, P., Frolova, N., Ganora, D., Gorbachova, L., Gül, A., Hannaford, J., Harrigan, S., Kireeva, M., Kiss, A., Kjeldsen, T., Kohnová, S., Koskela, J.J., Ledvinka, O., Macdonald, N., Mavrova-Guirguinova, M., Mediero, L., Merz, R., Molnar, P., Montanari, A., Murphy, C., Osuch, M., Ovcharuk, V., Radevski, I., Salinas, J.L., Sauquet, E., Sraj, M., Szolgay, J., Volpi, E., Wilson, D., Zaimi, K., and Živković, N., 2019: Changing climate both increases and decreases European river floods. *Nature* 573(7772), 108–111. <https://doi.org/10.1038/s41586-019-1495-6>
- Crnogorac, C. and Rajčević, V., 2019: Climate Change and Protection Against Floods. In: (Eds. Leal Filho, W., Trbić, G. Filipović, D.): Climate Change Adaptation in Eastern Europe: Climate Change Management. Springer, Cham, pp. 127–136. https://doi.org/10.1007/978-3-030-03383-5_9
- Cuevas, J.G., Arumi, J.L., and Dörner, J., 2019: Assessing methods for the estimation of response times of stream discharge: the role of rainfall duration. *J. Hydrol. Hydromech.* 67(2), 143–153. <https://doi.org/10.2478/johh-2018-0043>
- Dimkić, D., 2018: Observed Climate and Hydrological Changes in Serbia — What Has Changed in the Last Ten Years. In: (Eds. Kanakoudis, V., Keramaris, E.): Proc. The 3rd EWaS Int. Conf. Insights on the Water-Energy-Food-Nexus (Lefkada Island, 2018). Proceedings, 2 (11), MDPI, 616. <https://doi.org/10.3390/proceedings2110616>
- Dimkić, D. and Despotović, J., 2012: Analysis of the changes of the streamflows in Serbia due to climate changes. In: (Eds. Berger, A., Mesinger F., Sijacki, D.): Climate Change. Springer, Vienna, 167–177. https://doi.org/10.1007/978-3-7091-0973-1_13

- Dissanayaka, K.D.C.R. and Rajapakse, R.L.H.L., 2019: Long-term precipitation trends and climate extremes in the Kelani River basin, Sri Lanka, and their impact on the streamflow variability under climate change. *Paddy Water Environ.* 17, 281–289. <https://doi.org/10.1007/s10333-019-00721-6>
- Dorđević, B., Dašić, T., and Plavšić, J., 2020: Impact of climate change on Serbian water management and measures for protection against adverse impacts. *Vodoprivreda* 52, 303–305, 39–68. (in Serbian)
- Gavrilović, Lj. and Dukić, D., 2014: Reke Srbije (Rivers of Serbia). Zavod za udžbenike i nastavna sredstva, Belgrade. (in Serbian)
- Gilbert, R.O., 1987: Statistical methods for environmental pollution monitoring. Wiley, New York
- Gnjato, S., Popov, T., Adžić, D., Ivanišević, M., Trbić, G., and Bajić, D., 2021: Influence of climate change on river discharges over the Sava River watershed in Bosnia and Herzegovina. *Időjárás* 125, 449–462. <https://doi.org/10.28974/idojaras.2021.3.5>
- Gnjato, S., Popov, T., Trbić, G., and Ivanišević, M., 2019: Climate Change Impact on River Discharges in Bosnia and Herzegovina: A Case Study of the Lower Vrbas River Basin. In: (Eds. Leal Filho, W., Trbic, G. Filipovic, D.) Climate Change Adaptation in Eastern Europe: Climate Change Management. Springer, Cham, 79–92. https://doi.org/10.1007/978-3-030-03383-5_6
- Gnjato, S., 2018: Analysis of the Water Discharge at the Sana River. *Herald* 22, 103–116. <https://doi.org/10.7251/HER2218103G> (in Serbian)
- Gocić, M., Martić Bursać, N., and Radivojević, A., 2016: Statistical analysis of annual water discharge of Jablanica and Toplica Rivers. *Serbian J. Geosci.* 2, 101–110.
- Haddeland, I., Langsholt, E., Lawrence, D., Wong, W.K., Andjelic, M., Ivkovic, M., and Vujadinovic, M., 2013: Effects of climate change in the Kolubara and Toplica catchments, Serbia. Report No 62, Norwegian Water Resources and Energy Directorate, Oslo, 3–60.
- Helsel, D.R. and Hirsch, R.M., 1992: Statistical methods in water resources. 1st edition Elsevier, Amsterdam.
- Helsel, D.R., Hirsch, R.M., Ryberg, K.R., Archfield, S.A. and Gilroy, E.J., 2020: Statistical methods in water resources. Book 4, Chapter A3, U.S. Geological Survey, Reston.
- Hirsch, R.M., Slack, J.R. and Smith, R.A., 1982: Techniques of trend analysis for monthly water quality data. *Water Resour. Res.* 18(1), 107–121. <https://doi.org/10.1029/WR018i001p00107>
- Hirsch, R.M. and Slack, J.R., 1984: Non-parametric trend test for seasonal data with serial dependence. *Water Resour. Res.* 20(6), 727–732. <https://doi.org/10.1029/WR020i006p00727>
- Hydrological Yearbooks (1961–2020): Republic Hydrometeorological Service of Serbia. https://www.hidmet.gov.rs/latin/hidrologija/povrsinske_godisnjaci.php (assessed 22 January 2023)
- Imamović, A. and Trožić-Borovac, S., 2013: Climate change impacts on the water regime of the River Bosnia. *Our Forests* 12(30–31), 34–41. (in Croatian)
- Jiang, Y., Zhou, C., and Cheng, W., 2007: Streamflow trends and hydrological response to climatic change in Tarim headwater basin. *J. Geogr. Sci.* 17, 51–61. <https://doi.org/10.1007/s11442-007-0051-8>
- Kendall, M.G., 1975: *Rank correlation methods*. 4th edition, Charles Griffin, London
- Kovačević-Majkić, J. and Urošev, M., 2014: Trends of mean annual and seasonal discharges of rivers in Serbia. *J. Geogr. Inst. Cvijic* 64(2), 143–160. <https://doi.org/10.2298/IJGI1402143K>
- Langović, M., Manojlović, S., and Čvorović, Z., 2017: Trends of mean annual river discharges in the Zapadna Morava river basin. *The Bulletin* 97(2), 19–45. <https://doi.org/10.2298/GSGD1702019L>
- Langović, M., Živković, N., Dragičević, S., and Luković, J., 2023: Repeatability cycles of river discharges: Can we identify discharge patterns? A case study of the South Morava River (Serbia). *Carpath. J. Earth Env.* 18(2), 369–383. <https://doi.org/10.26471/cjees/2023/018/266>
- Leščešen, I., Šraj, M., Pantelić, M., and Dolinaj, D., 2022: Assessing the impact of climate on annual and seasonal discharges at the Sremska Mitrovica station on the Sava River, Serbia. *Water Supply* 22(1), 195–207. <https://doi.org/10.2166/ws.2021.277>
- Mallakpour, I., Sadegh, M., and AghaKouchak, A., 2018: A new normal for streamflow in California in a warming climate: Wetter wet seasons and dryer dry seasons. *J. Hydrol.* 567, 203–211. <https://doi.org/10.1016/j.jhydrol.2018.10.023>

- Malede, D.A., Agumassie, T.A., Kosgei, J.R., Linh, N.T.T., and Andualem, T.G. 2022: Analysis of rainfall and streamflow trend and variability over Birr River watershed, Abbay basin, Ethiopia. *Environ. Chall.* 7, 100528. <https://doi.org/10.1016/j.envc.2022.100528>
- Mann, H.B., 1945: Non-parametric tests against trend. *Econometrica* 13(3), 245–259. <http://dx.doi.org/10.2307/1907187>
- Manojlović, S., Manojlović, P., and Djokić, M., 2016: Dynamics of suspended sediment load in the Morava River (Serbia) in the period 1967–2007. *Rev. Geomorfol.* 18(1), 47–58. <https://doi.org/10.21094/rg.2016.076>
- Manzano, J.E. and Barkdoll, B.D., 2022: Precipitation and streamflow trends in Michigan, USA. *Sustain. Water Resour. Manag.* 8, 56. <https://doi.org/10.1007/s40899-022-00606-3>
- Martić Bursać, N., Radovanović, M., Radivojević, A., Ivanović, R., Stričević, Lj., Gocić, M., Golubović, N., and Bursać, B., 2022: Observed climate changes in the Toplica River valley — Trend analysis of temperature, precipitation and river discharge. *Időjárás* 126, 403–423. <https://doi.org/10.28974/idojaras.2022.3.8>
- Meteorological Yearbooks* (1961–2020). Republic Hydrometeorological Service of Serbia. https://www.hidmet.gov.rs/latin/meteorologija/klimatologija_godisnjaci.php (assessed 22 January 2023)
- Milanović Pešić, A., 2019: Water regime and discharges trends of the rivers in the Šumadija region (Serbia). In: Proceedings of the International Scientific Symposium “New Trends in Geography” (Ohrid, North Macedonia, 2019). Macedonian Geographical Society, Ohrid, 3–13.
- Milanović Pešić, A. and Milovanović, B., 2016: The thermic regime and air temperature trends in Šumadija region (Serbia). *J. Geogr. Inst. Cvijic* 66(1), 19–34. <https://doi.org/10.2298/IJGI1601019M>
- Milanović Pešić, A., 2015: *Geographical aspects of natural disasters in Šumadija*. PhD thesis, University of Belgrade, Faculty of Geography, Belgrade, Serbia. (in Serbian)
- Milentijević, N., Bačević, N., Ristić, D., Valjarević, A., Pantelić, M., and Kičović, D., 2020: Application of Mann-Kendal (MK) test in trend analysis of air temperature and precipitation: Case of Mačva district (Serbia). *Bulletin of Natural Sciences Research* 10(1), 37–43. <https://doi.org/10.5937/univtho10-24774>
- Milovanović, B., Ducić, V., Radovanović, M., and Milivojević, M., 2017: Climate regionalization of Serbia to Köppen climate classification. *J. Geogr. Inst. Cvijic* 67(2), 103–114. <https://doi.org/10.2298/IJGI1702103M>
- Milovanović, B., Radovanović, M., and Schneider, C., 2020: Seasonal distribution of urban heat island intensity in Belgrade (Serbia). *J. Geogr. Inst. Cvijic* 70(2), 163–170. <https://doi.org/10.2298/IJGI2002163M>
- Orkodjo, T.P., Kranjac-Berisavićević, G. and Abagale, F.K., 2022: Impact of climate change on future precipitation amounts, seasonal distribution, and streamflow in the Omo-Gibe basin, Ethiopia. *Heliyon* 8, e09711. <https://doi.org/10.1016/j.heliyon.2022.e09711>
- Ouyang, Y., Parajuli, P.B., Li, Y., Leininger, T.D., and Feng, G., 2017: Identify the temporal trend of air temperature and its impact on forest stream flow in the Lower Mississippi River Alluvial Valley using wavelet analysis. *J. Environ. Manage.* 198, 21–31. <https://doi.org/10.1016/j.jenvman.2017.05.014>
- Plavšić, J., Blagojević, B., Todorović, A., and Despotović, J., 2016: Long-term behaviour of precipitation at three stations in Serbia. *Acta Hydrotech.* 29(50), 23–36.
- Rajčević, V. and Mislicki-Tomić, T., 2021: The impact of climate change on the water regime in the Vrbanja River Basin. In: Proceedings of International Scientific Conference GEOBALCANICA 2021, (Ohrid, North Macedonia 2021). Ohrid, 111–123.
- Rajčević, V. and Crnogorac B.Č., 2011: Rijeka Vrbanja — fiziogena svojstva sliva i riječnog sistema (Vrbanja River — Physiogenic features of the basin and river system). Art print, Banja Luka. (in Serbian)
- Republic Hydrometeorological Institute – Republic of Srpska (2023): <https://rhmzrs.com/> (assessed 22 January 2023)
- Salmi, T., Määttä, A., Anttila, P., Ruoho-Airola, T. and Amnell, T., 2002: Detecting trends of annual values of atmospheric pollutants by the Mann-Kendall test and Sen's slope estimates—the Excel

- template application MAKESENS. Finish Meteorological Institute, Helsinki, http://www.fmi.fi/organisation/kontakt_11.html (assessed 22 January 2023)
- Shahgedanova, M., Afzal, M., Severskiy, I., Usmanova, Z., Saidaliyeva, Z., Kapitsa, V., Kasatkin, N., and Dolgikh, S., 2018: Changes in the mountain river discharge in the northern Tien Shan since the mid-20th Century: Results from the analysis of a homogeneous daily streamflow data set from seven catchments. *J. Hydrol.* 564, 1133–1152. <https://doi.org/10.1016/j.jhydrol.2018.08.001>
- Shrestha, R.R., Pesklevits, J., Yang, D., Peters, D.L., and Dibike, Y.B., 2021: Climatic controls on mean and extreme streamflow changes across the permafrost region of Canada. *Water* 13(5), 626. <https://doi.org/10.3390/w13050626>
- Silva, W.L., Xavier, L.N.R., Maceira, M.E.P., and Rotunno, O.C., 2019: Climatological and hydrological patterns in precipitation and streamflow in the basins of Brazilian hydroelectric plants. *Theor. Appl. Climatol.* 137, 353–371. <https://doi.org/10.1007/s00704-018-2600-8>
- Singh, P., Kumar, A., Kumar, N., and Kishore, N., 2010: Hydro-meteorological correlations and relationships for estimating streamflow for Gangotri Glacier basin in Western Himalayas. *IJWREE* 2(3), 60–69.
- Student, 1908: The probable error of a mean. *Biometrika* 6(1), 1–25. <https://doi.org/10.2307/2331554>
- Swain, S.S., Mishra, A., Chatterjee, C., and Sahoo, B., 2021: Climate-changed versus land-use altered streamflow: A relative contribution assessment using three complementary approaches at a decadal time-spell. *J. Hydrol.* 596, 126064. <https://doi.org/10.1016/j.jhydrol.2021.126064>
- Talchabhadel, R., Aryal, A., Kawaike, K., Yamanoi, K., and Nakagawa, H., 2021: A comprehensive analysis of projected changes of extreme precipitation indices in West Rapti River basin, Nepal under changing climate. *Int. J. Climatol.* 41(51), E2581–E2599. <https://doi.org/10.1002/joc.6866>
- Xu, Z.P., Li, Y.P., Huang, G.H., Wang, S.G., and Liu, Y.R., 2021: A multi-scenario ensemble streamflow forecast method for Amu Darya River Basin under considering climate and land-use changes. *J. Hydrol.* 598, 126276. <https://doi.org/10.1016/j.jhydrol.2021.126276>
- Zhong, D., Dong, Z., Fu, G., Bian, J., Kong, F., Wang, W., and Zhao, Y., 2021: Trend and change points of streamflow in the Yellow River and their attributions. *J. Water Clim. Change* 12(1), 136–151 <https://doi.org/10.2166/wcc.2020.14>

IDŐJÁRÁS

*Quarterly Journal of the HungaroMet Hungarian Meteorological Service
Vol. 129, No. 1, January – March, 2025, pp. 89–105*

Clustering of the Black Sea Region meteorological stations of Türkiye with fuzzy c-means, k-means, and silhouette index analysis methods by precipitation, temperature and wind speed

Ash Ulke Keskin¹, Gurkan Kır¹, and Utku Zeybekoglu^{2,*}

¹*Faculty of Engineering, Ondokuz May University
55139, Atakum, Samsun, Türkiye*

²*Boyabat Vocational School of Higher Education,
Sinop University, 57200 Boyabat, Sinop, Türkiye*

* *Correspondening Author E-mail: utkuz@sinop.edu.tr*

(Manuscript received in final form April 11, 2024)

Abstract— Recent years have seen a marked increase in the number of disasters caused by the effects of global climate change. In response, a range of studies have been conducted in Türkiye and worldwide with the aim of reducing the impact of climate change. The classification of regions affected by climate change into similar classes in terms of climate parameters is crucial for the application of consistent methods in studies conducted in these regions. Consequently, the formulation of effective strategies to mitigate the repercussions of climate change in these regions is contingent upon the accurate determination of the aforementioned strategy. The observation records evaluated within the scope of the study were obtained from 31 stations of the Turkish State Meteorological Service in the Black Sea Region, encompassing the period between 1982 and 2020, encompassing precipitation, temperature, and wind speed records. The maximum number of clusters was determined as 5, the cluster analysis study was carried out by using fuzzy c-means and k-means methods for 2, 3, 4, and 5 cluster numbers according to these three data together form a matrix. The determination of the optimum cluster numbers was carried out by silhouette index analysis. For the data matrix where precipitation, temperature, and wind speed were evaluated together, the most appropriate classification was obtained by the k-means method by choosing the number of clusters as 4.

Key-words: cluster analysis, silhouette index analysis, wind speed, precipitation, temperature, fuzzy c-means, k-means, Türkiye

1. Introduction

Climate, defined as the extreme values of various meteorological parameters such as precipitation, temperature, and wind, is the collective state of the atmosphere for a specific location and time period (*Demircan et al.*, 2017). It was widely accepted that there was no change in the long-term averages of the parameters of this collective structure until the mid-1950s. However, as the 20th century progressed, the rapid advancements in industry led to unplanned consumption of natural resources, escalating environmental pollution levels relative to the population, and substantial increases in greenhouse gas emissions into the atmosphere. Consequently, the increasing presence of greenhouse gases, which are capable of trapping heat in the atmosphere, has initiated a series of alterations in climate parameters over time. These alterations in climate parameters are designated as global climate change (*Türkeş*, 2010; *Özkoca*, 2015). The phenomenon of climate change, in its global manifestation, has been demonstrated to manifest locally in the form of various disasters, including but not limited to floods, droughts, and storms. The escalating impact of global climate change, a subject that has been extensively documented in numerous articles in recent years, has been shown to exert a detrimental effect on human life in economic and social spheres. In this regard, studies undertaken to comprehend climate change and to devise measures in this context are also assuming increasing significance. The classification of regions exhibiting analogous climatic characteristics is believed to facilitate various studies, including those focused on combating climate change, safeguarding water resources, and strategising land use. Cluster analysis is a methodology that has been used in climatology research for at least 30 years (*Kalkstein et al.*, 1987; *Fovell and Fovell* 1993). *Erinç* (1949) classified precipitation and temperature data obtained from 53 meteorological stations in Türkiye for 4 different climate zones using the Thornthwaite method. With this study, the regional and detailed classification of Türkiye's geography with sufficient data was carried out for the first time. *Türkeş* (1996) classified the precipitation data of Türkiye with the help of the normalization procedure method proposed by *Kraus* in 1977. In the study, in which the aspirations of the 1930-1993 period were used, 7 different regions were determined. *Kulkarni and Kripalani* (1998), using the fuzzy c-means method, determined the similar classes of Indian precipitation data. Using the precipitation data for the 1871–1984 period, 306 meteorological stations were divided into 4 different clusters. *Unal et al.* (2003) determined the similar classes of temperature and precipitation data covering the period 1951–1998 in Türkiye with 5 different clustering methods. In the study where the single linkage, complete linkage, centroid, Ward's minimum variance, and average distance methods were used, it was stated that the most effective method was the Ward's method. *Soltani and Modarres* (2006) divided the precipitation data of 28 stations in Iran into similar classes with the help of hierarchical and non-hierarchical clustering methods. In

the study in which 8 different classes were determined, the Ward's method and the k-means algorithm were used. *Sönmez and Kömüşcü (2008)* used the k-means algorithm in their study in which they determined the precipitation regions of Türkiye. In the study, in which monthly total precipitation series covering the years 1977–2006 obtained from 148 stations were used, 6 different precipitation regions were determined. *Şahin (2009)* used monthly average temperature, monthly relative humidity, and monthly total precipitation data obtained from 150 stations to determine similar climate classes in Türkiye. Using the Ward's method, the Kohonen artificial neural network, and the fuzzy artificial neural network, 7 different regions were determined. *Dikbas et al. (2012)* determined 6 different precipitation regions by using the 1967-1998 records of 188 stations in Türkiye using the fuzzy c-means method. *Şahin and Cığızoğlu (2012)* determined the sub-climate and sub-precipitation regime classes of Türkiye by using the Ward's method and the fuzzy artificial neural network. Using the precipitation, temperature, and humidity data of 232 stations in the 1974–2002 period, 7 precipitation regime regions and 7 climate regions were determined. *Firat et al. (2012)* determined 7 different regions with similar characteristics by using the k-means method of the classes of annual total precipitation, which was measured at 188 precipitation observation stations in Türkiye covering the period of 1967–1998. In the study of *İyigün et al. (2013)*, a clustering analysis study was carried out with precipitation, temperature, and relative humidity data using the Ward's method. It was obtained from 244 stations in Türkiye and its period covered the years 1970–2010. As a result of the study, 14 different clusters were identified. *Rau et al. (2017)* divided the precipitation data of the Peruvian Pacific slope and coast into regions with similar characteristics. Using the regional vector method and the k-means algorithm, 9 different precipitation regions were determined. *Zeybekoğlu and Ülke Keskin (2020)* realized clustering analysis by adding the latitudes, longitudes, and elevations of the stations to the precipitation intensity series using the fuzzy c-means algorithm. It has been determined that 95 meteorological observation stations in Türkiye form 5 different clusters.

A plethora of studies have been conducted on the determination of climate classes in the literature. A close examination of these studies reveals that they predominantly emphasise precipitation and temperature data as climate parameters. Furthermore, the utilisation of silhouette index analysis for the evaluation of clusters determined by using fuzzy c-means and k-means methods is not a prevalent practice in climate studies, to the best of the authors' knowledge (*Kır, 2021*). The Black Sea Region, selected as the study area, has been experiencing the impacts of global climate change, manifesting in the form of disasters such as floods, droughts, and severe storms. The objective of this study is to identify similar clusters in the wind speed series of the Black Sea Region by employing various clustering algorithms. The analyses conducted for different cluster numbers using the fuzzy c-means and k-means methods were used to determine the most suitable cluster number by means of the silhouette index

analysis. This analysis, conducted using a matrix encompassing wind speed parameters alongside precipitation and temperature metrics, represents a pioneering endeavour within the context of the Black Sea Region, particularly within the context of Türkiye.

2. Materials and methods

2.1. Materials

The present study utilised observations of annual precipitation, annual temperature, and annual wind speed, which were recorded over a period of 39 years (1982–2020) at 31 observation stations operated by the Turkish State Meteorological Service in the Black Sea Region of Türkiye. In order to ensure sufficient statistical validity, it was imperative to consider a minimum record length of 30 years (Kite, 1991). The observation stations utilised in this study are situated in 17 distinct provinces across the Black Sea Region. Eleven of the stations are located in the western Black Sea region, including Duzce, Akçakoca, Bolu, Zonguldak, Bartın, Amasra, Kastamonu, İnebolu, Bozkurt, Tosya, Sinop. The remaining ten stations are situated in the central Black Sea region, Samsun, Bafra, Çorum, Osmaniye, Amasya, Merzifon, Tokat, Zile, Ordu and Ünye. The final ten stations are located in the eastern Black Sea Region, including Giresun, Şebinkarahisar, Trabzon, Akçaabat, Gümüşhane, Bayburt, Rize, Pazar, Artvin and Hopa. Comprehensive details concerning the stations are delineated in Table 1, while the geographical distribution of the stations is exhibited in Fig. 1.

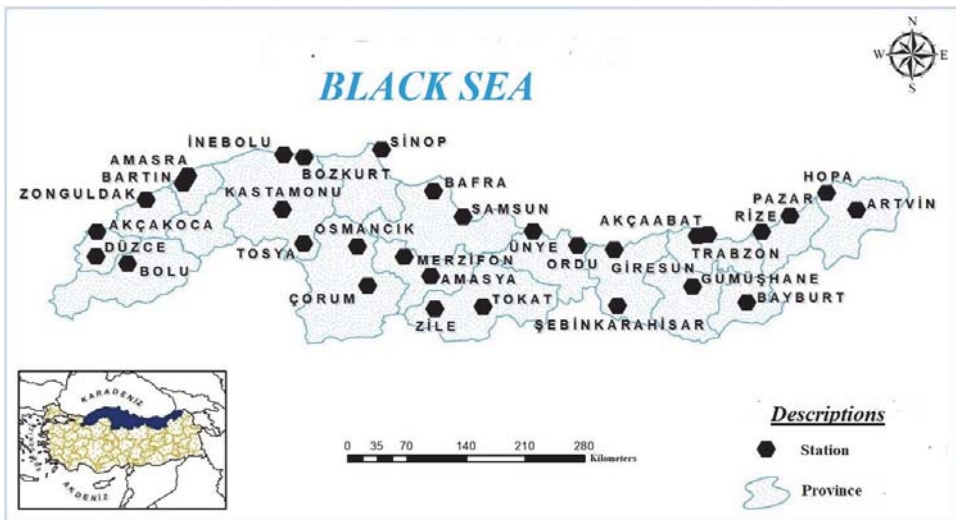


Fig. 1. Geographical distribution of meteorological stations

Table 1. List of meteorological stations and geographical details

Station Name	Station No	Latitude (N)	Longitude (E)	Elevation (m)	Period
Düzce	17072	40°50'37.3"	31°08'55.7"	146	1982-2020
Akçakoca	17015	41°05'22.2"	31°08'14.6"	10	1982-2020
Bolu	17070	40°43'58.4"	31°36'07.9"	743	1982-2020
Zonguldak	17022	41°26'57.3"	31°46'40.5"	135	1982-2020
Bartın	17020	41°37'29.3"	32°21'24.8"	33	1982-2020
Amasra	17602	41°45'09.4"	32°22'57.7"	73	1982-2020
Kastamonu	17074	41°22'15.6"	33°46'32.2"	800	1982-2020
İnebolu	17024	41°58'44.0"	33°45'49.0"	64	1982-2020
Kastamonu/Bozkurt	17606	41°57'34.9"	34°00'13.3"	167	1982-2020
Tosya	17650	41°00'47.5"	34°02'12.1"	870	1982-2020
Çorum	17084	40°32'46.0"	34°56'10.3"	776	1982-2020
Osmancık	17652	40°58'43.3"	34°48'04.0"	419	1982-2020
Sinop	17026	42°01'47.6"	35°09'16.2"	32	1982-2020
Amasya	17085	40°40'00.5"	35°50'07.1"	409	1982-2020
Merzifon	17083	40°52'45.5"	35°27'30.6"	754	1982-2020
Samsun Bölge	17030	41°20'39.0"	36°15'23.0"	4	1982-2020
Bafra	17622	41°33'05.4"	35°55'28.9"	103	1982-2020
Tokat	17086	40°19'52.3"	36°33'27.7"	611	1982-2020
Zile	17681	40°17'45.6"	35°53'25.8"	719	1982-2020
Ordu	17033	40°59'01.7"	37°53'08.9"	5	1982-2020
Ünye	17624	41°08'34.8"	37°17'34.8"	16	1982-2020
Giresun	17034	40°55'21.7"	38°23'16.1"	38	1982-2020
Şebinkarahisar	17682	40°17'13.9"	38°25'09.5"	1364	1982-2020
Gümüşhane	17088	40°27'35.3"	39°27'55.1"	1216	1982-2020
Trabzon Bölge	17037	40°59'54.6"	39°45'53.6"	25	1982-2020
Akçaabat	17626	41°01'57.0"	39°33'41.4"	3	1982-2020
Bayburt	17089	40°15'16.9"	40°13'14.5"	1584	1982-2020
Rize	17040	41°02'24.0"	40°30'04.7"	3	1982-2020
Rize/Pazar	17628	41°10'39.7"	40°53'57.5"	78	1982-2020
Artvin	17045	41°10'30.7"	41°49'07.3"	613	1982-2020
Hopa	17042	41°24'23.4"	41°25'58.8"	33	1982-2020

2.2. k-means algorithm

K-means, one of the oldest clustering algorithms, was developed in 1967 by MacQueen (*MacQueen*, 1967). The assignment mechanism of k-means, one of the most widely used unsupervised learning methods, allows each data to belong to only one cluster. Therefore, it is a sharp clustering algorithm. It is a method based on the main idea that the central point represents the cluster (*Han and Kamber*, 2006). It tends to find globular clusters of equal size (*Isık and Camurcu*, 2007).

The sum of squared errors criterion (SSE) is most commonly used in the evaluation of the k-means clustering method. The clustering result with the lowest

SSE value gives the best results. The sum of the squares of the distances of the objects from the center points of the cluster they are located in is calculated with the following formula (Pang-Ning *et al.*, 2006; Isik and Camurcu, 2007):

$$SSE = \sum_{i=1}^K \sum_{x \in C_i} dist^2(m_i, x). \quad (1)$$

As a result of this criterion, it is aimed to result in k clusters as dense and separate from each other as possible. The algorithm tries to identify k pieces that will reduce the quadrature-error function. The k-means algorithm divides the data set consisting of n data into k clusters with the k parameter given to the algorithm by the user. Cluster similarity is measured by the mean value of the objects in the cluster, which is the center of gravity of the cluster (Xu and Wunsch, 2005; Isik and Camurcu, 2007).

2.3. Fuzzy c-means (FCM) algorithm

Fuzzy c-means (FCM) algorithm is the best known and widely used method among fuzzy division clustering techniques. The fuzzy c-means algorithm was introduced by Dunn (1974) and developed by Bezdek (1981) (Höppner *et al.*, 2000). The fuzzy c-means algorithm is also an objective function-based method. The FCM allows objects to belong to two or more clusters. According to the fuzzy logic principle, each data belongs to each of the clusters with a membership value varying between $[0,1]$. The sum of the membership values of a data to all classes must be “1”. Whichever cluster center the object is close to, the membership of that cluster will be larger than the membership of other clusters. The clustering process is completed when the objective function converges to the determined minimum progress value (Isik and Camurcu, 2007).

The algorithm works to minimize the following objective function, which is a generalization of the least squares method (Höppner *et al.*, 2000; Isik and Camurcu, 2007):

$$J_m = \sum_{i=1}^N \sum_{j=1}^C u_{ij}^m \|x_i - c_j\|^2; 1 \leq m < \infty. \quad (2)$$

The algorithm is started by randomly assigning the U membership matrix. In the second step, the center vectors are calculated. The centers are calculated with the following formula (Höppner *et al.*, 2000; Isik and Camurcu, 2007):

$$c_j = \frac{\sum_{i=1}^N u_{ij}^m x_i}{\sum_{i=1}^N u_{ij}^m}. \quad (3)$$

According to the calculated cluster centers, the U matrix is recalculated using the following formula:

$$u_{ij} = \frac{1}{\sum_{k=1}^C \left(\frac{\|x_i - c_j\|}{\|x_i - c_k\|} \right)^{2/(m-1)}}. \quad (4)$$

The old U matrix and the new U matrix are compared, and the process continues until the difference is less than ε (Moertini, 2002; Isık and Camurcu, 2007). As a result of the clustering operation, the U membership matrix containing fuzzy values reflects the result of the clustering. If desired, these values can be rounded to 0 and 1 by clarification (Isık and Camurcu, 2007).

2.4. Silhouette index analysis

In this method developed by Rousseeuw (1987), the suitability of each element in the data set to the cluster to which it is assigned is defined by the silhouette index value obtained between $[-1, +1]$. A positive silhouette index value indicates that the element is assigned to the correct cluster, and a negative value indicates that the element is assigned to the wrong cluster. The amount of the silhouette index value indicates the degree of membership in the cluster to which the element is assigned. The silhouette index value is calculated by the following formula (Günay Atbaş, 2008; Sönmez and Kömüşcü 2008):

$$S(i) = \frac{\min\{b(i,m) - a(i)\}}{\max\{a(i), \min(b(i,m))\}}, \quad (5)$$

where $a(i)$ is the average distance between point i and all other points in the same cluster, $b(i,m)$ represents the average distance between the i th point and all the points in the m th cluster.

3. Results and discussion

In this study, the k-means and FCM methods were employed to ascertain clusters exhibiting analogous characteristics. This was achieved by utilising a matrix comprising annual total precipitation, annual average temperature, and annual average wind speed observations, encompassing the period between 1982 and 2020, for a total of 31 stations. The analyses were conducted within the MATLAB R2016a software framework. The number of clusters was determined to be five, ensuring that the total number of clusters was less than the square root of the number of stations (Pal and Bezdek, 1995; Zhang et al., 2008; Karahan, 2011, 2019). Since precipitation, temperature, and wind speed are variables with different scales, these data were standardized before classification (Ünal et al., 2003; Lin and Chen, 2006; Cannarozzo et al., 2009; Lim and Voeller, 2009; Dikbas et al., 2012; Firat et al., 2012) as follows:

The classification results obtained when the number of clusters is selected as 3 using the k-means method is shown in *Fig. 2*. When the results are examined, it is seen that cluster C is separated as a subset of cluster A in the previous distribution. Here, clusters A and B consist of 14 stations located in the western, central, and eastern Black Sea Regions. Cluster C consists of 3 stations located in the eastern Black Sea coast. The maximum, minimum, and mean values of the observations in the determined clusters are presented in *Table 3*.

Table 3. Minimum, maximum, and mean values, and standard deviations for meteorological records from 3 clusters solution for k-means

Cluster	Precipitation (mm)				Temperature (°C)				Wind speed (m s ⁻¹)			
	Min.	Max.	Mean	Std. Dev.	Min.	Max.	Mean	Std. Dev.	Min.	Max.	Mean	Std. Dev.
A	444.3	1308.1	952.7	253.1	12.6	15.0	14.1	0.7	1.2	4.8	2.3	0.9
B	423.4	1051.1	563.2	181.0	7.2	13.6	11.3	1.9	0.5	1.9	1.3	0.4
C	2105.4	2329.7	2239.8	118.6	13.8	14.8	14.4	0.5	1.2	2.3	1.8	0.6

The classification results obtained when the number of clusters is selected as 4 using the k-means method is shown in *Fig. 2*. When the results are examined, it is seen that cluster D is separated as a subset of cluster A in the previous distribution. In addition, it is seen that cluster C maintains its integrity in the previous distribution. Thus, cluster A consists of 17 stations located in the western, central, and eastern Black Sea Regions. Cluster B consists of 9 stations located in the inner parts of the western, central, and eastern Black Sea Regions. Clusters C and D, on the other hand, consist of 2 and 3 stations located in the western and eastern Black Sea coastal areas, respectively. The maximum, minimum, and average values of the observations in the determined clusters are presented in *Table 4*.

Table 4. Minimum, maximum, and mean values, and standard deviations for meteorological records from 4 clusters solution for k-means

Cluster	Precipitation (mm)				Temperature (°C)				Wind speed (m s ⁻¹)			
	Min.	Max.	Mean	Std. Dev.	Min.	Max.	Mean	Std. Dev.	Min.	Max.	Mean	Std. Dev.
A	423.4	1308.1	869.5	285.3	12.2	15.0	13.9	0.8	1.0	2.8	1.8	0.5
B	444.4	568.6	489.4	49.1	7.2	11.9	10.3	1.4	0.5	1.9	1.3	0.5
C	2105.4	2329.7	2239.8	118.6	13.8	14.8	14.4	0.5	1.2	2.3	1.8	0.6
D	981.6	1053.8	1017.7	51.0	13.5	14.0	13.7	0.3	3.6	4.8	4.2	0.9

The classification results obtained when the number of clusters is selected as 5 using the k-means method is shown in *Fig.2*. When the results are examined, it is seen that cluster E is separated as a subset of cluster C in the previous distribution. Thus, cluster A consists of 17 stations located in the western, central, and eastern Black Sea Regions. Cluster B consists of 9 stations located in the inner parts of the western, central, and eastern Black Sea Regions. Clusters C and E consist of 2 and 1 stations, respectively, located in the Eastern Black Sea coast. Cluster D consist of 2 stations located in the western Black Sea coast. The maximum, minimum, and mean values of the observations in the determined clusters are presented in *Table 5*.

Table 5. Minimum, maximum, and mean values, and standard deviations for meteorological records from 5 clusters solution for k-means

Cluster	Precipitation (mm)				Temperature (°C)				Wind speed (m s ⁻¹)			
	Min.	Max.	Mean	Std. Dev.	Min.	Max.	Mean	Std. Dev.	Min.	Max.	Mean	Std. Dev.
A	423.4	1308.1	869.5	285.3	12.2	15.0	13.9	0.8	1.0	2.8	1.8	0.5
B	444.4	568.6	489.4	49.1	7.2	11.9	10.3	1.4	0.5	1.9	1.3	0.5
C	2105.4	2329.7	2217.6	158.6	13.8	14.8	14.3	0.7	1.8	2.3	2.1	0.3
D	981.6	1053.8	1017.7	51.0	13.5	14.0	13.7	0.3	3.6	4.8	4.2	0.9
E	2284.4	2284.4	2284.4	-	14.7	14.7	14.7	-	1.2	1.2	1.2	-

The classification results obtained when the number of clusters is selected as 2 using the FCM is shown in *Fig.3*. When the results are examined, cluster A consists of 17 stations located in the western, central, and eastern Black Sea coastal areas. Cluster B consists of 14 stations located in the inner parts of the western, central, and eastern Black Sea Regions. The maximum, minimum, and mean values of the observations in the determined clusters are presented in *Table 6*.

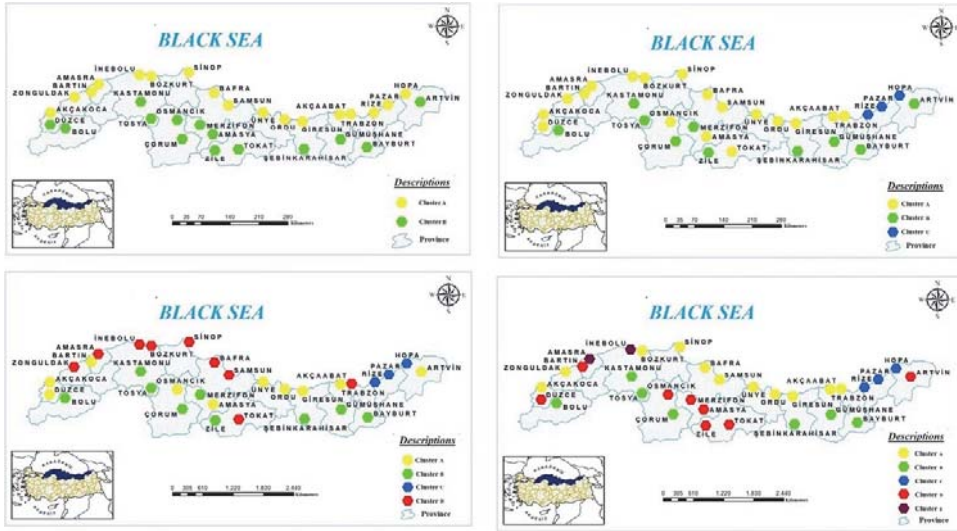


Fig. 3. Geographical distribution of stations for FCM

Table 6. Minimum, maximum, and mean values, and standard deviations for meteorological records from 2 clusters solution for FCM

Cluster	Precipitation (mm)				Temperature (°C)				Wind speed (m s ⁻¹)			
	Min.	Max.	Mean	Std. Dev.	Min.	Max.	Mean	Std. Dev.	Min.	Max.	Mean	Std. Dev.
A	716.5	2329.7	1215.5	524.9	12.9	15.0	14.2	0.7	1.2	4.8	2.2	0.9
B	423.4	818.4	519.8	116.2	7.2	13.6	11.3	1.8	0.5	2.2	1.4	0.5

The classification results obtained when the number of clusters 3 is selected using the FCM is shown in Fig.3. When the results are examined, it is seen that cluster C is separated as a subset of cluster A in the previous distribution. Thus, cluster A consists of 18 stations located in the western, central, and eastern Black Sea Regions. Cluster B consists of 10 stations located in the inner parts of the western, central, and eastern Black Sea Regions. Cluster C consists of 3 stations located in the eastern Black Sea coast. The maximum, minimum, and mean values of the observations in the determined clusters are presented in Table 7.

Table 7. Minimum, maximum, and mean values, and standard deviations for meteorological records from 3 clusters solution for FCM

Cluster	Precipitation (mm)				Temperature (°C)				Wind speed(m s ⁻¹)			
	Min.	Max.	Mean	Std. Dev.	Min.	Max.	Mean	Std. Dev.	Min.	Max.	Mean	Std. Dev.
A	423.4	1308.1	894.2	278.3	12.6	15.0	13.9	0.7	1.0	4.8	2.1	0.9
B	444.4	721.4	512.6	86.8	7.2	12.2	10.5	1.5	0.5	1.9	1.4	0.5
C	2105.4	2329.7	2239.8	2239.8	13.8	14.8	14.4	14.4	1.2	2.3	1.8	1.8

The classification results obtained when the number of clusters is selected as 4 using the FCM is shown in Fig.3. When the results are examined, it is seen that Rize, Pazar, and Hopa stations maintain their integrity. It is seen that cluster B is separated as a subset of cluster A in the previous distribution. Thus, clusters A and D consist of 10 and 9 stations, respectively, located in the western, central, and eastern Black Sea Regions. Cluster B consists of 9 stations located in the inner parts of the western, central and eastern Black Sea Regions. Cluster C consists of 3 stations located in the eastern Black Sea coast. The maximum, minimum, and mean values of the observations in the determined clusters are presented in Table 8.

Table 8. Minimum, maximum, and mean values, and standard deviations for meteorological records from 4 clusters solution for FCM

Cluster	Precipitation (mm)				Temperature (°C)				Wind speed (m s ⁻¹)			
	Min.	Max.	Mean	Std. Dev.	Min.	Max.	Mean	Std. Dev.	Min.	Max.	Mean	Std. Dev.
A	423.4	1308.1	888.1	304.2	12.2	14.8	13.8	0.9	1.0	1.9	1.5	0.3
B	444.4	568.6	489.4	49.1	7.2	11.9	10.3	1.4	0.5	1.9	1.3	0.5
C	2105.4	2329.7	2239.8	118.6	13.8	14.8	14.4	0.5	1.2	2.3	1.8	0.6
D	444.3	1226.7	881.8	252.9	12.6	15.0	13.9	0.7	2.1	4.8	2.7	0.9

The classification results obtained when the number of clusters is selected as 5 using the FCM is shown in Fig.3. When the results are examined, it is seen that only cluster C preserves its integrity. Here, clusters A and D consist of 11 and 8 stations located in the western, central, and eastern Black Sea coastal areas, respectively. Cluster B consists of 7 stations located in the inner parts of the western, central, and eastern Black Sea Regions. Cluster C consists of 3 stations located in the Eastern Black Sea coast. Cluster E consists of 2 stations located in the western Black Sea Region. The maximum, minimum, and mean values of the observations in the determined clusters are presented in Table 9.

Table 9. Minimum, maximum, and mean values, and standard deviations for meteorological records from 5 clusters solution for FCM

Cluster	Precipitation (mm)				Temperature (°C)				Wind speed (m s ⁻¹)			
	Min.	Max.	Mean	Std. Dev.	Min.	Max.	Mean	Std. Dev.	Min.	Max.	Mean	Std. Dev.
A	716.5	1308.1	987.1	234.5	13.2	15.0	14.3	0.6	1.2	2.8	2.0	0.5
B	450.2	568.6	502.2	48.5	7.2	11.4	9.8	1.4	0.9	1.9	1.5	0.3
C	2105.4	2329.7	2239.8	118.6	13.8	14.8	14.4	0.5	1.2	2.3	1.8	0.6
D	423.4	1051.1	601.6	235.4	11.6	13.6	12.7	0.8	0.5	2.2	1.3	0.5
E	981.6	1053.8	1017.7	51.0	13.5	14.0	13.7	0.3	3.6	4.8	4.2	0.9

Silhouette index values of stations in clusters for each number of clusters are presented in Figs. 4 and 5 for k-means and FCM, respectively. Average silhouette index values and negative silhouette index numbers for each cluster determined by k-means and FCM from the clusters 2 to 5 are presented in Tables 10 and 11, respectively.

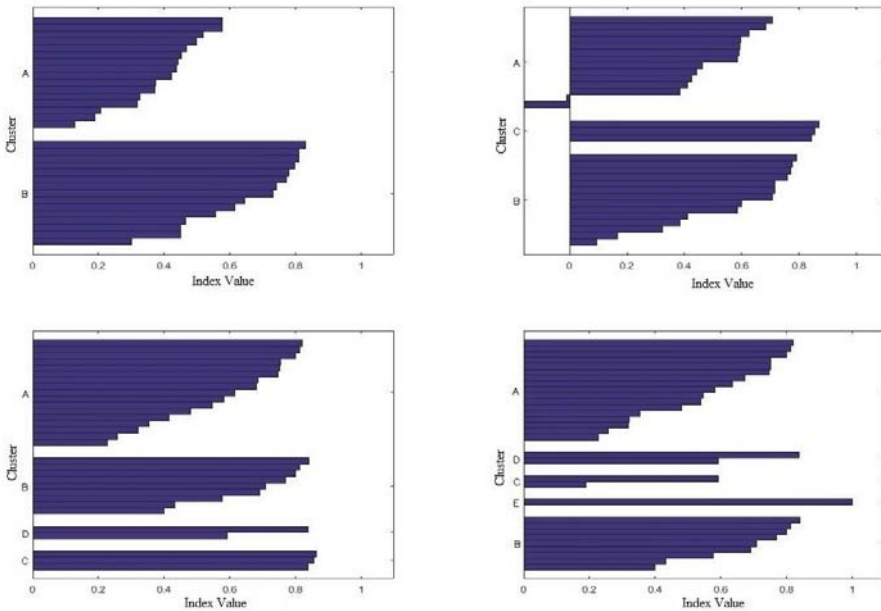


Fig. 4. Silhouette index analysis results of clusters for k-means

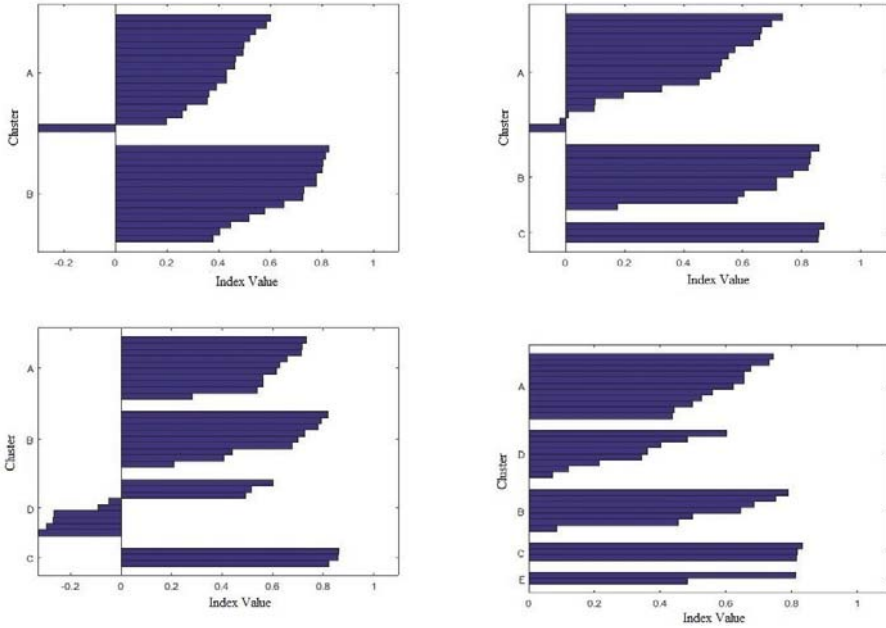


Fig. 5. Silhouette index analysis results of clusters for FCM

Table 10. Silhouette index analysis results for k-means

Cluster number	2	3	4	5
Mean silhouette index value	0.518	0.539	<u>0.641</u>	0.608
Number of negative silhouette indexes	-	2	-	-

Table 11. Silhouette index analysis results for FCM

Cluster number	2	3	4	5
Mean silhouette index value	0.510	0.535	0.464	0.542
Number of negative silhouette indexes	1	2	6	-

As a result of the silhouette analysis (Figs. 4 and 5, Tables 10 and 11) among the clusters determined using k-means and FCM, it was determined that the most suitable clusters were 4 clusters formed by the k-means method.

As a result of the analysis, the Black Sea Region stations were determined as 4 similar clusters in terms of precipitation, temperature, and wind speed characteristics. When compared with the studies covering the Black Sea Region (Turkes, 1996; Unal et al., 2003; Iyigun et al., 2013; Ozturk et al., 2017; Zeybekoglu and Ulke Keskin, 2020), the methods used in the clustering analysis of the different clusters resulted in hydrometeorological parameters, different observation periods, sea effect, and the parallelism of the mountains to the coast, mountainous and rugged. It is thought to be caused by regional geographical features.

4. Conclusion

- In this study, the Black Sea Region of Türkiye was selected as the subject of analysis. The precipitation, temperature, and wind speed parameters of meteorological observation stations in this region were analysed to determine clusters with similar characteristics. The K-means and fuzzy c-means algorithms were utilised to identify the clusters. Cluster analysis was conducted for four different cluster numbers, ranging from two to five, and the optimal number of clusters was determined through the implementation of the silhouette index analysis. The findings of this study, incorporating both cluster analysis and silhouette index analysis, indicate that the most appropriate classification result is achieved through the delineation of four clusters employing the k-means method. While the outcomes derived from the k-means and FCM methods appear to be analogous, it is evident that the k-means method yields more favourable results. The subsequent phase of this study will entail: It is recommended to determine climate classes with different and new combinations that are not used much in the literature, by including hydro-meteorological parameters such as flow, humidity, and evaporation, as well as precipitation, temperature, and wind speed parameters.
- Apart from non-hierarchical clustering algorithms, clustering analyses containing different hierarchical clustering algorithms such as Ward's method should be performed in the literature, and comparative studies should be conducted.
- The cluster analysis study should also be applied to other regions in Türkiye's geography.

In the modern understanding of disaster management (Gunduz, 2022; Usta, 2023), activities should be carried out to identify risks and hazards to take all necessary precautions, to take responsibility for disasters, and to raise awareness of all individuals who make up the society, in order to reduce or prevent the damages of disasters.

Data availability: The meteorological data used in this manuscript were obtained from the Turkish State Meteorological Service (TSMS) for the master's thesis titled "Evaluation of the meteorological data of the Black Sea Region using clustering analysis methods" written by Gurkan Kir under the supervision of Asli Ulke Keskin.

Acknowledgements: The authors thank the Turkish State Meteorological Service for providing the meteorological data. The authors also thank the reviewers for their constructive criticisms which have considerably improved this manuscript.

References

- Bezdek, J.C., 1981: *Pattern recognition with fuzzy objective function algorithms*. Plenum Press, USA.
- Cannarozzo, M., Noto, L.V., Viola, F., and La Loggia, G., 2009: Annual run-off regional frequency analysis in Sicily. *Phys. Chem. Earth* 34, 679–687. <https://doi.org/10.1016/j.pce.2009.05.001>
- Demircan, M., Arabacı, H., Coşkun, M., Türkoğlu, N., and Çiçek, İ., 2017: İklim değişikliği ve halk takvimi: Maksimum sıcaklık desenleri ve değişimi. IV. Türkiye İklim Değişikliği Kongresi İstanbul Medipol Üniversitesi, İstanbul. (In Turkish)
- Dikbas, F., Firat, M., Koc, A.C., and Gungor M., 2012: Classification of precipitation series using fuzzy cluster method. *Int. J. Climatol.* 32(10), 1596–1603. <https://doi.org/10.1002/joc.2350>
- Dunn, J.C., 1974: A fuzzy relative of the ISODATA process and its use in detecting compact, well-separated clusters. *J. Cybernetics* 3, 32–57. <https://doi.org/10.1080/01969727308546046>
- Eriñç, S., 1949: The climates of Turkey according to Thornthwaite's classifications. *Ann. Assoc. Am. Geograp.* 39, 26–46. <https://doi.org/10.1080/00045604909351994>
- Firat, M., Dikbaş, F., Koç, A.C., and Güngör, M., 2012: Classification of annual precipitations and identification of homogeneous regions using k-means method. *Techn. J.* 23(113), 6037-6050.
- Fovell, B., and Fovell, M., 1993: Climate zones of the conterminous United States defined using cluster analysis. *J. Climate* 6, 2103–2135. [https://doi.org/10.1175/1520-0442\(1993\)006<2103:CZOTCU>2.0.CO;2](https://doi.org/10.1175/1520-0442(1993)006<2103:CZOTCU>2.0.CO;2)
- Gündüz, F., 2022: Lessons Learned from the Perspective of Women and Gender in Disasters, The Case of Haiti, and Japan Earthquake. *IBAD J. Social Scie.* 12, 440–460. <https://doi.org/10.21733/ibad.1039215>
- Günay Atbaş, A.C., 2008: A study on determining the number of clusters in cluster analysis. MSc Thesis, Ankara University, Ankara, Turkey.
- Han, J., and Kamber, M., 2006: *Data Mining Concepts and Techniques*. Morgan Kaufmann Publishers Inc.
- Höppner, F., Klawonn, F., Kruse, R., and Runkler, T., 2000: *Fuzzy Cluster Analysis*. John Wiley&Sons, Chichester.
- Işık, M., and Çamurcu, A.Y., 2007: Applied Performance Determination Of K-Means, K-Medoids And Fuzzy C-Means Algorithms. *İstanbul Commerce Univ. J. Sci.* 6(11), 31–45.
- Iyigun, C., Türkes, M., Batmaz, İ., Yozgatlıgil, C., Purutçuoğlu, V., Kartal Koç, E., and Öztürk, M.Z., 2013: Clustering current climate regions of Turkey by using a multivariate statistical method. *Theor. Appl. Climatol.* 114, 95–106. <https://doi.org/10.1007/s00704-012-0823-7>
- Kalkstein, L.S., Tan, G., and Skindlov, J.A., 1987: An evaluation of three clustering procedures for use in synoptic climatological classification. *J. Climate. Appl. Meteor.* 26, 717–730. [https://doi.org/10.1175/1520-0450\(1987\)026<0717:AEOTCP>2.0.CO;2](https://doi.org/10.1175/1520-0450(1987)026<0717:AEOTCP>2.0.CO;2)
- Karahan, H., 2011: Determination of Rainfall Intensity-Duration-Frequency Relationships Using Differential Evolution Algorithm. 108Y299, Research Project, The Scientific and Technological Research Council of Turkey (TUBITAK), Final Report, Ankara, Türkiye.

- Karahan, H., 2019: Determination of homogeneous sub-regions by using intensity-duration-frequency relationships and cluster analysis: an application for the Aegean Region. *Pamukkale University J. Eng. Sci.* 25(8), 998–1013. <https://doi.org/10.5505/pajes.2019.09365>
- Kır, G., 2021: Evaluation of the meteorological data of the Black Sea Region using clustering analysis methods. MSc Thesis, Ondokuz May University, Samsun, Turkey.
- Kite, G., 1991: Looking for Evidence of Climatic Change in Hydrometeorological Time Series. Western Snow Conference. Washington, Alaska.
- Kulkarni, A. and Kripalani, R., 1998: Rainfall patterns over India: Classification with fuzzy c-means method. *Theor. Appl. Climatol.* 59, 137–146. <https://doi.org/10.1007/s007040050019>
- Lim, Y.H., and Voeller, D.L., 2009: Regional flood estimations in red river using L-moment-based index-flood and bulletin 17B procedures. *J. Hydrol. Eng.* 14, 1002–1016. [https://doi.org/10.1061/\(ASCE\)HE.1943-5584.0000102](https://doi.org/10.1061/(ASCE)HE.1943-5584.0000102)
- Lin, G.F., and Chen, L.H., 2006: Identification of homogeneous regions for regional frequency analysis using the self-organizing map. *J. Hydrol.* 324, 1–9. <https://doi.org/10.1016/j.jhydrol.2005.09.009>
- Macqueen, J.B., 1967: Some Methods for Classification and Analysis of Multivariate Observations. *Proc. Symp. Math. Statist. and Probability* (5th), 281–297.
- Moertini, V.S., 2002: Introduction to Five Clustering Algorithms. *Integral* 7(2), 87–96.
- Özkoca, T., 2015: Trend analysis of hydrometeorological parameters at middle blacksea region coast band. MSc Thesis, Ondokuz May University, Samsun, Turkey.
- Öztürk, M.Z., Çetinkaya, G., and Aydın, S., 2017: Climate Types of Turkey According to Köppen-Geiger Climate Classification. *J. Geography* 35, 17–27. <https://doi.org/10.26650/JGEOG295515>
- Pal, N.R., and Bezdek, J.C., 1995: On Cluster validity for the fuzzy c-means model. *IEEE Transactions On Fuzzy Syst.* 3, 370–379. <https://doi.org/10.1109/91.413225>
- Pang-Ning Tan, P.N., Steinbach, M., and Kumar, V., 2006: Introduction to Data Mining. Addison Wesley.
- Rau, P., Bourrel, L., Labat, D., Melo, P., Dewitte, B., Frappart, F., Lavado, W., and Felipe, O., 2017: Regionalization of rainfall over the Peruvian Pacific slope and coast. *Int. J. Climatol.* 37(1), 143–158. <https://doi.org/10.1002/joc.4693>
- Rousseuw, P.J., 1987: Silhouettes: A graphical aid to the interpretation and validation of cluster analysis. *J. Comput. Appl. Math.* 20, 53–65. [https://doi.org/10.1016/0377-0427\(87\)90125-7](https://doi.org/10.1016/0377-0427(87)90125-7)
- Soltani, S., and Modarres, R., 2006: Classification of spatio temporal pattern of rainfall in Iran using a hierarchical and divisive cluster analysis. *J. Spatial Hydrol.* 6(2), 1–12.
- Sönmez, İ., and Kömüscü, A., 2008: Redefinition rainfall regions using k-means clustering methodology and changes of sub period. *İklim Değişikliği ve Çevre* 1, 38–49.
- Şahin, S., 2009: *Applying artificial neural networks on determining climate zones and comparison with the Ward's method.* PhD Thesis, Istanbul Technical University, Istanbul, Turkey.
- Şahin, S., and Çiğzoğlu, H.K., 2012: The sub-climate regions and the sub-precipitation regime regions in Turkey. *J. Hydrol.* 450–451, 180–189. <https://doi.org/10.1016/j.jhydrol.2012.04.062>
- Türkeş, M., 1996: Spatial and temporal analysis of annual rainfall variations in Turkey. *Int. J. Climatol.* 16, 1057–1076. [https://doi.org/10.1002/\(SICI\)1097-0088\(199609\)16:9<1057::AIDJOC75>3.0.CO;2-D](https://doi.org/10.1002/(SICI)1097-0088(199609)16:9<1057::AIDJOC75>3.0.CO;2-D)
- Türkeş, M., 2010: Küresel iklim değişikliği: Başlıca Nedenleri, gözlenen ve öngörülen değişiklikler ve etkileri. Uluslararası Katılımlı 1. Meteoroloji Sempozyumu, Devlet Meteoroloji İşleri Genel Müdürlüğü, Ankara. (In Turkish)
- Usta, G., 2023: Statistical Analysis of Disasters in the World (1900-2022). *Gümüşhane University Journal of Social Sciences Institute* 14(1), 172–186.
- Ünal Y., Kındap, T., and Karaca, M., 2003: Redefining the climate zones of Turkey using cluster analysis. *Int. J. Climatol.* 23, 1045–1055. <https://doi.org/10.1002/joc.910>
- Xu, R., and Wunsch, II D., 2005: Survey of Clustering Algorithms. *IEEE Transactions On Neural Networks* 16(3), 645–678. <https://doi.org/10.1109/TNN.2005.845141>
- Zeybekoğlu, U., and Ülke Keskin, A., 2020: Defining rainfall intensity clusters in Turkey by using the fuzzy c-means algorithm. *Geofizika* 37(2), 181–195. <https://doi.org/10.1016/j.ins.2007.10.004>
- Zhang, Y., Wang, W., Zhang, X., and Li, Y., 2008: A cluster validity index for fuzzy clustering. *Information Sciences* 178, 1205–1218. <https://doi.org/10.1016/j.ins.2007.10.004>

INSTRUCTIONS TO AUTHORS OF *IDŐJÁRÁS*

The purpose of the journal is to publish papers in any field of meteorology and atmosphere related scientific areas. These may be

- research papers on new results of scientific investigations,
- critical review articles summarizing the current state of art of a certain topic,
- short contributions dealing with a particular question.

Some issues contain “News” and “Book review”, therefore, such contributions are also welcome. The papers must be in American English and should be checked by a native speaker if necessary.

Authors are requested to send their manuscripts to

Editor-in Chief of IDŐJÁRÁS
P.O. Box 38, H-1525 Budapest, Hungary
E-mail: journal.idojaras@met.hu

including all illustrations. MS Word format is preferred in electronic submission. Papers will then be reviewed normally by two independent referees, who remain unidentified for the author(s). The Editor-in-Chief will inform the author(s) whether or not the paper is acceptable for publication, and what modifications, if any, are necessary.

Please, follow the order given below when typing manuscripts.

Title page should consist of the title, the name(s) of the author(s), their affiliation(s) including full postal and e-mail address(es). In case of more than one author, the corresponding author must be identified.

Abstract: should contain the purpose, the applied data and methods as well as the basic conclusion(s) of the paper.

Key-words: must be included (from 5 to 10) to help to classify the topic.

Text: has to be typed in single spacing on an A4 size paper using 14 pt Times New Roman font if possible. Use of S.I.

units are expected, and the use of negative exponent is preferred to fractional sign. Mathematical formulae are expected to be as simple as possible and numbered in parentheses at the right margin.

All publications cited in the text should be presented in the *list of references*, arranged in alphabetical order. For an article: name(s) of author(s) in Italics, year, title of article, name of journal, volume, number (the latter two in Italics) and pages. E.g., *Nathan, K.K.*, 1986: A note on the relationship between photo-synthetically active radiation and cloud amount. *Időjárás* 90, 10–13. For a book: name(s) of author(s), year, title of the book (all in Italics except the year), publisher and place of publication. E.g., *Junge, C.E.*, 1963: *Air Chemistry and Radioactivity*. Academic Press, New York and London. Reference in the text should contain the name(s) of the author(s) in Italics and year of publication. E.g., in the case of one author: *Miller* (1989); in the case of two authors: *Gamov and Cleveland* (1973); and if there are more than two authors: *Smith et al.* (1990). If the name of the author cannot be fitted into the text: (*Miller*, 1989); etc. When referring papers published in the same year by the same author, letters a, b, c, etc. should follow the year of publication. DOI numbers of references should be provided if applicable.

Tables should be marked by Arabic numbers and printed in separate sheets with their numbers and legends given below them. Avoid too lengthy or complicated tables, or tables duplicating results given in other form in the manuscript (e.g., graphs). *Figures* should also be marked with Arabic numbers and printed in black and white or color (under special arrangement) in separate sheets with their numbers and captions given below them. JPG, TIF, GIF, BMP or PNG formats should be used for electronic artwork submission.

More information for authors is available: journal.idojaras@met.hu

Published by the HungaroMet Hungarian Meteorological Service

Budapest, Hungary

ISSN 0324-6329 (Print)

ISSN 2677-187X (Online)